Old Dominion University

ODU Digital Commons

Isolation and Functional Mapping of Human T-Cell Leukemia Virus Type 1 Tax Oncoprotein DNA-Damage Complexes

Sarah Saionz Durkin
Old Dominion University

Follow this and additional works at: https://digitalcommons.odu.edu/biomedicalsciences_etds

Part of the Cell Biology Commons, Molecular Biology Commons, and the Virology Commons

ISOLATION AND FUNCTIONAL MAPPING OF HUMAN T-CELL

LEUKEMIA VIRUS TYPE 1 TAX ONCOPROTEIN DNA-DAMAGE

COMPLEXES

by

Sarah Saionz Durkin
B.A. May 2000, University of Pennsylvania
M.A. August 2000, University of Pennsylvania

A Thesis Submitted to the Faculty of
Old Dominion University and Eastern Virginia Medical School
in Partial Fulfillment of the
Requirement for the Degree of

DOCTOR OF PHILOSOPHY

BIOMEDICAL SCIENCES

OLD DOMINION UNIVERSITY
December 2006

Approved by:

_____
O. John Semmes (Chair)

_____
Ann Campbell (Member)

_____
Richard Drake (Member)

_____
Julie Kerry (Member)

ABSTRACT

ISOLATION AND FUNCTIONAL MAPPING OF HUMAN T-CELL LEUKEMIA VIRUS TYPE 1 TAX ONCOPROTEIN DNA-DAMAGE COMPLEXES

Sarah Saionz Durkin
Old Dominion University, 2006
Chair: Dr. O. John Semmes

Human T-cell Leukemia Virus Type 1 (HTLV-1) is a transforming retrovirus which causes Adult T-cell Leukemia (ATL) and HTLV-1 Associated Myelopathy/Tropical Spastic Paraparesis (HAM/TSP). Cellular transformation can be caused by a single viral *trans*-activating protein, Tax. Tax may contribute to transformation through interaction with components of the DNA damage response pathway, promoting cellular genomic instability. We examined cellular Tax complexes in an effort to elucidate potential protein-protein interactions that can model the Tax-induced molecular events. We also investigated the role of post-translational modification in regulating Tax function.

We employed a direct physical analysis of Tax complexes isolated from mammalian cells using affinity purification followed by liquid chromatography/tandem mass spectrometry (LC-MS/MS) analysis, in order to identify both Tax-interacting proteins as well as post-translational modifications of the Tax protein itself. We identified the DNA-dependent Protein Kinase catalytic subunit (DNA-PKcs) as a novel Tax-interacting protein. Using bioinformatics analysis, we created a database of Tax-interacting proteins and, using this tool, identified DNA-PKcs as a predicted member of the Tax complex.

Physical mapping of purified Tax protein revealed novel phosphorylation sites at T48, T184, T215 and S336. Mutational analysis demonstrated phosphorylation at T215 is associated with loss of Tax *trans*-activation of CREB and NF-κB-responsive promoters, while T48 preferentially affects NF-κB-responsive promoters, and T184 and S336 have no effect on these Tax functions.

We confirm the presence of DNA-PKcs and the regulatory protein Ku70 in the Tax complex by co-immunoprecipitation. Tax increases phosphorylation of DNA-PKcs and co-localizes with phosphor-DNA-PKcs within nuclear Tax Speckled Structures (TSS). Cytoplasmically-localized Tax deletion mutants cause a redistribution of phosphor-DNA-PK to the cytoplasm. Tax-expressing cells harbor significantly increased DNA-PK kinase activity, as measured in an *in vitro* kinase assay. Inhibition of DNA-PK activity dramatically reduces Tax-induced autophosphorylation of Chk2, a known DNA-PK substrate.

Suppression of DNA-PKcs expression by siRNA has no significant effect on Tax-induced G2/M arrest. Tax shows no significant effect on cellular end-joining repair as measured by a plasmid-based *in vivo* end-joining assay. Tax-expressing cells show delayed dissolution of damage-induced nuclear speckles containing DNA-PK, γ-H2AX and Tax, suggesting a mechanism for impaired repair response.

This dissertation is dedicated to my family, who provided support and encouragement throughout my studies.

ACKNOWLEDGMENTS

I would like to thank my committee members, Dr. Julie Kerry, Dr. Ann Campbell and Dr. Richard Drake, and especially my adviser Dr. John Semmes for his support in conducting my research. I would also like to acknowledge members of my laboratory, Dr. Saurabh Gupta and Kimberly Fryrear, who provided technical assistance in many of the experiments presented here. In addition, their advice, discussion, and companionship were invaluable to me in the completion of this work.

TABLE OF CONTENTS

Page

LIST OF TABLES

LIST OF FIGURES

Figure   Page

SECTION 1

INTRODUCTION

Human T-Cell Leukemia Virus Type 1

Human T-Cell Leukemia Virus Type 1 (HTLV-1) was the first human retrovirus to be discovered (1,2). Retroviruses are a family of enveloped double-stranded RNA viruses that can be divided into two categories—simple and complex—based on the organization of their genomes. All retroviruses contain four major coding regions: *gag, pro, pol,* and *env* (3). Complex retroviruses code for additional regulatory proteins.

Retroviruses carry two copies of the RNA genome encased in a nucleocapsid and surrounded by an envelope. In brief, the replication cycle begins with attachment of the virion to a cell surface receptor followed by fusion and entry of the core into the cell. The key feature of a retrovirus is reverse transcription of the RNA genome into double-stranded DNA. This provirus, in association with virion proteins, is transported into the nucleus and the viral DNA is integrated into the chromosomal DNA of the cell at more or less random sites. The proviral DNA is transcribed by cellular RNA polymerase II. Transcripts are processed to become both full-length and spliced messenger RNAs as well as full length viral RNA genome. Messenger RNA is translated by cellular machinery in the cytoplasm to produce virion proteins. Virion proteins and viral genome are assembled and virions are released by budding. Mature virions are produced by proteolytic processing of capsid proteins to produce infectious virus. This brief overview describes the life cycle of retroviruses, including HTLV-1 (3,4).

This dissertation follows the format of *The Journal of Biological Chemistry.*

HTLV-1 is a complex retrovirus and a member of the Deltaretroviruses which also include Bovine Leukemia Virus (BLV), Simian T-cell Leukemia Virus (STLV), HTLV-2, HTLV-3 and HTLV-4. The HTLV-1 genome is 9 kb and, like other retroviruses, contains 5' and 3' long terminal repeats (LTRs) which contain signals for transcriptional control of viral gene expression (4). In addition to the retroviral *gag, pro, pol,* and *env* genes, the HTLV-1 genome includes the *pX* region encoding unique regulatory and accessory proteins (4). The HTLV-1 *gag* gene encodes 19-kD matrix (MA), 24-kD capsid (CA), and 15-kD nucleocapsid (NC) structural proteins (5). The *pro* gene encodes the 14-kD protease which is responsible for processing mature gag products (6). The *pol* gene encodes the 95-kD reverse transcriptase (3). The *env* gene encodes envelope proteins which include the 46-kD surface glycoprotein (SU) and 21-kD transmembrane protein (TM) (7). Within the *pX* region are overlapping reading frames encoding for accessory proteins $p12^I$, $p13^{II}$ and $p30^{II}$, and regulatory proteins 27-kD Rex and 40-kD Tax (8). While the accessory proteins, $p12^I$, $p13^{II}$ and $p30^{II}$, are not required for viral replication *in vitro,* they may be essential for establishment of persistent viral infection *in vivo* (8). The regulatory proteins, Rex and Tax, however, are essential for viral replication, and are involved in regulation of viral expression. Rex is involved in controlling gene expression by activating nuclear export of unspliced viral RNA (9). Tax is a *trans*-acting transcriptional activator that regulates transcription from the viral promoter as well as certain cellular promoters (10). Many additional functions of Tax contribute to the unique pathogenesis of HTLV-I, which will be discussed in depth below.

Cellular Tropism and Viral Entry

HTLV-1 preferentially infects CD4$^+$ T-cells in the peripheral blood, however infection of other hematopoietic cells, including CD8$^+$ T-cells, may also occur *in vivo* (11,12). Although CD8$^+$ T-cells are infected by HTLV-1, only CD4$^+$ T-cells present a pre-leukemic phenotype (13). Viral binding and entry depends upon interaction of the HTLV-1 Env receptor with a cellular receptor, the ubiquitous glucose transporter, GLUT-1 (14,15). Extracellular virions have very low infectivity, and efficient spread of HTLV-1 infection requires cell-to-cell contact (16-18). The virus can induce cell-cell fusion and syncytium formation, both of which require envelope glycoproteins (19,20). A study using confocal microscopy to examine the cell-to-cell spread of HTLV-1 identified a structure at the cell-cell junction termed a 'virological synapse' (17). This structure describes a virus-induced polarization of the cytoskeleton of the infected cell at the cell-cell junction, accompanied by accumulation of the HTLV-1 core protein Gag and the viral genome at the same site (17). After 2 h, both the Gag protein and viral genome were transferred from the infected cell to the uninfected cell (17). The ability of HTLV-1 to spread from cell to cell directly without forming extracellular virions may limit its exposure to the immune system (16). Further immune evasion may be attributed to a latent phase where viral replication occurs not through viral gene expression but via persistent clonal expansion of infected T-cells harboring the integrated viral genome (21).

Epidemiology

There are an estimated 20-30 million people in the world infected with HTLV-1 (22,23). Studies of seroprevalence indicate that HTLV-1 is endemic in distinct

geographic areas, including Japan, parts of Africa, Central and South America, and the Caribbean basin (24-32). In the Caribbean, 3-4% of the population is seropositive for HTLV-1 (24); and in Japan, an estimated 1.2 million individuals are HTLV-1-infected (25,26). The major modes of viral transmission occur from mother-to-child via breastfeeding, intravenously through blood transfusion or injection drug use, or sexually (22,24,27-30). In the United States, HTLV-1 infection is found primarily among intravenous drug users, sex workers and immigrants from endemic areas (24,31). The seroprevalence of HTLV-1 in US blood donors was found to be 0.025% (32). Due to the risk of viral transmission through blood transfusion, in November 1988, the Food and Drug Administration (FDA) issued recommendations to screen all whole blood donations in the United States for HTLV-1 (33). Screening of blood donations for HTLV-1 has also been implemented in Japan, Canada, Brazil and several European countries (31).

Diseases of HTLV-I Infection

HTLV-1 infection is linked to two life-threatening and incurable diseases, Adult T-cell Leukemia (ATL) and HTLV-1 Associated Myelopathy/Tropical Spastic Paraparesis (HAM/TSP), as well as other chronic inflammatory conditions, including uveitis, infective dermatitis, polymyositis, bronchioalveolar pneumonitis, auto-immune thyroiditis and arthritis (31,34,35).

Adult T-Cell Leukemia

The first link between a retrovirus and a human cancer was demonstrated in 1980, when Poiesz et al. discovered a retrovirus in a cell line derived from a patient with

cutaneous T-cell lymphoma, and designated it Human T-cell Leukemia Virus Type 1 (36). In the next two years, the linkage between ATL and HTLV-1 was demonstrated by the presence of an antibody against HTLV-1 in sera from a patient with ATL, and the finding of proviral DNA in ATL cell lines (37,38). The following year, the virus was molecularly cloned and the complete nucleotide sequence of the 9 kb proviral genome was determined (39).

More than 800 cases of ATL are diagnosed in Japan each year (25,26). The cumulative lifetime risk of an HTLV-1-infected individual developing ATL or HAM/TSP is estimated at 2 to 5 percent, and this number increases if the individual has other illnesses (23,24,40). Furthermore, there is evidence that co-infection with HTLV-1 and Human Immunodeficiency Virus Type 1 (HIV-1) accelerates progression to Acquired Immunodeficiency Syndrome (AIDS) (23,41). ATL develops after decades of chronic, latent infection, indicating that the mechanism of T-cell transformation must involve multiple, complex events over an extended period of time.

ATL is classified into four clinical subtypes: acute, chronic, smoldering, and lymphoma-type, based on disease presentation, progression, and response to treatment (42). Acute ATL, comprising 55-75% of all ATL cases, is characterized by fever, cough, lymphoadenopathy, skin lesions, hepatosplenomegaly, marked leukocytosis, and hypercalcemia frequently associated with lytic bone lesions (22,34). Without treatment, ATL is rapidly fatal, often with complications from immunodeficiency, and cause of death is frequently from pulmonary complications, opportunistic infections, sepsis or uncontrolled hypercalcemia (34).

The prognosis of ATL patients is poor. ATL cells are resistant to anti-cancer agents, and conventional chemotherapy is ineffective for treating aggressive forms of ATL. The median survival time of patients with acute ATL is 13 months, despite treatment with the most intensive chemotherapy (43). Other treatment regimens include nucleoside analogues, topoisomerase inhibitors, interferon-α, and arsenic trioxide, often in combination (44). Other therapies are targeted at inhibiting NF-κB activity, which increases transcription of anti-apoptotic genes in ATL cells (45). Monoclonal antibodies targeted at cell differentiation markers on the malignant cells provide an alternative therapeutic approach (44). Finally, some success has been achieved with the use of allogeneic stem cell transplantation following cytoreductive chemotherapy and total body irradiation (46).

HTLV-1 Associated Myelopathy/Tropical Spastic Paraparesis and Other Diseases

Like ATL, HAM/TSP only occurs in a small percentage of HTLV-1-infected individuals, with gradual onset decades after infection (31). HAM/TSP is a neurodegenerative disorder characterized by chronic inflammatory changes in the spinal cord, with the principle disability being spasticity of the lower legs (34). The pathogenesis is thought to be caused by an immunological response to HTLV-1 infection (31). Treatment approaches include anti-retroviral drugs, corticosteroids and immunosuppressive drugs, and interferon-α immunotherapy, none of which have good success (31,34).

Other autoimmune diseases have been associated with HTLV-1-infection, including uveitis, infective dermatitis, polymyositis, bronchioalveolar pneumonitis, auto-

immune thyroiditis and arthritis (31,34,35). Uveitis is the only HTLV-associated disease in which HTLV viral sequences and HTLV-1 infected T-cells have been detected in patients (47). The other diseases have only epidemiological evidence of association with HTLV-1.

Prevention

Disease prevention relies on public health initiatives aimed at preventing HTLV-1 infection, including routine screening of blood donations, avoidance of breast-feeding by infected mothers, protected sex, and vaccine development. A prototype vaccine containing the envelope gene in a live recombinant vaccine provided some protection in a rabbit model of infection (48). Other vaccine development focuses on peptide vaccines developed from Tax, naked DNA vaccines, and passive immunization with HTLV-1 immune serum (49-51). No HTLV-1 vaccine has been tested in clinical trials.

The Tax Oncoprotein

The HTLV-1 Tax protein plays a central role in initiating cellular transformation leading to the development of ATL. Tax is a 353 amino acid, 40 kD protein encoded by the *pX* region of the HTLV-1 genome. While Tax has a predominantly nuclear localization, it shuttles between the nucleus and cytoplasm, and has important functions in both compartments (52). It specifically localizes to discrete subnuclear foci, designated Tax Speckled Structures (TSS) (53). Post-translational modifications of Tax, including phosphorylation, ubiquitination and sumoylation at multiple sites, are an important mechanism of regulation (54-58). Sequence analysis of Tax and mutagenesis

experiments have revealed a number of important functional domains including a nuclear localization signal (59,60), nuclear export signal (52,61), activation specific region (62), leucine zipper-like domains (63,64), dimerization domains (63,65,66), PDZ-domain binding motif (67,68), KIX-interacting domain (69-71), and zinc-finger domain (59). The Tax protein is widely regarded as a key element in HTLV-1-mediated transformation.

Transforming Potential of Tax

A number of studies have demonstrated the transforming potential of Tax both *in vivo* and *in vitro*. Introduction of Tax alone or in combination with Ras in rodent fibroblasts transforms cells, which are tumorigenic when injected into nude mice (72,73). Tax expression also immortalizes primary human T-cells (74,75). Expression of the *tax* gene *in vivo* induces tumors in transgenic mice (76-78). Collectively, these observations demonstrate a critical role for Tax in HTLV-1-mediated transformation and ATL pathogenesis.

In addition to this direct evidence for Tax's role in transformation, there is a tremendous wealth of data demonstrating oncogenic activity of Tax *in vitro*. Oncogenesis can occur through an accumulation of mutations in the cellular genome which can be mechanistically attributed to chromosomal instability or loss of DNA repair function. Chromosomal instability results in polyploidy and aneuploidy, while loss of DNA repair function results in structurally damaged chromosomes bearing point mutations, deletions, substitutions, and translocations. Many of these features are demonstrated in HTLV-1-mediated transformation. Aneuploidy is a striking feature of

ATL cells, which have multilobulated nuclei, commonly referred to as "flower" cells (25). Meanwhile, Tax expression alone causes multi-nucleated (polyploid) cells (79,80). HTLV-1-transformed lymphocytes derived from patients contain a variety of chromosomal abnormalities, including translocations, rearrangements, duplications and deletions (81). Chromosomal damage is a characteristic of Tax-expressing cells, as observed by the induction of micronuclei (MN), which represent fragmented chromosomes indicative of DNA damage, or defects in DNA repair or in chromosomal segregation (82). Additional evidence of genomic instability comes from a study showing a 2.8-fold increase in mutation frequency in mammalian cells expressing Tax (83). An increased mutation rate has also been observed in Tax-expressing yeast (84). The mutations induced in the presence of Tax are random, suggesting impairment in the ability of the cell to repair accumulated DNA damage introduced during the normal life cycle of the cell (83).

While HTLV-1 can infect both $CD4^+$ and $CD8^+$ T-cells, only $CD4^+$ infected cells exhibit a preleukemic phenotype, and this is correlated with evidence of genomic instability and Tax expression (85). A study examining the differences between $CD4^+$ and $CD8^+$ HTLV-1-infected T-cells demonstrated a high percentage of multinucleated cells, chromosomal bridges, and G2/M arrest only in the infected $CD4^+$ T-cell population (85). These data suggest that the restriction of the leukemic phenotype to the $CD4^+$ T-cell subtype is a result of genomic instability characterized by accumulated cellular defects and cell cycle redistribution correlated with Tax expression (13).

Tax-induced genomic instability is attributed to its multiple functional activities; however, the exact mechanism is still unknown. In general, as will be discussed below,

many Tax functions, including transactivation, cell cycle dysregulation and interference with DNA repair are dependent on Tax protein-protein interactions with cellular factors. Tax activity results in inactivation of cell cycle checkpoints combined with inhibition of DNA repair, leading to an accumulation of mutations, and ultimately cellular transformation.

Tax Transactivation Functions

While transcriptional activation by Tax allows for regulation of viral transcription through its ability to *trans*-activate the viral long terminal repeat (LTR), this activity also allows Tax to influence transcription of key cellular genes. Tax activates the viral LTR through three 21-bp repeats known as Tax responsive elements (TxRE) (86). The TxRE contains a conserved 8-nucleotide core sequence TGACG(T/A)(C/G)(T/A) that closely mimics the consensus cAMP responsive element (CRE; TGACGTCA) (87). The CRE-binding protein (CREB) forms an unstable complex with the viral CRE, but is stabilized by direct interaction with Tax (88,89). Tax also recruits the co-activators CREB binding protein (CBP), p300, and p300/CBP-associated factor (P/CAF) to the complex, where they induce chromatin conformational modification at the promoter via histone acetylation (10). While Tax has limited direct contact with DNA through amino acid residues 89-110, interaction with transcriptional co-activators is required for transactivation (90,91). Aside from the viral LTR, Tax can *trans*-activate or -repress numerous cellular genes through direct interaction with CRE, CREB, CBP/p300, P/CAF, as well as other CREB/activating transcription factor (CREB/ATF) family members (70,92-95).

Tax also stimulates cellular transcription through activation of the NF-κB pathway via direct binding to the IκB kinase γ/NF-κB essential modulator (IKKγ/NEMO) protein in the cytoplasm, leading to IκB phosphorylation, proteasomal degradation, and persistent NF-κB activity (91,96-98). Furthermore, Tax can bind directly to IκBs to induce their proteasomal degradation (98,99). Additionally, Tax binds to other NF-κB family proteins within the nucleus including NF-κB p50, p65, c-Rel, and NF-κB-2 to enhance transcriptional activation of NF-κB-responsive promoters (100). Constitutive activation of NF-κB is found in ATL cells as well as in Tax-expressing cells (101-103).

Tax modulates the activity of the serum response element (SRE) promoter through direct interaction with serum response factor (SRF) and the SRF cofactor, ternary complex factor (TCF) (104,105). Activation of the SRE promoter by Tax results in increased expression of proto-oncogenes c-Fos, cJun, JunB, JunD and Fra-1, which are components of transcription factors that regulate the expression of genes essential for cell proliferation, differentiation and prevention of apoptosis (106).

Collectively, Tax-mediated modulation of transcription via the CREB, NF-κB, and SRF pathways leads to up- and down-regulation of a range of cellular genes involved in multiple processes. Examples of genes up-regulated by Tax include cytokines and receptors such as IL-2 and IL-2Rα, chemokine receptors, proto-oncogenes, cell cycle regulators, and anti-apoptotic gene *bcl-x$_L$* (34). Tax represses transcription of genes including DNA repair enzyme DNA β polymerase, DNA topoisomerase I, TGF-β1, and pro-apoptotic gene *bax* (34). Microarray analysis of transcriptional changes in HTLV-1-infected or Tax-expressing cells as compared to normal cells reveals altered expression of

many genes relevant for maintaining genomic integrity, including those involved in cell cycle, DNA repair, and apoptosis (107-111).

Cell Cycle Dysregulation by Tax

The effect of Tax on transcription of genes involved in cell cycle regulation can directly contribute to genomic instability. In addition to transcriptional control, Tax influences cell cycle regulation through direct interaction with cellular proteins. Maintenance of genomic integrity requires precise replication and segregation of chromosomes, and impaired cell cycle regulation directly interferes with this process. Tax activity, through a combination of transcriptional activation and interaction with cellular proteins, results in inactivation of cell cycle checkpoints, including accelerated G1/S progression, impaired G2/M transition, and loss of the mitotic spindle assembly checkpoint (80,112-114).

Cell cycle genes transcriptionally regulated by Tax include cyclins A, C, D2 and E; cyclin-dependent kinases (CDK) cdk2 and cdk4; CDK inhibitors (CKI) $p18^{INK4c}$, $p19^{INK4d}$ and $p21^{Wafl/Cip1}$, $p27^{Kip1}$; and E2F (115,116). Physical interaction of Tax with cellular proteins also promotes dysregulation of the cell cycle. Direct binding of Tax with CKI, $p16^{INK4a}$ and $p15^{INK4b}$, interferes with the inhibition of Cdk4/6, resulting in progression through the G1/S phase of the cell cycle (117,118). Furthermore, Tax physically interacts with Cdk4/6, forming an active complex capable of phosphorylating Rb protein and stimulating the G1 to S transition (119). Direct binding of Tax with Rb also targets this protein for proteasomal degradation (120). Along with Rb, the activity of another important tumor suppressor protein, p53, is also regulated by Tax. In contrast to

many other types of cancers which have mutated p53, p53 is wild-type in HTLV-1-infected cells, although Tax inhibits p53 transcriptional activity (121). Evidence from our laboratory shows that Tax inactivation of the p53-mediated G1/S checkpoint promotes cell cycle progression even in the presence of DNA damage (114).

Besides the G1/S checkpoint, Tax activity can abrogate the G2/M checkpoint (80,112,122). Studies in our laboratory have shown that Tax binds directly to Chk2, resulting in Chk2 activation/phosphorylation, and causes cells to accumulate in the G2/M phase of the cell cycle (112). In addition, Tax impairs mitotic spindle checkpoint function through direct binding to mitotic arrest defective protein 1 (MAD1), repressing its function and resulting in defective cytokinesis and subsequent aneuploidy (79). Aneuploidy may also occur as a result of Tax interaction with APC^{cdc20}, leading to premature securin degradation and improper chromatid separation (122,123). Furthermore, centrosome fragmentation has been attributed to the direct binding of Tax with Ran and Ran-binding protein-1 (Ran-BP1) located at the spindle poles (124).

Collectively, these studies demonstrate that transcriptional activation by Tax along with direct interaction with cell cycle proteins leads to dysregulation of the cell cycle. Defects in cell cycle checkpoints combined with improper chromosome segregation caused by Tax effectively promotes loss of genomic integrity.

Tax Interference with DNA Repair

The impairment of cell cycle checkpoints caused by Tax is particularly detrimental to the genomic integrity of the cell when DNA damage occurs. As cells move through the cell cycle and replicate their DNA, they naturally acquire spontaneous

mutations. In a normal cell, the DNA damage response pathway acts to pause the cell cycle and allow for proper repair before the mutations are passed on to daughter cells. Tax contributes to genomic instability not only through abrogation of cell cycle checkpoints, but there is increasing evidence that Tax interferes with the cellular DNA damage response. It does this through transcriptional activation of cellular genes as well as through direct protein-protein interactions.

Damaged DNA is repaired through several pathways, including base excision repair (BER), nucleotide excision repair (NER), homologous recombination (HR), and non-homologous end-joining (NHEJ). Tax represses transcription of β-polymerase, a DNA polymerase enzyme involved specifically in DNA repair (125). Meanwhile, BER activity is reduced in HTLV-1 virus-transformed cells (126). Tax suppresses NER, which correlates with its ability to *trans*-activate proliferating cell nuclear antigen (PCNA) (127). Transcriptional repression of human telomerase (hTert) by Tax may inhibit the addition of telomeric repeats to stabilize the ends of double-stranded DNA breaks (128,129). Recent evidence suggests that the ability of Tax to induce micronuclei is dependent on Ku80, a component of the NHEJ pathway of DNA repair (130). Gene expression of NHEJ pathway components, Ku and DNA-PKcs, were shown to be reduced in Tax-expressing cells by microarray analysis (108). Studies in our laboratory show Tax colocalizes with DNA damage response pathway components, Chk2 and 53BP1, at nuclear sites of DNA damage (112). The multiple effects of Tax activity on DNA repair pathways in the cell have negative implications for the maintenance of genomic integrity.

SECTION 2

SPECIFIC AIMS

Human T-cell Leukemia Virus Type 1 (HTLV-1) is a human transforming retrovirus. Cellular transformation of T-cells in HTLV-1-infected individuals can cause Adult T-cell Leukemia (ATL), and a neurodegenerative disease, HTLV-1 Associated Myelopathy/Tropical Spastic Paraparesis (HAM/TSP). Research shows that cellular transformation can be caused by expression of a single viral transactivating protein, Tax. Although the specific mechanism is not fully known, it is evident that Tax affects diverse cellular processes through direct interaction with various cellular proteins.

Tax may contribute to cellular transformation through induction of genomic instability. Increasing evidence from our laboratory indicates that Tax interacts with components of the cellular DNA damage pathway. In this study we show that Tax specifically interacts with a DNA repair enzyme, DNA-dependent Protein Kinase catalytic subunit (DNA-PKcs). Identification and functional analysis of Tax-interacting proteins, especially those involved in cellular DNA damage-response pathways, can bring forth new insights into the mechanism of Tax-induced genomic instability. Furthermore, a detailed analysis of the physical structure of Tax is critical to understanding how the regulation of this protein affects its function. The objective of this research is to investigate the structural and functional characteristics of Tax complexes. The hypothesis of the research is that Tax interacts with and functionally alters cellular proteins involved in the DNA-damage response pathway. This study will make a significant contribution to our understanding of how Tax transforms cells.

The objective of this proposal will be accomplished by pursuing the following specific aims:

Aim 1. Isolate and identify Tax-interacting proteins.

Identification of Tax-interacting proteins is critical to ascertaining the cellular processes that Tax has an impact on, including the DNA damage-response pathway. We will isolate Tax using a stable, inducible system, as well as a transient expression model, followed by purification of Tax complexes. The components of the Tax complex will be characterized using both mass spectrometry and molecular techniques. Bioinformatics analysis will be used to develop a database of Tax interactions currently documented in the research literature, which can be used for predictive modeling of the Tax interactome.

Aim 2. Characterize functionally significant phosphorylation sites in Tax.

Physical mapping of the Tax structure is critical for developing an understanding of its regulation. Studies have shown that phosphorylation of Tax affects function. First, we will physically map the sites of phosphorylation in the Tax protein using mass spectrometry. Then we will use mutational analysis to determine the functional significance of these modifications.

Aim 3. Determine the functional significance of the interaction of Tax with DNA-PKcs.

We will examine the biological consequence of the Tax-DNA-PK interaction as it relates to genomic instability. We will investigate the effects of Tax on several measurable activities of DNA-PK, including kinase activity and DNA damage response. We will examine the effect of Tax on end-joining repair. Further, using an assay for G2/M arrest, we will determine the functional impact of DNA-PK on Tax-induced genomic instability.

SECTION 3

ISOLATION OF TAX-INTERACTING PROTEINS

Introduction

The transforming retrovirus, Human T-cell Leukemia Virus Type 1 (HTLV-1) is the causative agent of two life-threatening and incurable diseases, Adult T-cell Leukemia (ATL) and HTLV-1 Associated Myelopathy/Tropical Spastic Paraparesis (HAM/TSP), as well as other subneoplastic conditions (25,36,38,131,132). The 40-kDa oncoprotein Tax, encoded by HTLV-1, plays a central role in HTLV-1 pathogenesis (115). Importantly, Tax promotes cellular transformation through its influence on multiple cellular pathways including transcriptional activation, cell cycle control, DNA damage response, signal transduction, tumor suppressor function and apoptosis (34,115). The primary function of Tax is to regulate HTLV-1 gene expression via *trans*-activation of the viral LTR, however, Tax can also regulate host gene transcription (10). The activation and repression of genes involved in diverse cellular pathways is a significant factor in Tax-mediated transformation.

The ability of Tax to regulate gene expression and influence cellular pathways depends upon its protein-protein interactions with diverse host cell factors. The transactivation function of Tax is conferred by interaction with cellular transcription factors and coactivators, including cAMP responsive element binding protein (CREB), CREB-binding protein (CBP) and p300, p300/CBP-associated factor (P/CAF), and activating transcription factor (ATF) family members ATF-1, ATF-2, ATF-4 and ATFx (98-101,112,139-142). Tax also modulates the activity of the nuclear factor-κB (NF-κB)

promoter through interacting directly with IκB kinase γ/ NF-κB essential modulator (IKKγ/NEMO), NF-κB p50, p65, c-Rel, NF-κB-2, mitogen activated kinase kinase (MEKK1), and NIK (96-98,100,133-135). Direct binding of Tax to serum response factor (SRF) and ternary complex factor (TCF) mediates activation of the serum response element (SRE) promoter, resulting in increased gene expression of transcription factors essential for cell proliferation and prevention of apoptosis, including c-Fos, c-Jun, JunB, JunD, and Fra-1 (104,106). Microarray analysis of transcriptional changes induced by Tax reveals a broad range of affected genes involved in such critical cellular processes as cell cycle control, DNA repair response, and apoptosis induction (108,109).

In addition to transcriptional activity, Tax can influence many cellular processes through direct protein-protein interactions. Tax has several structural domains important for mediating protein-protein interactions including a PDZ domain-binding motif (PBM) and coiled-coil domain-binding motif (68,136). The interaction between Tax and PDZ domain-containing proteins such as the discs large (Dlg) tumor suppressor has been associated with the transforming activity of Tax in a colony formation in soft agar (CFSA) assay (137). Another domain in Tax is responsible for interacting with a set of proteins containing a coiled-coiled motif, a conserved structure for protein-protein interaction, and this Tax domain is implicated in the interaction with the spindle assembly checkpoint protein MAD1, the centrosomal protein TXBP121, and a nuclear transcription factor for regulation of cell growth and proliferation, TXBP151 (136). Considering the range of cellular activities influenced by Tax through its interaction with host cell factors, it is of great interest to identify new Tax-binding proteins.

Here, we have attempted to define Tax-interacting proteins in the mammalian cell. We have designed a stable, inducible Tax expression system as well as a transient expression model to purify Tax complexes from human cell lines. Our approach relies on isolating Tax complexes from cells and identifying the cellular components using liquid chromatography tandem mass spectrometry (LC-MS/MS). Using this method, we have identified the novel Tax-binding protein, the catalytic subunit of the DNA-dependent Protein Kinase (DNA-PKcs), a key enzyme in the DNA damage response pathway. Finally, we have conducted a large-scale bioinformatics analysis to generate a digital library containing interactions between HTLV-1 Tax and cellular proteins.

Experimental Procedures

Plasmids

The *tax-Egfp* fusion was originally cloned in frame with a *6XHis* tag in *pcDNA4*. *HisTaxGFP* was subcloned using restriction digestion with *Afl*II and *Not*I into a plasmid with a tetracycline-responsive DNA element, *pcDNA5/FRT/TO/TOPO* (Invitrogen, Carlsbad, CA).

The S-tagged expression vectors *STaxGFP*, *STax*, and *SGFP* were constructed by PCR amplification of the *tax-EGFP* fusion, *tax*, or *EGFP* ORF respectively, using *Pfu Turbo* DNA polymerase (Stratagene, La Jolla, CA) to produce an insert with blunt ends which was subcloned into the *Sma*I site of *pTriEx4-Neo* (Novagen, Madison, WI) in frame with the amino-terminal S-tag and His-tag and a thrombin cleavage site.

Cell Culture and Generation of Stable Cell Line

293T cells were maintained at 37°C in a humidified atmosphere of 5% CO_2 in air, in Iscove's modified Dulbecco's medium supplemented with 10% fetal bovine serum (Cambrex, East Rutherford, NJ) and 1% penicillin-streptomycin (Invitrogen, Carlsbad, CA).

The Flp-In TREx 293 cell line (Invitrogen), which contains a Flp recombination target (FRT) site in its genome, was maintained in Dulbecco's modified Eagle's medium (DMEM) (Invitrogen) supplemented with 10% fetal bovine serum (Cambrex, East Rutherford,NJ), 1% penicillin-streptomycin (Invitrogen), 2 mM L-glutamine (Invitrogen), 200 μg/mL zeocin (Fisher Scientific, Hampton, NH), and 15 μg/mL blasticidin S (ICN Biomedicals, Irvine, CA). To establish a tetracycline-inducible system in 293 cells, pcDNA5/FRT/TO vectors encoding HisTaxGFP and pOG44 vector (Invitrogen), which expresses Flp recombinase, were cotransfected at a molar ratio of 1:9 into Flp-In TREx 293 cells using Lipofectamine 2000 reagent (Invitrogen), according to the manufacturer's protocol. 48 h post-transfection, 50 μg/mL hygromycin B (Invitrogen) was added to the culture for selection. After 2 weeks, hygromycin-resistant cells were harvested and pooled together for further analysis. The stable Flp-In TREx 293-HisTaxGFP cells were maintained in DMEM supplemented with 10% Tet System Approved fetal bovine serum (Clontech, Mountain View, CA), 1% penicillin-streptomycin, 2 mM L-glutamine, 15 μg/mL blasticidin S, and 50 μg/mL hygromycin B. Expression of HisTaxGFP was induced by incubation of cells with 1 μg/mL tetracycline (Fisher, Hampton, NH) for 24 h.

Transient Transfection

Transfections of 293T cells were performed by standard calcium phosphate precipitation. Cells were plated at 1×10^5 cells/mL. The following day, plasmid DNA in 2M $CaCl_2$ and 2X HBS were added dropwise to cells in fresh medium. Cells were incubated at 37°C for 5 h to overnight and fresh medium was added. The cells were harvested 48 h post-transfection, following a single wash with 1X PBS, in 500 µl M-Per mammalian protein extraction reagent (Pierce, Rockford, IL) with protease inhibitor cocktail (Roche, Palo Alto, CA) and immediately frozen at –80°C.

Metal Affinity Protein Purification

Prepared cell lysate (1.5 mL) in M-Per with EDTA-free protease inhibitor cocktail (Roche, Palo Alto, CA), was incubated with 100 µl pre-equilibrated Talon Metal Affinity Resin (Clontech, Mountain View, CA) and incubated for 30 min rotating at room temperature, then washed 3 times with 1 mL 1X Equilibration/Wash Buffer (50 mM sodium phosphate, 300 mM NaCl, pH 7.0). Washed beads were eluted in 1X Imidazole Elution Buffer (50 mM sodium phosphate, 300 mM NaCl, 150 mM imidazole, pH 7.0). An equal volume of Laemmli Sample Buffer (Bio-Rad, Hercules, CA) with β-mercaptoethanol was added to the eluate, followed by boiling for 5 min. Samples were electrophoresed in a 10% SDS polyacrylamide gel and visualized by SilverQuest silver staining (Invitrogen, Carlsbad, CA). Bands of interest were manually excised from the gel for further analysis.

S-tag Protein Purification

Prepared cell lysate (1.5 mL) was incubated with 75 µl bed volume of S-protein agarose (Novagen, Madison, WI) for 30 min rotating at room temperature, then washed 3 times with 1 mL Bind/Wash Buffer (20 mM Tris-HCl pH 7.5, 150 mM NaCl, 0.1% TritonX-100). Washed beads were eluted by resuspension in 150 µl Laemmli Sample Buffer (Bio-Rad, Hercules, CA) with β-mercaptoethanol, followed by boiling for 5 min. Eluates were electrophoresed in a 10% SDS polyacrylamide gel and visualized by SilverQuest silver staining (Invitrogen, Carlsbad, CA). Bands of interest were manually excised from the gel for further analysis.

LC-MS/MS Analysis

Protein bands were excised from 1-D polyacrylamide gels. Gel slices were cut into 1-2 mm cubes; washed 3X with 500 µL ultra-pure water and incubated in 100% acetonitrile for 45 minutes. The material was dried in a speed-vac, rehydrated in a 12.5 ng/µL modified sequencing grade trypsin solution (Promega, Madison, WI) and incubated in an ice bath for 40-45 min. The excess trypsin solution was then removed and replaced with 40-50 µL of 50mM ammonium bicarbonate, 10% acetonitrile, pH 8.0 and the mixture was incubated overnight at 37°C. Peptides were extracted 2X with 25 µl 50% acetonitrile, 5% formic acid and dried in a speed-vac. Digests were resuspended in 20 µL Buffer A (5% acetonitrile, 0.1% formic acid, 0.005% heptafluorobutyric acid) and 3-6 µL were loaded onto a 12-cm x 0.075 mm fused silica capillary column packed with 5 µM diameter C-18 beads (The Nest Group, Southboro, MA) using a N2 pressure vessel at 1100 psi. Peptides were eluted over 55 minutes, by applying a 0-80% linear gradient

of Buffer B (95% acetonitrile, 0.1% formic acid, 0.005% heptafluorobutyric acid) at a

flow rate of 130 μL/min with a pre-column flow splitter resulting in a final flow rate of

~200 nl/min directly into the source. In some cases the gradient was extended to 150

minutes to acquire more MS/MS spectra. A LCQ™ Deca XP (ThermoFinnigan, San

Jose, CA) was run in an automated collection mode with an instrument method composed

of a single segment and 4 data-dependent scan events with a full MS scan followed by 3

MS/MS scans of the highest intensity ions. Normalized collision energy was set at 30,

activation Q was 0.250 with minimum full scan signal intensity at 5×10^5 and a minimum

MS2 intensity at 1×10^4. Dynamic exclusion was turned on utilizing a three minute

repeat count of 2 with the mass width set at 1.50 Da. Sequence analysis was performed

with TurboSEQUEST™ (ThermoFinnigan, San Jose, CA) or MASCOT (Matrix

Sciences, London, GB) using an indexed human subset database of the non-redundant

protein database from National Center for Biotechnology Information (NCBI) web site

(http://www.ncbi.nlm.nih.gov/). An additional database was created containing only the

ORF sequence for the expressed Tax protein.

Immunoblot Analysis

Cell extracts were derived as described above. Total protein concentrations were

determined by Protein Assay (Bio-Rad, Hercules, CA). An equal volume of Laemmli

sample buffer (Bio-Rad, Hercules, CA) with β-mercaptoethanol was added to the lysate,

boiled for 5 min, and a normalized amount of total protein was loaded in each lane and

electrophoresed through a 10% SDS-polyacrylamide gel. The proteins were transferred

onto an Immobilon-P (Millipore, Billerica, MA) membrane using a Trans-blot SD semi-

dry transfer cell (Bio-Rad, Hercules, CA) at 400 mA for 50 min in transfer buffer (25 mM Tris, 200 mM glycine, 20% methanol, 0.1% SDS). Following blocking in 5% non-fat milk in PBS/0.1% Tween-20, blots were incubated in primary antibody overnight, followed by 1 h incubation in secondary horseradish-peroxidase conjugated anti-mouse or anti-rabbit antibody (Bio-Rad, Hercules, CA). Immunoreactivity was detected via Immunstar enhanced chemiluminescence protein detection (Bio-Rad, Hercules, CA).

Immunoprecipitation

Whole cell lysate (~2 mg) in 500 µl volume were incubated with 5 µl anti-Tax pep3 polyclonal antibody at 4°C overnight, with constant rotation. The lysate was then incubated with 100 µl Protein A Sepharose beads (Zymed, San Francisco, CA) while rotating for 1 h at 4°C. The beads were washed 3X with 1 mL each 1X SNNTE buffer (5% sucrose, 500 mM NaCl, 1% Nonidet P-40, 50mM Tris-HCl [pH 7.4], 5 mM EDTA). Proteins were eluted from beads with 100 µl Laemmli sample buffer (Bio-Rad, Hercules, CA) with β-mercaptoethanol, and boiled for 5 min.

Fluorescent Microscopy

293T cells were seeded onto 22-mm diameter coverslips in 6-well plates at $1x10^5$ cells/well. Transfections were performed as described above, and 48 h later cells were washed twice with PBS and fixed in 4% paraformaldehyde. Coverslips were mounted on glass slides in Vectashield containing DAPI (Vector Laboratories, Burlingame, CA). Fluorescent images were acquired using a Zeiss LSM 510 confocal microscope at 40X

magnification with a 2.8X zoom using Argon (488 nm) and HeNe2 (633 nm) lasers, and imaged with LSM Image Browser software (Carl Zeiss, Jena, Germany).

Luciferase Assay

293T cells, plated at $2x10^5$ cells per well of a 6-well plate, were transfected as described with 1 to 5 µg of Tax expression plasmid, and 1 µg of *HTLV-LTR-Luc* reporter plasmid. The parental vector used for Tax expression, *pTriEx4-Neo* (Novagen, Madison, WI), was added to normalize for the total amount of transfected DNA. Luciferase activity was measured 48 h after transfection. Cells were washed twice with 1X PBS and then lysed in 1X Reporter Lysis Buffer (Promega, Madison, WI) and subjected to one freeze-thaw at -80°C. Luciferase assay substrate was used according to the manufacturer's protocol, and activity was measured in a TD-20/20 luminometer (Turner Designs, Sunnyvale, CA). Luciferase activity was normalized for total cell protein determined from whole cell extracts by Protein Assay (Bio-Rad, Hercules, CA), according to manufacturer's direction.

Bioinformatics Analysis

The Human Virus Interactome Resource (HVIR), including a Tax-interaction map and digital library of Tax-interacting cellular proteins, was generated as part of a collaboration of Dr. O. John Semmes and Sarah Durkin with a research group at Old Dominion University led by Dr. Alex Pothen, Dr. Mohammad Zubair, Dr. Kurt Maly and Dr. Chris Osgood, and including Emad Ramadan, Mahmoud Abu-Elela, Khaled Ibrahim, and Praveen Namburi. Databases used for bioinformatics analysis were from the

following public websites: PubMed, www.ncbi.nlm.nih.gov/PubMed/; Yale Medical Library, www.med.yale.edu/library/; Human Protein Reference Database, www.hprd.org; Database of Interacting Proteins, dip.doe-mbi.ucla.edu; and Biomolecular Interaction Network Database, www.bind.ca.

Results

Efficient Expression of Tax in a Stable, Inducible Cell Line

In order to isolate cellular proteins that interact with Tax *in vivo,* we created a tandem affinity-tagged Tax construct that could be stably expressed in a human cell line, and purified in a complex with cellular binding proteins. Human embryonic kidney 293 (HEK293) cells were chosen as the parental cell line due to the characteristics of high transfection efficiency and immortality which are advantageous for construction of a stable cell line. We have previously demonstrated that Tax has measurable activity in this cell line (data not shown). A stable cell line provides an efficient method to harvest large numbers of cells expressing Tax protein. The Flp-In System (Invitrogen) allows for stable integration of the *tax* gene into a specific genomic location in the host cell chosen for optimal protein expression via recombinase-mediated DNA recombination. Tax expression is under the control of a tetracycline-responsive promoter, such that uninduced cells can be passaged without expression of Tax. This is advantageous because the Tax protein can induce cellular toxicity when expressed continuously. The *HisTaxGFP* vector expresses full-length Tax protein fused to amino-terminal His_6- and Xpress tags and carboxy-terminal green fluorescent protein (GFP) (Fig. 1*A*). The His_6 tag, which has metal-binding properties, is included for purification using immobilized metal affinity

A

His	Xpress	Tax	GFP	HisTaxGFP

His	Xpress	GFP		HisGFP

B

- Tet   + Tet

C

C   0   1   2   3   µg/ml
—75
◄——HisTaxGFP
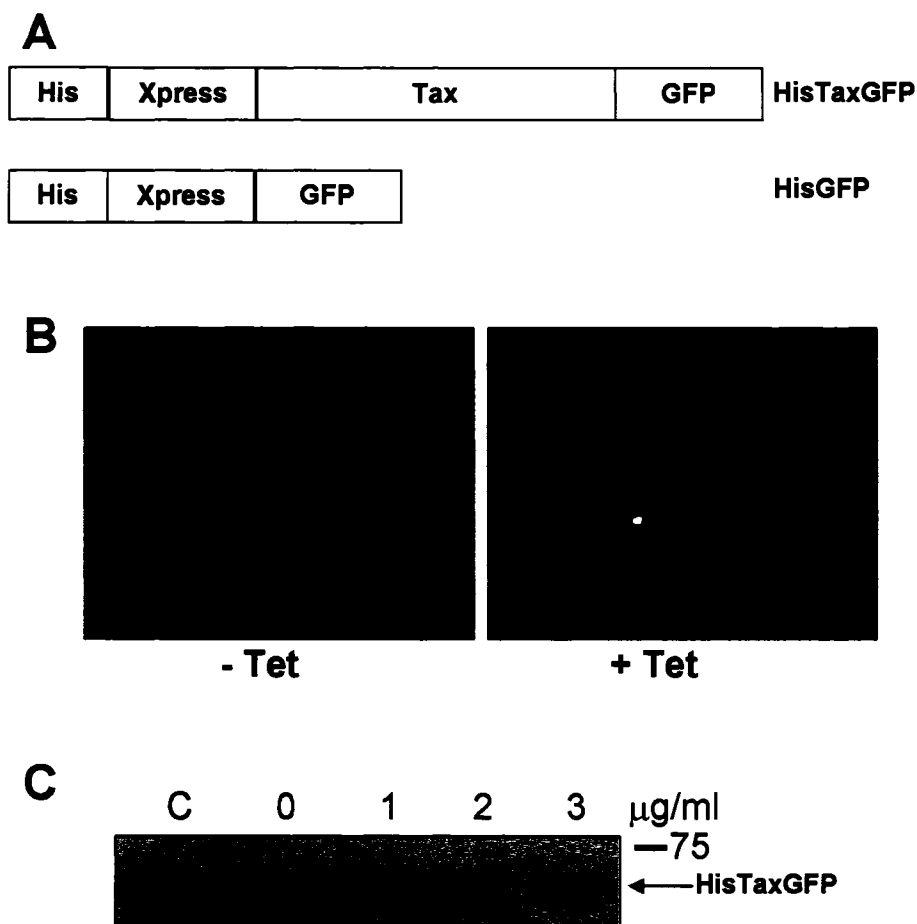
FIG. 1. **Efficient expression of Tax in a stable, inducible cell line.** *A*, a depiction of *HisTaxGFP* and control *HisGFP* expression vector constructs. *B*, induction of HisTaxGFP expression in Flp-In TREx 293-HisTaxGFP cells by incubation of with 1 µg/ml tetracycline for 24 h. Left panel shows uninduced cells. *C*, Flp-In TREx 293-HisTaxGFP cells harvested 24 h after induction of HisTaxGFP with the indicated concentrations of tetracycline were subjected to immunoblot analysis and probed with anti-Xpress antibody (Invitrogen). Cell lysate from 293T cells transiently transfected with *HisTaxGFP* was loaded as a control in the lane marked C.

resin. The *HisGFP* vector is used as a control for nonspecific binding in the purification scheme (Fig. 1*A*). We included the GFP subunit to facilitate monitoring of protein expression and localization, and the Xpress tag to monitor the purification process. We efficiently expressed Tax from the Flp-In TREx 293-HisTaxGFP cell line by induction with 1 μg/ml tetracycline for 24 h (Fig. 1, *B* and *C*). Tax expression is undetectable by either fluorescence microscopy or immunoblot analysis in the absence of tetracycline (Fig. 1, *B* and *C*).

Affinity Purification of Tax Complex from Stable Cell Line

We successfully purified His₆-tagged Tax protein from induced FlpIn TREx 293-HisTaxGFP cells using immobilized metal affinity resin as described in Experimental Procedures. The majority of Tax protein was captured on the resin, as the flowthrough shows minimal Tax protein (Fig. 2*A*, *lane 2*), and minimal Tax protein was lost in the wash steps (Fig. 2*A*, *lanes 3* and *4*). Tax protein is not completely removed from the beads in a single elution step, as an almost equal amount is removed in a second elution step (Fig. 2*A*, *lanes 5* and *6*). Combined, the Tax protein from two elution steps equals roughly 10% of the input (Fig. 2A, compare *lane 1* showing 5% input to *lanes 5* and *6*).

In order to identify cellular proteins bound to Tax protein, we purified HisTaxGFP from the stable cell line and resolved the Tax complex by SDS-PAGE followed by visualization of the proteins by silver staining (Fig. 2*B*). Control cell lysates from 293 cells transiently transfected with *HisGFP* vector were purified in parallel and used as a control for non-specific binding to the metal affinity resin. There is considerable non-specific binding, and the most obvious unique band is HisGFP in the
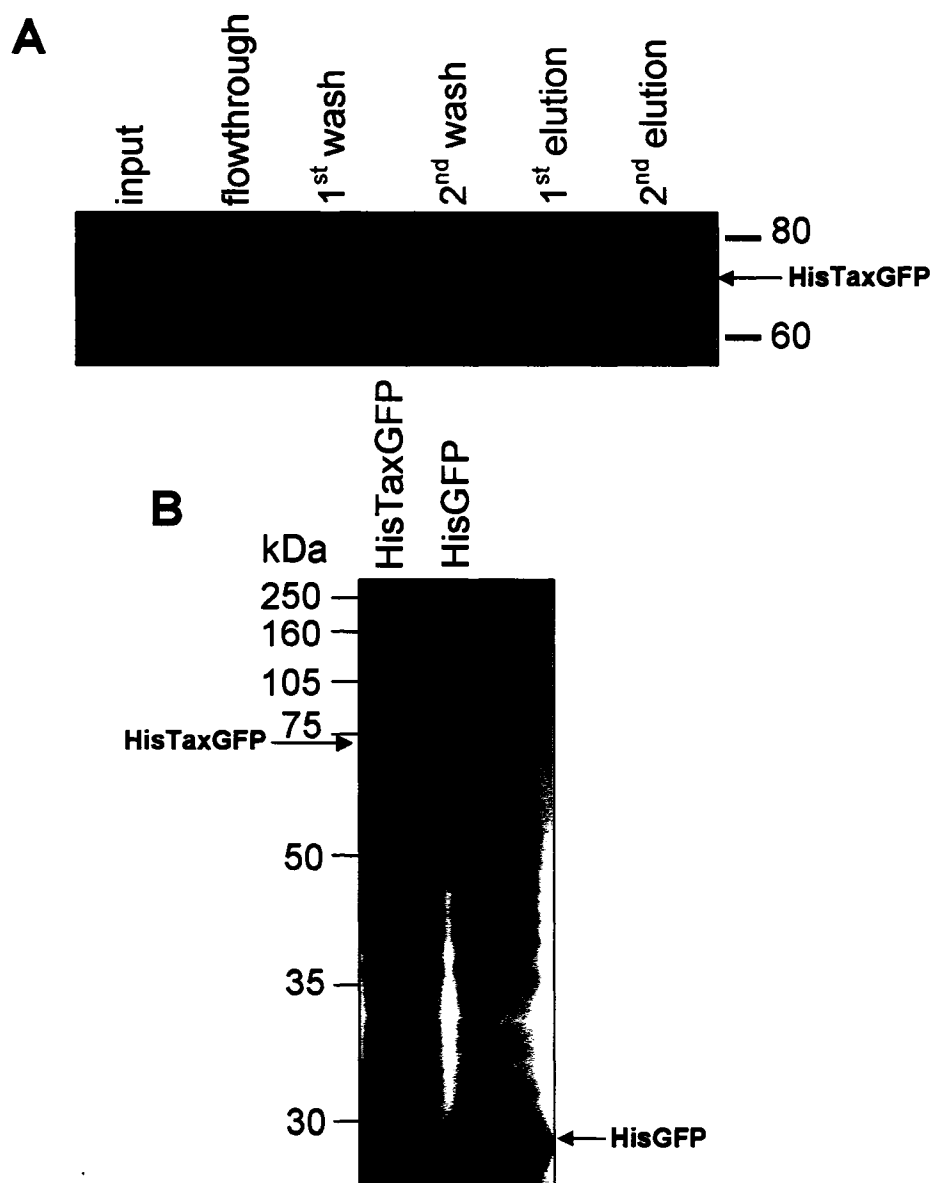
FIG. 2. **Affinity purification of Tax complex from stable cell line.** *A*, cell lysate from tetracycline-induced Flp-In TREx 293-HisTaxGFP cells (*input*) was incubated with immobilized metal affinity resin. Following incubation, resin was centrifuged and supernatant was removed (*flowthrough*); resin was washed twice and each wash was removed (1st *wash*, 2nd *wash*); bound protein was eluted twice with Laemmli Sample Buffer (1st *elution*, 2nd *elution*). Reserved fractions were subjected to immunoblot analysis and probed with anti-Tax polyclonal antibody. *B*, cell lysates from tetracycline-induced Flp-In TREx 293-HisTaxGFP cells (*HisTaxGFP*) and 293T cells transiently transfected with control HisGFP (*HisGFP*) were subjected to SDS-PAGE and proteins were visualized by silver staining.

control lane (Fig. 2B, *lane 2*). Using LC-MS/MS, we were able to successfully identify the proteins in 8 bands from a gel with HisTaxGFP isolated from the stable cell line (Fig. 3). One band was identified as Tax. Several of the bands were identified to contain chaperonin-containing TCP1 protein, however, in subsequent experiments this protein was shown to be present in purifications from both HisTaxGFP- and HisGFP-expressing cells, suggesting that TCP1 is binding non-specifically to the metal affinity resin (data not shown). The high background of non-specific binding using this method prompted us to change to a different type of tag for the purification scheme.

Efficient Expression of Biologically Active S-tagged Tax

We sought to utilize a more specific affinity purification tag to decrease the non-specific binding we saw with the metal affinity resin. We chose the S-tag purification system (Novagen), which is based on the strong interaction between a 15-amino acid S tag and S protein immobilized on agarose beads, both of which are derived from RNase S (138). We designed vectors expressing Tax with an amino-terminal S-tag (*STax*) or with an additional carboxy-terminal GFP tag to monitor transfection efficiency and protein localization (*STaxGFP*), and a control S-tagged GFP (*SGFP*) (Fig. 4A). An amino-terminal His$_6$-tag is included in all three vectors for tandem affinity purification and to facilitate monitoring of protein purification. An additional feature of this vector is a thrombin cleavage site located between the S-tag and the protein of interest (Fig. 4A, indicated by *arrow*). This design allows affinity binding of the S-tagged protein to the beads followed by thrombin cleavage of the tag to release the protein, rather than elution.
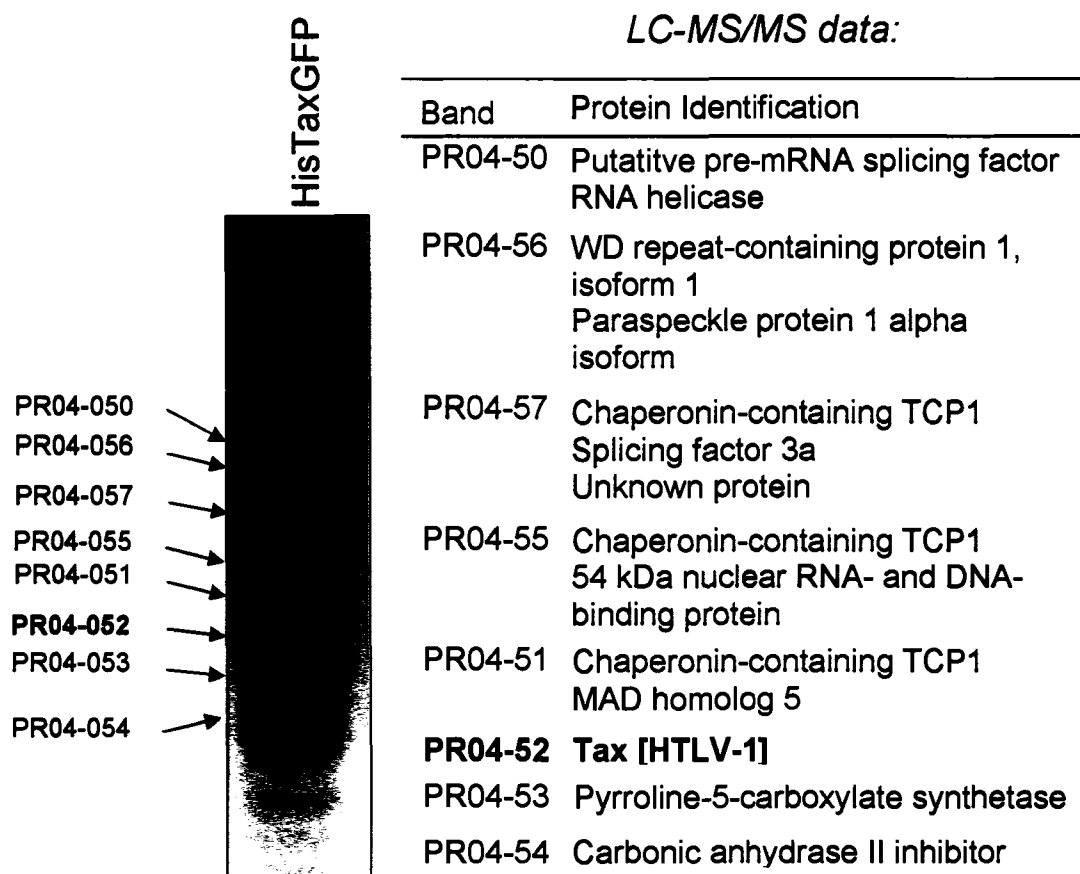
FIG. 3. **Identification of proteins affinity purified with HisTaxGFP.** Cell lysate from tetracycline-induced Flp-In TREx 293-HisTaxGFP cells was subjected to SDS-PAGE and proteins were visualized by silver staining. Individual bands, indicated by arrows, were manually excised from gel and assigned identification numbers (indicated), and analyzed by LC-MS/MS. Identified proteins from each band are listed with the corresponding band identification number.

A

S-Tag

KETAAAKFERQHMDSPPPSGLVPRGSM

| His | S-Tag | Tax | GFP | STaxGFP

| His | S-Tag | Tax | STax

| His | S-Tag | GFP | SGFP

B

C
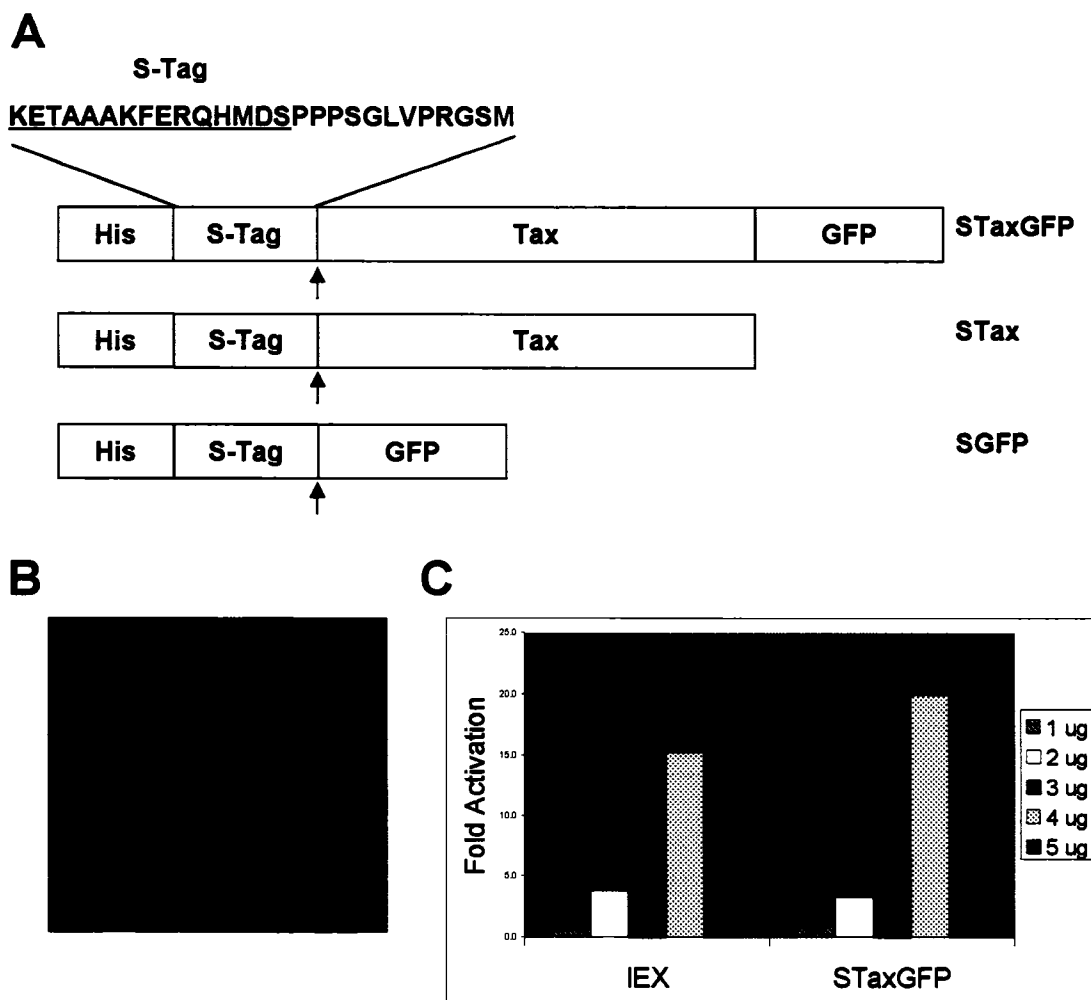
FIG. 4. **Efficient expression of biologically active S-tagged Tax.** *A*, a depiction of the *STaxGFP*, *STax*, and control *SGFP* expression vector constructs. *B*, 293T cells were transiently transfected with *STaxGFP* (green), fixed with 4 % paraformaldehyde, permeabilized with methanol and nuclei were stained with DAPI and TOPRO-3-iodide (blue). Fluorescent images were acquired with a Zeiss LSM 510 confocal microscope at 40X magnification using Argon (488 nm) and HeNe2 (633 nm) lasers and imaged with LSM Image Browser software. *C*, 293T cells were cotransfected with the HTLV-I LTR Luc reporter plasmid and increasing amounts of either Tax-expressing vector *IEX* or *STaxGFP*. Luciferase activity is shown as fold activation over non-Tax expressing cells.

The advantage of this method is that only the protein of interest along with interacting proteins will be removed from the beads by cleavage of the tag, whereas elution will release all proteins—specific and non-specific—bound to the beads.

The *STaxGFP* vector was transiently transfected into 293T cells, and the transfection efficiency and appropriate subcellular localization to Tax Speckled Structures (TSS) was confirmed by visualizing the GFP expression (Fig. 4*B*). In order to determine whether the S-tagged Tax-GFP fusion protein retains functional activity, we compared it to untagged Tax expressed from the *IEX* vector in *trans*-activation assays. 293T cells were cotransfected with the HTLV-1 LTR Luciferase reporter plasmid and either Tax-expressing vector *IEX* or *STaxGFP*. STaxGFP showed comparable transcriptional activity to untagged Tax (Fig. 4*C*). The activity of STaxGFP as measured by the ability to activate via the NF-κB-responsive promoter and to induce cell cycle accumulation in 4N was also comparable to untagged Tax (data not shown). Thus we showed that S-tagged Tax protein is biologically active and efficiently expressed in mammalian cells. Although the Flp-In TREx 293-HisTaxGFP stable cell line produces Tax protein in every cell, the protein expression of *STaxGFP* is much higher per cell and therefore overall expression of STaxGFP is higher than the stable cell line, even though it is a transient transfection. Therefore, we found this to be an efficient method for expressing Tax in mammalian cells.

Affinity Purification of S-tagged Tax from Mammalian Cells

We successfully purified S-tagged Tax protein from transiently transfected 293T cells using S-protein agarose beads as described in Experimental Procedures. The eluted

protein from the affinity purification was further resolved by SDS-PAGE and the STax and control SGFP proteins were detected by blotting with S-protein HRP-conjugate (Fig. 5A). Silver staining of a gel with STaxGFP and SGFP affinity purifications allowed visualization of interacting proteins (Fig. 5, B and C). Distinct bands corresponding to the predicted molecular weight of SGFP and STaxGFP are labeled (Fig. 5, B and C, arrows), indicating purification of a large quantity of S-tagged protein. Unlike the metal affinity purification process, the S-tag purification method produces limited non-specific binding, apparent in the presence of only one major band in the control SGFP lane which is also present in the STaxGFP lane (Fig. 5, B and C, open arrow).

Identification of Tax-interacting Proteins

Using LC-MS/MS, we successfully identified the proteins in 9 bands of a gel containing purified STaxGFP complexes from transiently transfected mammalian cells (Table I). Several of the bands contained Tax, and the lower molecular weight bands presumably contain Tax degradation products. The non-specific band present in the control SGFP lane (Fig. 5, B and C, open arrow) was identified as Raichu404X. Significantly, we identified a novel Tax-interacting protein, the catalytic subunit of the DNA-dependent Protein Kinase (DNA-PKcs), a key enzyme in the cellular response to DNA damage. Confirmation of this interaction and investigation of the functional significance is addressed in subsequent sections of this dissertation.
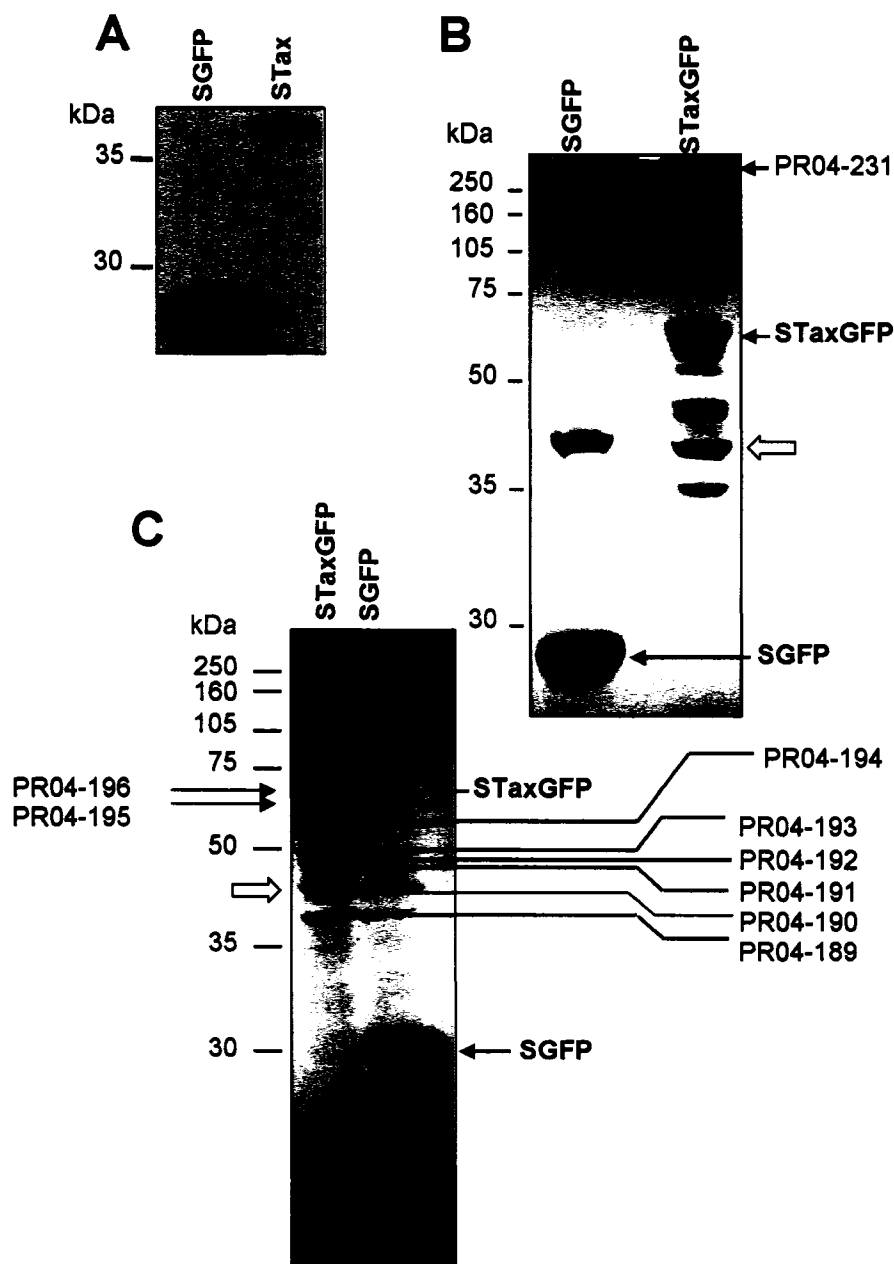
FIG. 5. **Affinity purification of S-tagged Tax from mammalian cells.** Cell lysates from 293T cells transiently transfected with SGFP, STax, or STaxGFP (indicated) were affinity purified on S-protein agarose beads as described under "Experimental Procedures" and subjected to SDS-PAGE and analysis using S-protein HRP-conjugate (Novagen) (A) or silver staining (B and C). Individual bands were manually excised from the silver stained gels (B and C), assigned identification numbers (indicated), and subjected to LC-MS/MS analysis (Table I).

TABLE I

Tax-binding protein candidates in Fig. 5 identified by LC-MS/MS analysis

Band	Protein identification
PRO-189	β-actin
	Tax [HTLV-1]
	Unknown protein
	F-box only protein 22 isoform a
PRO-190	Unknown protein
	Euk. Translation initiation factor 4a
PRO-191	β 5-tubulin
	Unnamed protein product
	Tax [HTLV-1]
	Raichu404X
	Vimentin
	Ribonuclease/angiogenin inhibitor
PRO-192	Tax [HTLV-1]
	Raichu404X
	β 5-tubulin
PRO-193	Tubulin alpha 6
	Tax [HTLV-1]
	Raichu404X
	ATP synthase, subunit
PRO-194	Raichu404X
	Tax [HTLV-1]
	TCP1, chaperonin, Hsp60
	KIAA0002
PRO-195	Tax [HTLV-1]
PRO-196	Tax [HTLV-1]
PRO-231	DNA-activated protein kinase, catalytic subunit

Bioinformatics Analysis

In addition to using experimental approaches to identify novel Tax-interacting proteins, we undertook a bioinformatics approach to categorize documented Tax interactions and provide a framework for predicting potential interactions. In collaboration with a research group at Old Dominion University, we built the Human Virus Interactome Resource (HVIR), designed as a digital library of Tax-interacting proteins. Furthermore, HVIR provides an interactive tool for researchers to visualize documented Tax-interacting proteins as well as 'second neighbors' of Tax, or binding partners of Tax-interacting proteins. This provides information to guide experiments in the laboratory which can determine if the 'second neighbors' are also in the Tax complex. Thus, HVIR provides a useful tool for predicting protein-protein interactions.

A database of known Tax-interacting proteins was created by extracting relevant information from selected journal articles in the online medical literature, using well-established text mining approaches. The extracted information was normalized and represented in a standardized format based on the Biomolecular Interactions Network Database (BIND) XML prototype, and stored in the HVIR digital repository. The quality of the text-mining data was validated manually by researchers. Several protein interaction databases available on public websites, including BIND, Human Protein Reference Database (HRPD), and Database of Interacting Proteins (DIP), were used as sources of information about 'second neighbors' of Tax. Finally, a network-drawing program was used for visualizing the Tax interactome network, and to present an interactive search service for the user. Clustering algorithms are also being developed to predict functional modules, protein complexes, and pathways from the proteomic

network. A schematic diagram indicating the workflow of HVIR development is included (Fig. 6*A*).

While development of the Tax interactome resource is still in progress, a current model incorporates 82 direct interacting proteins identified from selected journal articles, in addition to countless 'second neighbors' identified via protein interaction databases. (data not shown). Interestingly, by examining the network for relevant 'second neighbors' of Tax, the interaction of Tax and DNA-PKcs presented here could have been predicted based on a range of common binding partners (Fig. 6*B*). For example, Tax interacts with NFKB1, whose activity is regulated by IKK alpha, a phosphorylation target of DNA-PK (91,139). Another DNA-PK phosphorylation target is p53, a binding partner of 53BP1, which Tax also interacts with (112,140). The interaction could have been predicted through Chk2, a Tax-interacting protein that associates with mediator of DNA damage checkpoint protein 1 (MDC1), which interacts with DNA-PK (112,141-143). Collectively, this depiction of the Tax interactome predicts the presence of DNA-PKcs in the Tax complex.

Discussion

We used affinity purification to identify cellular proteins that interact with Tax in mammalian cells. Using a stable, inducible Tax expression system, we successfully purified His_6-tagged Tax protein with metal affinity resin. However, this method produced unsatisfactory levels of non-specific protein binding. Consequently, we developed a transient expression system for affinity purification of S-tagged Tax protein
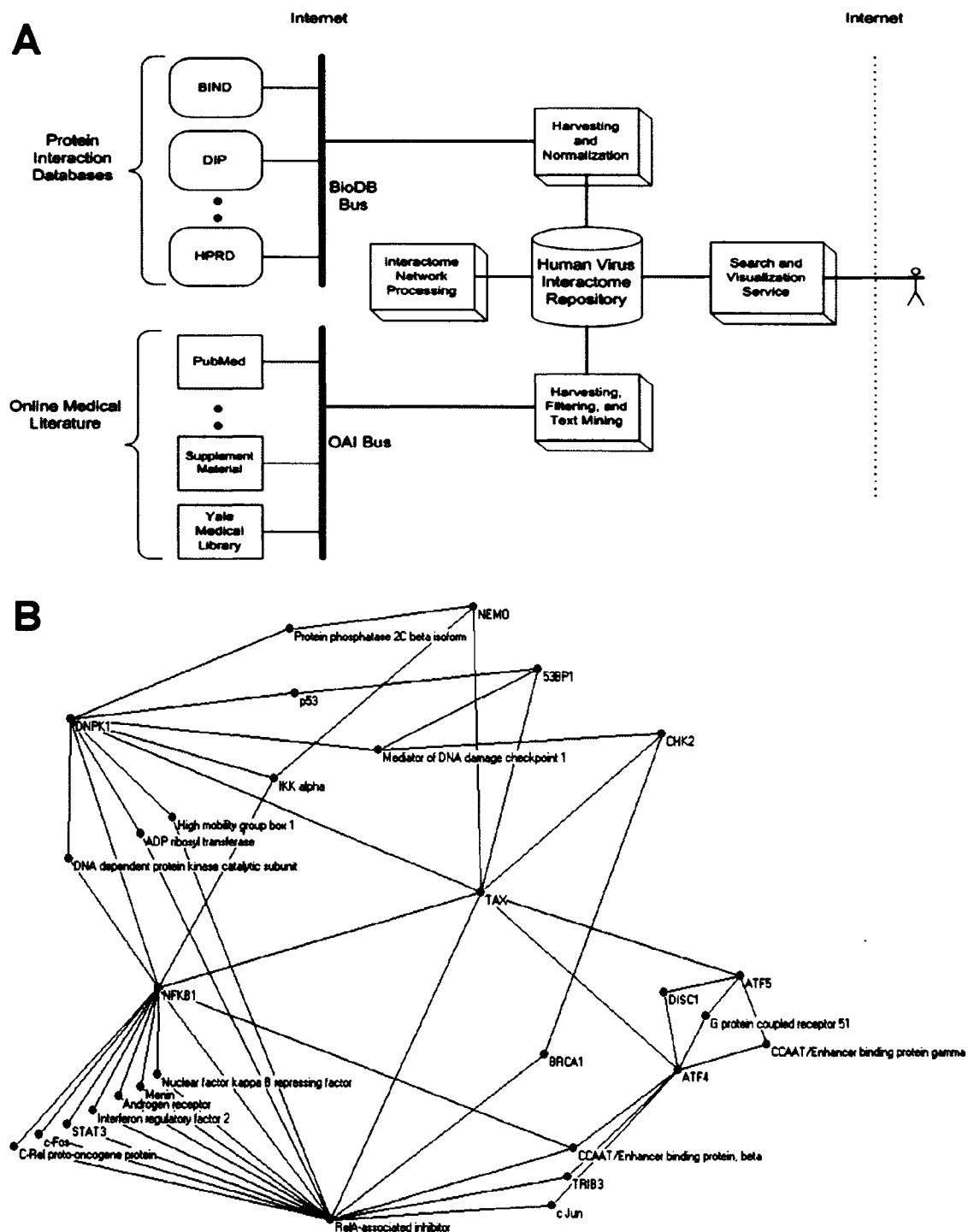
FIG. 6. **Bioinformatics analysis of Tax interactome.** *A*, a schematic diagram of Human Virus Interactome Repository (HVIR) development. *B*, a schematic display of a subset of interactions in the Tax-DNA-PK network, as identified by HVIR. Tax and DNA-PK are indicated, along with additional interacting proteins.

with S-protein beads. This process allowed us to efficiently purify Tax complexes from mammalian cells with limited non-specific binding to the beads. Protein-protein interactions account for many of the pleiotropic functions of Tax, and identification of novel cellular binding partners contributes to our understanding of how this oncoprotein induces genomic instability and transformation.

Using affinity purification, we identified the DNA damage response protein, DNA-PKcs, as a novel Tax-interacting protein. Previous studies in our laboratory and others have identified other components of the DNA damage response pathway that interact with Tax. Tax physically interacts with Chk2, and co-localizes with both Chk2 and 53BP1 in nuclear Tax Speckled Structures (TSS) (112,143). The Tax-Chk2 interaction promotes delayed progression through the G2/M checkpoint (112). Tax further impacts the DNA repair pathway through transcriptional activation and repression of key repair proteins, including β-polymerase and proliferating cell nuclear antigen (PCNA) (125,127,144). Base excision repair (BER) activity is reduced in HTLV-1 transformed cells and Tax suppresses nucleotide excision repair (NER) (114,126,127). Dysregulation of DNA repair by Tax can contribute to genomic instability (145). Thus, the interaction of Tax with DNA repair factor, DNA-PKcs, may influence the maintenance of genomic integrity.

DNA-PK is the key enzyme in the non-homologous end joining (NHEJ) pathway of DNA double strand break (DSB) repair (146-149). It is a nuclear serine/threonine kinase consisting of an approximately 470 kDa catalytic subunit (DNA-PKcs) and a regulatory subunit composed of the Ku70 and Ku86 heterodimer. Based on structural homology, DNA-PKcs belongs to a family of protein kinases known as

phosphatidylinositol 3-kinase-like protein kinases (PI3KK), which includes DNA damage response proteins, ATM and ATR. The kinase activity of DNA-PKcs is stimulated by physical association with double-strand DNA. Along with playing a key role in DNA repair via NHEJ, DNA-PK is also involved in other important responses to DSBs, including cell cycle arrest and apoptosis (148). A further role for DNA-PK has been shown in maintaining telomeres to prevent them from being recognized as DSBs. In fact, in the absence of DNA-PK, cells exhibit telomeric fusions and increased chromosomal instability (150). DNA-PK is thus critically involved in many important cellular responses to DNA damage and maintenance of genomic integrity. The interaction of Tax with DNA-PK may have deleterious effects on the cell, and is the subject of further investigation in our laboratory.

Our bioinformatics analysis of reported studies identifying Tax interactions combined with information from protein interaction databases led to development of the Human Virus Interactome Resource (HVIR). Current work is focused on increasing the search for Tax-interacting proteins via text-mining, and developing search and visualization methods for accessing and analyzing the data. Using the current model of the Tax interactome as presented in Fig. 6, we demonstrated that the interaction between Tax and DNA-PKcs could have been predicted using HVIR. A careful analysis of documented Tax interactions along with 'second neighbor' interactors using this resource could reveal many more members of the Tax complex. While there are many available databases documenting cellular protein interactions, HVIR provides the first digital library containing interactions between proteins from viruses and humans. A manual search of PubMed reveals over 1200 publications on the topic of HTLV-1 Tax, with more

added daily. Efficient evaluation of this literature to determine the complete network of Tax interactions requires automated processes. We chose to use a text-mining approach to collect these data, and then present it in a way that can be analyzed to address the functional significance of the Tax interactome. Combining this Tax network with information from available databases about cellular protein interactions gives a more complete picture of the impact of Tax on the cellular proteome. These data are invaluable for understanding the multiple pleiotropic functions of Tax. HVIR can provide researchers with a valuable tool to guide experimentation in the search for novel Tax interactions which contribute to its function.

SECTION 4

REGULATION OF TAX BY PHOSPHORYLATION

Introduction

Human T-cell Leukemia Virus Type 1 (HTLV-1) is a human transforming retrovirus. Infection with HTLV-1 can give rise to Adult T-cell Leukemia (ATL), HTLV-1 Associated Myelopathy/Tropical Spastic Paraperesis (HAM/TSP) as well as other subneoplastic conditions (25,131,151-153). Although cellular transformation can be achieved by expression of a single viral transactivating protein, Tax, the exact mechanism of transformation is not known (115). Tax is thought to induce genomic instability and thus contribute to cellular transformation through interaction with cellular proteins involved in cell cycle control and the DNA damage repair response (112,114,128,130,145). In addition, Tax can activate or repress a variety of cellular genes predominately through the CREB and NF-κB pathways (115,154). Thus, uncovering the regulatory mechanism for controlling the various Tax activities is critical to understanding HTLV-1-mediated cellular transformation.

There have been several structure-function studies of the Tax protein predominately utilizing molecular biology techniques. Specifically, with respect to the regulation of multiple Tax activities it has been noted that mutation or deletion of individual domains results in a selective loss of function (155). Important domains for Tax function include a nuclear localization signal (60,155), nuclear export signal (52,61), activation specific region (62), two leucine zipper-like domains (63,64), and a zinc-finger domain (59). Mutation of a number of individual serine residues in Tax have been shown

to alter its ability to *trans*-activate either CREB or NF-κB responsive promoters (155). In addition to phosphoryl-specific post-translational modifications, recent studies have uncovered an important regulatory role for ubiquitin/sumoyl-modifications (54,57). Clearly, Tax structural domains contribute to its regulation.

Phosphorylation is a common reversible regulatory event with a central role in controlling *trans*-acting/transcription (156). Earlier studies have demonstrated that Tax is a phosphoprotein (157) and that phosphorylation can regulate Tax activation of the HTLV-1-LTR (158,159). We conducted the first attempt toward identification of Tax phosphorylation sites using a scanning serine to alanine substitution mutational analysis. This study identified that substitution of serine residue at position 10 or 274 resulted in a Tax mutant which lost the ability to transactivate both CREB and NF-κB responsive promoters (155). A separate study showed that serine to alanine substitution at Tax amino acid 77 significantly reduced transactivation of a CREB-dependent promoter (160). However, 2-D mapping of tryptic fragments suggested that this site is not phosphorylated *in vivo*. Using tryptic peptide analysis, Bex et al. (1999) identified Tax phosphorylations on two serine residues at positions 300 and 301, and showed that they are critical for transcriptional activation by Tax. While the role of phosphorylation in the regulation of Tax is important, a complete map of the sites of phosphorylation within Tax has not been reported.

New methods for affinity purification and liquid chromatography tandem mass-spectrometry (LC-MS/MS) allow for direct interrogation of the presence of phosphoryl residues (161). In this study, we combined LC-MS/MS analysis of affinity purified Tax protein with a substitution mutational analysis to identify and functionally characterize

phosphorylation sites. The LC-MS/MS analysis achieved 77% coverage of the Tax sequence and identified four novel sites of phosphorylation on serine and threonine residues. Phosphorylation at specific amino acid residues provided both positive and negative regulatory signals. These results highlight the importance of phosphorylation in the regulation of Tax activity.

Experimental Procedures

Mammalian Expression Plasmid

The S-tagged expression vector *STaxGFP* was constructed by inserting the *tax-EGFP* fusion ORF into the *Sma*I site of *pTriEx4-Neo* (Novagen, Madison, WI) in frame with the amino-terminal S-tag and His-tag.

Cell Culture and Transfection

293T cells were maintained at 37°C in a humidified atmosphere of 5% CO_2 in air, in Iscove's modified Dulbecco's medium supplemented with 10% fetal bovine serum and 1% penicillin-streptomycin (Invitrogen, Carlsbad, CA). Jurkat cells were maintained in RPMI-1640 medium supplemented with 10% fetal bovine serum and 1% penicillin-streptomycin (Invitrogen, Carlsbad, CA).

Transfections of 293T cells were performed by standard calcium phosphate precipitation. Cells were plated in 150-mm plates at 4×10^6 cells per plate. The following day, 20 μg of plasmid DNA in 2M $CaCl_2$ and 2X HEPES-buffered saline were added dropwise to cells in fresh medium. Cells were incubated at 37°C for 5 h and fresh medium was added. The cells were harvested 48 h later, following a single wash with 1X

PBS, in 500 μl M-Per mammalian protein extraction reagent (Pierce, Rockford, IL) with protease inhibitor cocktail (Roche, Palo Alto, CA) and immediately frozen at –80°C.

Transfections of Jurkat cells were performed by electroporation with Bio-Rad Gene Pulser II with Capacitance Extender (Bio-Rad, Hercules, CA). $1x10^7$ cells were electroporated with 30 μg HTLV 1 LTR Luc reporter vector and 30 μg Tax plasmid in 250 μl RPMI with 10% fetal bovine serum in 0.2 cm electrode gap cuvette at 280 V and 960 μF. Following electroporation, cells were resuspended in 5 mL complete media. The cells were harvested 48 h later for luciferase assays in Reporter Lysis Buffer as described below.

Purification of Tax Protein

Prepared cell lysate (1.5 ml) was incubated with 75 μl bed volume of S-protein agarose (Novagen, Madison, WI) for 30 min at room temperature, then washed 3 times with 1 mL Bind/Wash Buffer (20 mM Tris-HCl pH 7.5, 150 mM NaCl, 0.1% TritonX-100). Washed beads were eluted by resuspension in 150 μl Laemmli Sample Buffer (Bio-Rad, Hercules, CA) with β-mercaptoethanol, followed by boiling for 5 min. Eluates were electrophoresed in a 10% SDS-polyacrylamide gel and visualized by Coomassie Blue staining. Bands of interest were manually excised from the gel for further analysis.

Immunoblot Analysis

Cell extracts were derived as described above. Total protein concentrations were determined by Protein Assay (Bio-Rad, Hercules, CA). A normalized volume of Laemmli sample buffer (Bio-Rad, Hercules, CA) with β-mercaptoethanol was added to

the lysate, boiled for 5 min, and a normalized amount of total protein was loaded in each lane and electrophoresed through a 10% SDS-polyacrylamide gel. The proteins were transferred onto an Immobilon-P (Millipore, Billerica, MA) membrane by semi-dry electroblotting and probed with anti-GFP monoclonal antibody (Santa Cruz Biotechnology, Santa Cruz, CA) and secondary horseradish-peroxidase conjugated anti-mouse antibody (Bio-Rad, Hercules, CA). Immunoreactivity was detected via Immunstar enhanced chemiluminescence protein detection (Bio-Rad, Hercules, CA).

LC-MS/MS Analysis

Protein bands were excised from SDS-polyacrylamide gels. Gel slices were cut into 1-2 mm cubes; washed 3X with 500 μL Ultra-pure water and incubated in 100% acetonitrile for 45 minutes. The material was dried in a speed-vac, rehydrated in a 12.5 ng/μL modified sequencing grade trypsin solution (Promega, Madison, WI) and incubated in an ice bath for 40-45 min. The excess trypsin solution was then removed and replaced with 40-50 μL of 50mM ammonium bicarbonate, 10% acetonitrile, pH 8.0 and the mixture was incubated overnight at 37°C. Elastase digestion was performed as described for trypsin at an enzyme concentration of 15 ng/μL without acetonitrile in the reaction buffer. Peptides were extracted 2X with 25 μl 50% acetonitrile, 5% formic acid and dried in a speed-vac. Digests were resuspended in 20 μL Buffer A (5% acetonitrile, 0.1% Formic Acid, 0.005% heptafluorobutyric acid) and 3-6 μL were loaded onto a 12-cm x 0.075 mm fused silica capillary column packed with 5μM diameter C-18 beads (The Nest Group, Southboro, MA) using a N2 pressure vessel at 1100 psi. Peptides were eluted over 55 minutes, by applying a 0-80% linear gradient of Buffer B (95%

acetonitrile, 0.1% formic acid, 0.005% heptafluorobutyric acid) at a flow rate of 130 μL/min with a pre-column flow splitter resulting in a final flow rate of ~200 nl/min directly into the source. In some cases the gradient was extended to 150 minutes to acquire more MS/MS spectra. A LCQ™ Deca XP (ThermoFinnigan, San Jose, CA) was run in an automated collection mode with an instrument method composed of a single segment and 4 data-dependent scan events with a full MS scan followed by 3 MS/MS scans of the highest intensity ions. Normalized collision energy was set at 30, activation Q was 0.250 with minimum full scan signal intensity at 5×10^5 and a minimum MS2 intensity at 1×10^4. Dynamic exclusion was turned on utilizing a three minute repeat count of 2 with the mass width set at 1.50 Da. Sequence analysis was performed with TurboSEQUEST™ (ThermoFinnigan, San Jose, CA) or MASCOT (Matrix Sciences, London, GB) using an indexed human subset database of the non-redundant protein database from National Center for Biotechnology Information (NCBI) web site (http://www.ncbi.nlm.nih.gov/). An additional database was created containing only the ORF sequence for the expressed Tax protein.

MALDI-TOF Analysis

Tryptic digests of purified Tax protein were resuspended in 20 μL 70% acetonitrile, 0.1% formic acid and 2 μL applied to a MP384 steel MALDI target (Brucker Daltonics, Bilaricka, MA). Spectra were acquired in reflectron mode using 96.3 μjoules laser power at 20 Hz with a total shot count of approximately 500.

Site-Directed Mutagenesis

Site-directed mutagenesis was performed using QuikChange II (Stratagene, La Jolla, CA) site-directed mutagenesis kit to introduce single amino acid changes by altering one or two nucleotides at the mutation site in the *STaxGFP* template. Both forward and reverse primers were designed to contain the desired mutation according to the manufacturer's protocol. Methylated original *STaxGFP* plasmid derived from bacteria was used as the template, and mutagenic primers were extended with *PfuUltra* high-fidelity DNA polymerase during a 16-cycle PCR, incorporating the desired mutation into newly synthesized strands. The remaining methylated template was digested with the DpnI provided, and the PCR product was used to transform XL-1 Blue competent bacteria. Bacterial colonies growing under ampicillin selection were selected for further processing and correct plasmids were purified using the Qiagen Maxiprep system (Qiagen, Valencia, CA). Introduction of each mutation was confirmed by DNA sequence analysis (Davis Sequencing, Davis, CA), and expression was confirmed by transfection and western analysis using anti-GFP monoclonal antibody (Santa Cruz Biotechnology, Santa Cruz, CA).

Luciferase Assays

293T cells, plated at 2×10^5 cells per well of a 6-well plate, were transfected as described with 2 to 8 µg of Tax expression plasmid, and 1 µg of *HTLV-LTR-Luc* or *pNF-κB-Luc* (Clontech, Mountain View, CA) reporter plasmid. The parental vector used for Tax expression, *pTriEx4-Neo* (Novagen, Madison, WI), was added to normalize for the total amount of transfected DNA. Luciferase activity was measured 48 h after

transfection. Cells were washed twice with 1X PBS and then lysed in 1X Reporter Lysis Buffer (Promega, Madison, WI) and subjected to one freeze-thaw at -80°C. Luciferase assay substrate was used according to the manufacturer's protocol, and activity was measured in a TD-20/20 luminometer (Turner Designs, Sunnyvale, CA). Luciferase activity was normalized for total cell protein determined from the whole cell extracts by Protein Assay (Bio-Rad, Hercules, CA), according to manufacturer's direction.

Results

Functional Domains of HTLV-1 Tax

As a reference point for structure-function determination, we present a composite representation of known functional domains of HTLV-1 Tax protein in Fig. 7. The specific sites/motifs were assembled from a manual search of the peer-reviewed literature. The potential phosphorylation sites at S10 and S274 were mapped based on substitution mutation analysis from our earlier studies (155). The S77 site was defined via 2-D mapping of tryptic fragments (160). Serine residues 300 and 301 have been previously identified as sites of phosphorylation by combined tryptic peptide and substitution mutational analysis (55). None of the previous studies utilized mass spectrometry and the physical mapping of the S300/301 tryptic peptide did not formally rule out phosphorylation at four possible alternative sites that are predicted to reside in the same tryptic fragment.
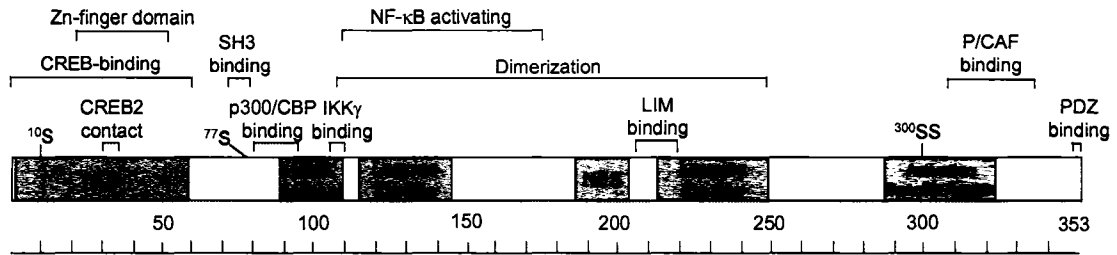
FIG. 7. **Functional domains and potential sites of phosphorylation in Tax.** Tax contains a nuclear localization signal (NLS) (155) and a nuclear export signal (NES) (61). Domains for binding CREB, SH3, p300/CBP, IKKγ, LIM, P/CAF, and PDZ are indicated (64,68,71,162). Tax contains multiple leucine zipper-like regions and an activation specific domain (62-64). Other regions are necessary for CREB2 contact and DNA contact (90,163). Also shown are the Zn-finger domain, and domains required for dimerization and NF-κB activation (59,66,164). Potential sites of phosphorylation at serine residues 10, 77, and 274 are indicated (155,160). Serine residues 300 and 301 have been previously identified as sites of phosphorylation (55).

Expression of Biologically Active Affinity-tagged Tax Protein

In order to facilitate the analysis of phosphopeptides in the Tax protein occurring *in vivo*, we created a tandem affinity tagged Tax construct that could be expressed in and purified from mammalian cells. The *STaxGFP* vector expresses full-length Tax protein fused to amino-terminal 6XHis- and S-tags, and carboxy-terminal green fluorescent protein (GFP) (Fig. 8A). We included the GFP subunit to facilitate protein expression and purification monitoring. The *STaxGFP* vector was transiently transfected into 293T cells, and the transfection efficiency and appropriate subcellular localization to Tax Speckled Structures (TSS) was confirmed by visualizing the GFP expression (Fig. 8C). In order to determine whether the tandem affinity tagged Tax-GFP retains functional activity, we compared it to untagged Tax expressed from the *IEX* vector in *trans-*activation assays. 293T cells were cotransfected with the HTLV-I LTR Luc reporter plasmid and either Tax-expressing vector *IEX* or *STaxGFP*. STaxGFP showed comparable transcriptional activity to untagged Tax expressed from the *IEX* vector (Fig. 4C). The activity of STaxGFP as measured by the ability to activate via NF-κB-responsive promoter and to induce cell cycle accumulation in 4N was also comparable to wild type Tax (data not shown). Thus efficient expression of functionally active tagged Tax was achieved in mammalian cells.

Affinity Purification of Tax from Mammalian Cells

We successfully purified S-Tagged Tax protein from transfected 293T cells using S-protein agarose beads as described in the methods section. The purification is based on

A

S-Tag
KETAAAKFERQHMDSPPPSGLVPRGSM

| 6His | S-Tag | Tax | GFP | STaxGFP
| 6His | S-Tag | GFP | | SGFP

B

kDa
200 —
116 —
97 —
66 — ◄—STaxGFP
45 —
31 —

C
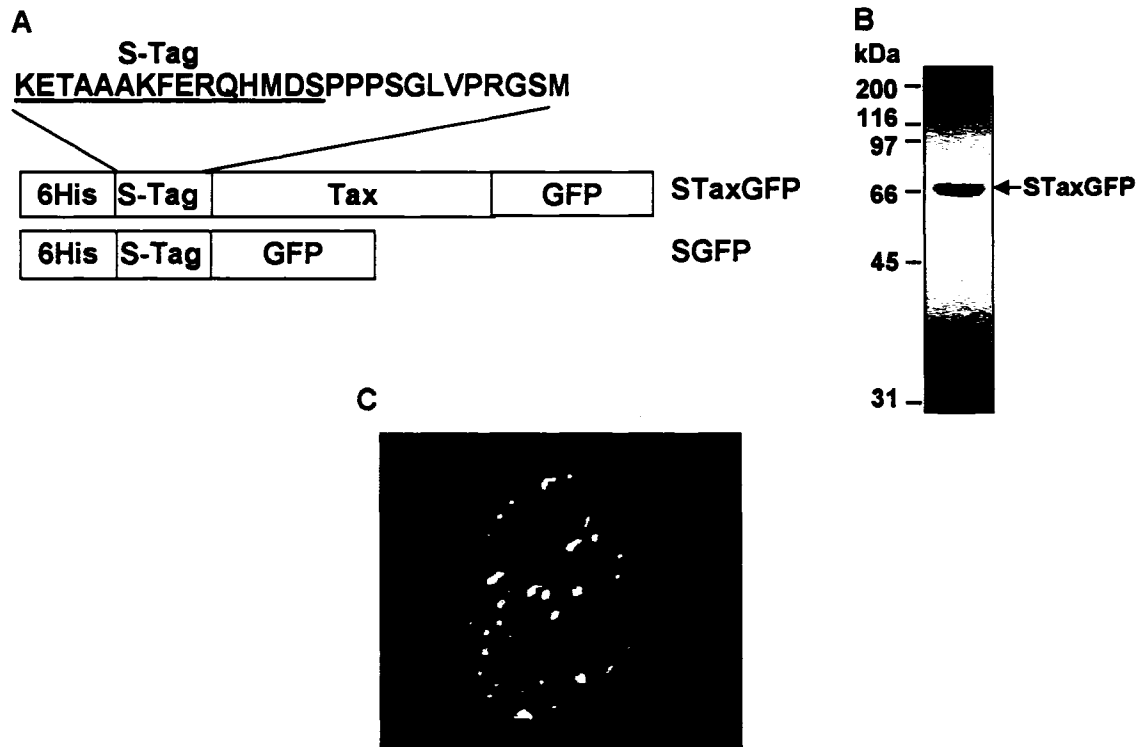
FIG. 8. **Efficient expression of biologically active affinity tagged Tax protein.** *A*, a depiction of the *STaxGFP* expression vector construct. *B*, affinity purification of S-tagged Tax from mammalian cells. 293T cells were transfected with *STaxGFP*, purified on S-protein agarose beads, eluted and resolved by SDS-PAGE, and detected by Coomassie staining. *C*, 293T cells were transiently transfected with *STaxGFP* (speckles), fixed with 4% paraformaldehyde, permeabilized with methanol and stained nuclei with TOPRO-3-iodide (Molecular Probes, Eugene, OR). Fluorescent images were acquired with a Zeiss LSM 510 confocal microscope at 40X magnification using Argon (488 nm) and HeNe2 (633 nm) lasers and imaged with LSM Image Browser software (Carl Zeiss, Jena, Germany).

the strong interaction between the 15 amino acid S-Tag and S-protein immobilized on agarose beads, both of which are derived from RNase S (165). The eluted protein from the affinity purification was further resolved by SDS-PAGE and a distinct STaxGFP band was detected by Coomassie blue staining (Fig. 8*B*). This process produced sufficient quantities of highly purified Tax protein from mammalian cells and allowed for the subsequent post-translational modification analysis by LC-MS/MS.

Phosphopeptide Mapping of Tax using LC-MS/MS

We employed several strategies in determining the phosphorylation sites in Tax. First, the purified STaxGFP protein was subjected to enzymatic digestion by trypsin resulting in approximately 15 peptides within the reproducible dynamic mass range of the ion trap accounting for nearly 50% of the sequence. Tryptic peptides that were too large to detect were either further digested with elastase or independently digested with elastase, resulting in an additional 27% sequence coverage. The combined analysis of all of the peptide fragments generated by digestion with either trypsin or elastase enabled us to obtain a detailed physical map covering 77% of the Tax sequence (Fig. 9*A*). We found only suggestive evidence that the previously reported S300/301 was phosphorylated (55). Specifically, of the 23 experimental runs conducted only a single instance of a base peak neutral loss from a non-tryptic peptide was found indicating a phosphate residing on either S300 or S301, but not both (Fig. 10). There was no evidence for phosphorylation at S10, S77 or S274.

We next employed a directed chemical derivatization of serine or threonine residues in order to rule out poor ionization efficiency or lability of the phosphates at

A

MAHFPGFGQSLLFGYPVYVFGDCVQGDWCPISGGLCSARLHFHALIATCPEHQITWDPIDGRVIGSALQFLIP

RLPSFPIQBTSKTLKNLTPFTHTTPNIPPSFLQAMRKYSPFNGYMEPILGQHLPTLSFPDPGLRPQNLYTLW

GGSVVCMYLYQLSPPTTWPLLPHVFCHPGQLGAFLTNVPYKRIEEILYKISLTTGALIILPEDCLPTILFQPAR

APVTLTAWQAGLLPFHSTLTTPGLIWTFTDGTPMISGACPKDGQPSLVLQSSRFFHKFQTKAYHPSFLLSHGLI

QYSSFHSLHLLFEEYINIPSLLFNEEEADDNDHEPQSPGGLEPPSEKHFRETEV

	# Residues mapped/Total	% Residues mapped
Serines (S)	22/26	85 %
Threonines (T)	28/29	97 %
Total amino acids	273/353	77 %

Trypsin Digest

Elastase Digest

B

48T   184T   215T   300SS 336S

Tax

FIG. 9. **Tax phosphopeptide map.** *A*, a compilation of the results obtained with LC-MS/MS analysis of Tax. The identified phosphorylation sites are indicated (bold). The Tax amino acid sequence assessed by enzymatic digestion with trypsin (solid line) and/or elastase (dotted line) is marked. The total analyzed sequence is highlighted. The inserted table shows % total amino acid, serine amino acids and threonine amino acids coverage of LC-MS/MS analysis. *B*, the novel phosphorylation sites and the 300/301 site are shown with the appropriate Tax sequence.
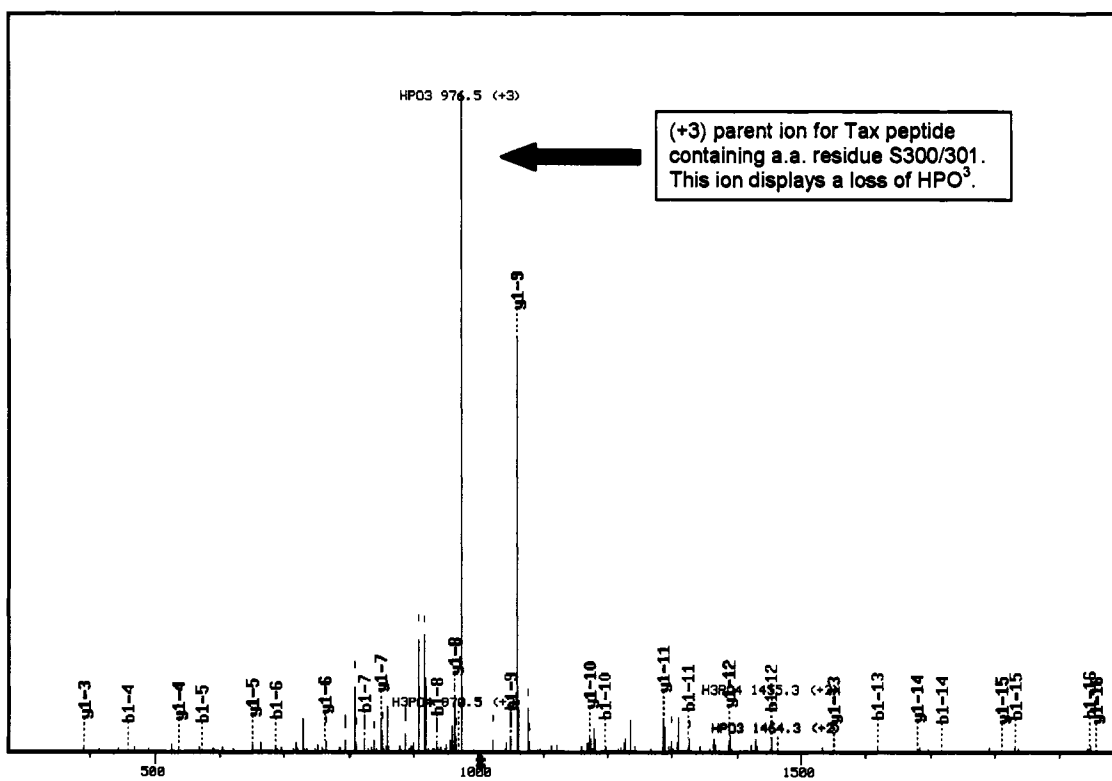
FIG. 10. **Neutral loss ion map of non-tryptic peptide containing S300/301.** MS/MS spectrum of a phosphorylated base peak ion indicating a loss of HPO_3 from the +3 parent ion. The inset shows the resulting matched ion series for the selected peptide. The database search was conducted without an enzyme restriction against the Tax-GFP sequence.

S300/301 (166). This approach utilizes a β-elimination/ethanediol addition which results in phosphoserine and phosphothreonine conversion to the more stable S-ethylcystein or β-methyl-S-ethylcystein respectively. These derivatives are then detected by an increase of 44 amu from the unmodified serine or threonine residues. This method failed to increase the incidence rate of the S300/301 phosphorylation event suggesting that the low incidence is not an artifact of ionization but rather indicative of native abundance. Results from the combined analysis detected three phosphothreonine residues at positions 48, 184 and 215, and two phosphoserine residues at positions 300/301 and 336 (Fig. 9B).

Mutational Analysis of the Identified Tax Phosphorylation Sites

Tax *trans*-activates viral and cellular gene expression through either the ATF/CREB or NF-κB activation pathways (60,155,167). Thus, we evaluated each substitution mutation for *trans*-activation activity via both CREB-dependent and NF-κB-dependent promoters. Tax mutants were transiently co-transfected into 293T cells with either HTLV-1 LTR Luc or NF-κB Luc reporter plasmid to assay for the ability of Tax to activate either the ATF/CREB or NF-κB pathways, respectively. To determine the possible regulatory role of phosphorylation at the specific sites determined by mass spectrometry, single amino acid substitutions were introduced at T48>A, T48>D, T184>A, T184>D, T215>A, T215>D, S300/301>A, S300/301>D, S336>A and S336>D. The stability of the expressed protein containing the specific substitution mutations was determined by Western blot analysis (Fig. 11A). These data were also used to normalize the extracts for the biological assays.
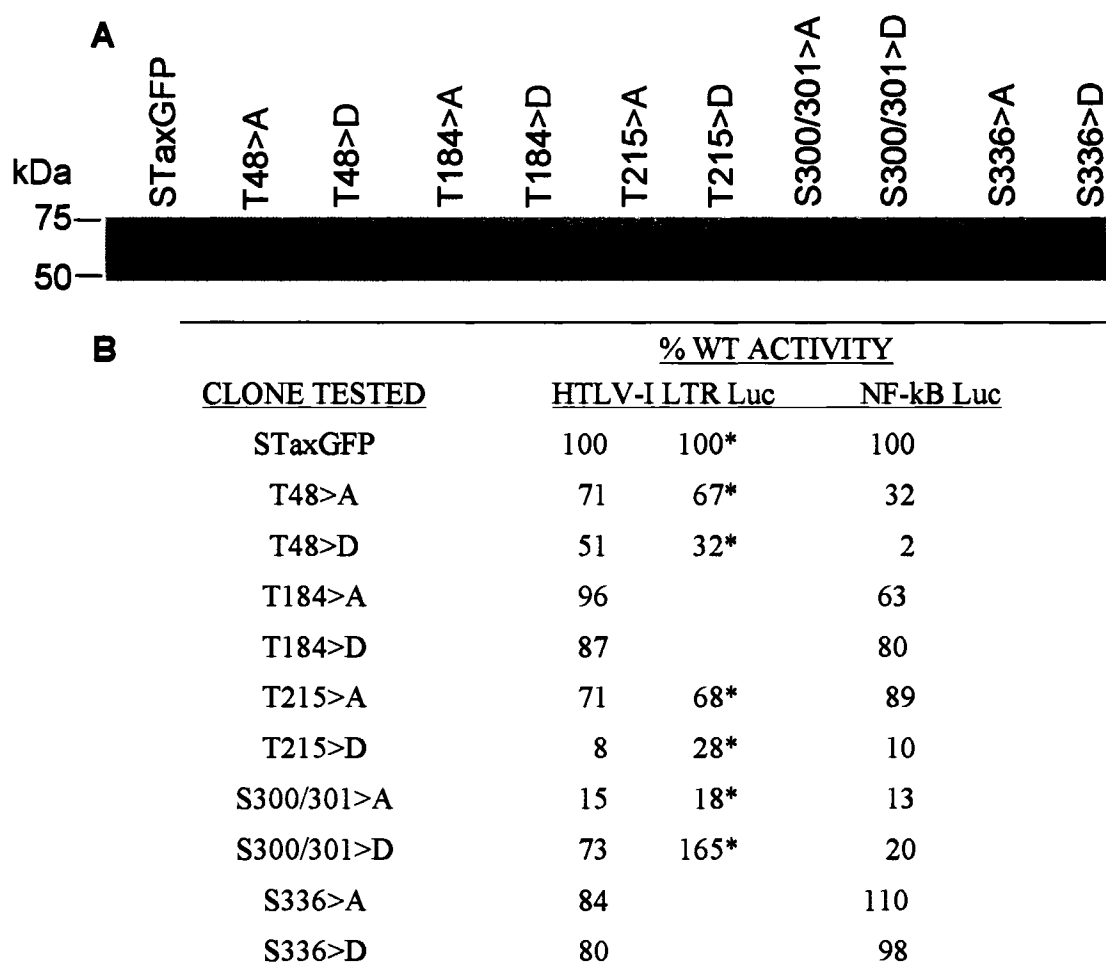
A — kDa, 75—, 50—; lanes: STaxGFP, T48>A, T48>D, T184>A, T184>D, T215>A, T215>D, S300/301>A, S300/301>D, S336>A, S336>D

B

CLONE TESTED	% WT ACTIVITY		NF-kB Luc
	HTLV-I LTR Luc		
STaxGFP	100	100*	100
T48>A	71	67*	32
T48>D	51	32*	2
T184>A	96		63
T184>D	87		80
T215>A	71	68*	89
T215>D	8	28*	10
S300/301>A	15	18*	13
S300/301>D	73	165*	20
S336>A	84		110
S336>D	80		98

FIG. 11. **Mutational analysis of Tax phospho-specific mutants.** *A*, immunblot analysis of the expression of Tax mutants in cells compared to wild type Tax-expressing cells. 10 µg of wild type *STaxGFP* DNA (STaxGFP) or 20 µg of mutant *STaxGFP* DNA (indicated) was transfected into 293T cells. Equal amounts of whole cell lysate were loaded on the gel, and blotted with anti-GFP antibody. *B*, *trans*-activation assay. 293T cells were co-transfected with either the HTLV-I LTR Luc or the NF-κB Luc reporter plasmid (indicated), and vectors expressing either wild-type STaxGFP (STaxGFP) or a Tax mutant (indicated). The specific amino acid substitution for each Tax mutant is shown. Luciferase activity is shown as a percentage of the activity relative to wild-type Tax. In some experiments (indicated by an asterisk) Jurkat cells were used to analyze activation of HTLV-I LTR Luc plasmid. The values presented are the median of replicate measurements with an average CV of 0.083 (CV range from 0.012 to 0.2)

The results of the *trans*-activation assays are shown in Fig. 11*B*. Substitution mutations at T184 and S336 showed only a slight reduction in activity although each of these sites is clearly phosphorylated. Substitutions at T48 had a more pronounced effect upon NF-κB activity than was measurable via CREB activation. Interestingly, the T48>A mutation retained both CREB and NF-κB activation when compared to the phosphomimetic substitution T48>D. This result implies that phosphorylation at this site provides a negative regulatory signal. Likewise, Tax T215>A retained full activity in both assays where as the phosphomimetic substitution T215>D was inactive for each assay suggesting that phosphorylation at this site results in significant decrease of both Tax activities. Examination of the S300/301 substitution mutations confirmed a previous report that S300/301>A retains only partial activity for either NF-κB or CREB activation and the phosphomimetic substitution S300/301>D specifically recovers the CREB activity but not the NF-κB activity (55). To determine whether the functional activity of these mutants is retained in a cell type targeted by HTLV-1, we tested mutants in luciferase assays measuring transactivation of HTLV-1 LTR in Jurkat cells (Figure 11*B*). We found that those mutants with significant differences in functional activity from wild type showed the same pattern of activity in both 293T cells and Jurkat cells.

Semi-quantitation of Phosphorylated Tax Protein

Although not directly quantitative it is possible to evaluate the stoichiometric relationship between phosphorylated and unphosphorylated protein by determining the frequency that a phosphoryl-peptide is detected. We re-examined all spectra of sufficient quality to identify Tax phosphopeptides and counted the relative incidence of

phosphorylated ions versus all ions arising from the same sequence. The results of this analysis are shown in Table II. The establishment of an absolute percentage of the peptide form is not reliable through this method; however a general conclusion can be drawn that the majority of Tax is phosphorylated at T48 and S336. In addition a minor but significant portion of the protein is phosphorylated at T184 and T215.

The much broader dynamic mass range of MALDI-TOF allowed analysis of tryptic peptides too large for the ion trap, such as the 40 amino acid tryptic peptide containing S300/301. In addition, since ion acquisition is temporally static and devoid of data-dependent activation, MALDI-TOF analysis facilitates ion counting for semi-quantitation of modified peptides. We were able to easily observe several of the large predicted tryptic masses corresponding to unmodified/modified peptides as well as the most abundant Tax-specific ionic masses seen with the ion trap instrument. MASCOT searches of these peak lists yielded identification of Tax as well as the GFP fusion protein, confirming that the predominant analyte was our fusion protein. We conducted 5 identical experiments and compared the relative average area under each of the peaks to obtain an estimate of <5% of all peptides were phosphorylated. An example of the spectral trace from one experiment is shown in Fig. 12. All of the resolvable features were consistent with a single phosphorylation event. Thus, our data suggests that phosphorylation of Tax at S300/301 occurs at a single site and is a rare event.

Discussion

The oncoprotein, Tax, encoded by the Human T-cell Leukemia Virus Type 1 (HTLV-1), is implicated in viral pathogenicity through its multiple pleiotropic functions.

TABLE II

Relative incidence of phosphorylated ions

Amino acid	Sequence	Ion Ratio[1]	%P[2]
T48	HALLATYPEHQITWDPIDGR	23/23	100%
T184	FLTNVPYKRIEEL	4/11	36%
S336	EADDNDHEPQISPGGLEPPSEK	17/21	81%
T215	ISLTTGALIILPEDCLPTTLFQPAR	4/13	31%

High quality spectra from 23 experimental runs were examined for the presence of indicated ions.

[1]Ion ratio is the number of times the phosphoryl-ion was detected over the total number of times any ion was detected.

[2]Percent of phosphorylated ions was determined by solving the ion ratio formula.
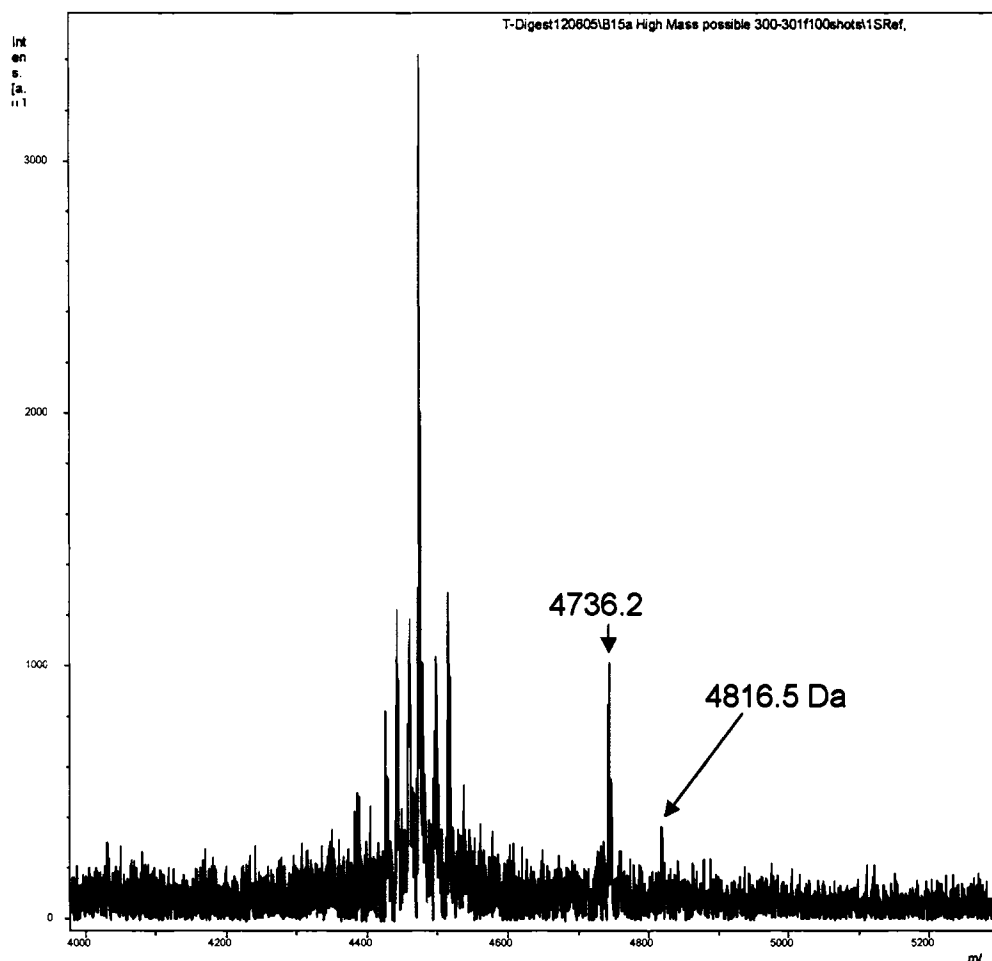
FIG. 12. **Partial MALDI-TOF spectrum of a Tax tryptic digest.** Peptide masses equivalent to the phosphorylated and non-phosphorylated tryptic peptide containing S300/301 are shown. Area under the curve was calculated from the total isotopic distribution of each peptide. This spectrum represents the highest percentage of phosphorylated S300/301 peptide observed in five separate experiments.

While this *trans*-acting factor is essential for effective viral replication through its ability to activate viral transcription, Tax can also activate and repress transcription of a variety of cellular genes. This process occurs through targeting of both the CREB and NF-κB pathways. In addition, there have been many models proposed in which Tax interacts with cellular proteins, to promote cellular transformation via dysregulation of the cell cycle, inhibition of tumor suppressor proteins, and modulation of the DNA damage repair response (100,145). The specific regulation of all or a subset of these activities represents the functional impact of Tax on cell proliferation, increased mutation rate, and ultimately cellular transformation and leukemogenesis. Clearly then, a complete understanding of Tax-mediated oncogenesis is dependent upon a better understanding of how the activities of the protein are regulated.

As a central molecular regulatory mechanism, phosphorylation has been shown to modulate transcription factor function by multiple mechanisms including regulation of DNA binding, cellular localization, protein-protein interactions and protein stability (168). Examples can be found in the scientific literature of both positive and negative regulation of transcription factors by phosphorylation. Regulation of transcription factor DNA binding activity may be negatively regulated due to the introduction of a negative charge within or nearby a DNA binding domain, generating electrostatic repulsion with the phosphates on the DNA and thus inhibiting DNA binding (168,169). In other cases, the phosphorylation sites are located distal to the DNA binding domain, and regulation of DNA binding is mediated via phosphorylation-induced alteration in protein conformation. An example of negative regulation of DNA binding by distal site phosphorylation has been described for the transcription factor c-myb, in which

phosphorylation at sites ~50 residues from the DNA-binding domain inhibit transcription factor docking (169). The DNA binding activity of the transcriptional repressor, Wilms' tumor gene product WT1, is similarly inhibited by phosphorylation within a distal zinc-finger region (168,170). Sometimes phosphorylation of transcription factors regulates transactivation function via post-binding mechanisms. For example, phosphorylation of yeast transcription factor ADR1 does not affect DNA binding activity, but instead negatively regulates the interaction with general transcriptional machinery and thus controls transactivation function (171).

Given the preponderance of regulatory mechanisms involving phosphorylation, there have been some efforts directed at determining the role of phosphorylation in the regulation of HTLV-1 Tax. The first investigation, resulting in the determination that the native protein was phosphorylated predominately on serine, utilized two-dimensional thin layer chromatography and tryptic peptide analysis (24). Subsequently, we conducted a mutational analysis of Tax protein that targeted all 47 serine residues (155). This study was followed by a combined mutational analysis and 2-D mapping of Tax tryptic fragments (160). Neither of these studies could conclusively identify functionally relevant phosphorylation sites within Tax. However, Bex et al identified a specific phosphorylation of serine residues 300/301 by reverse-phase high-performance liquid chromatography of Tax tryptic fragments (55). These investigators also employed substitution analysis directed at amino acids 300 and 301 to demonstrate that "active" Tax protein required phosphorylation at this site. However, there were several theoretical scenarios, such as phosphorylation at other sites within the same tryptic fragment and dual phosphorylation at 300/301, which were not formally ruled out. In our current

study, we report the phosphorylation of Tax at four novel sites; threonine residues 48, 184, and 215, and serine residue 336, as well as confirming the phosphorylation at either serine residue 300 or 301. One explanation for why the other phosphorylation sites were not identified in this earlier study may be that the HPLC fractionation procedure may have resulted in a loss of other phosphopeptides in the protein. The selective loss of phosphopeptides can result from the addition of a phosphate group thus reducing hydrophobicity which may cause it to fail to be retained on the reversed-phase material used in purification (172). An additional consideration is that this study analyzed Tax protein derived from BHK21 (hamster kidney) cells, which may produce alternative post-translational modification patterns when compared to human cells. Although not without it's own limitations, our approach provides a more robust method for the comprehensive mapping of phosphorylation sites (161,172-174). We were able to identify phosphorylated Tax peptides as well as assign the sites of phosphorylation to specific residues by peptide sequencing using tandem mass spectrometry. Contrary to previous reports, however, our studies show that Tax is predominantly phosphorylated on threonine residues.

In addition to the dominance of threonine phosphorylation, we identified phosphorylation sites that were found to be negative regulators of Tax activity. Specifically, while alanine substitution at threonine residues 48 or 215 resulted in Tax mutants that retained the ability to activate gene expression, substitution with the phosphomimetic aspartic acid residue resulted in a dramatic loss of activity. For threonine residue 48, this effect was more pronounced for activation of the NF-κB pathway than the CREB pathway. Although the Tax protein was abundantly

phosphorylated at threonine residue 184 and serine residue 336, the mutational analysis revealed no significant effect on the ability of Tax to activate gene expression. This result is consistent with the known existence of functionally silent phosphorylation events.

One logical model for our combined results is that phosphorylation at either S300 or S301 along with dephosphorylation at T48 and T215 confers an activation state for Tax. A second aspect of our analysis allowed for inference toward the relative stoichiometry of individual phosphorylation events by determining the relative abundance of specific ions across 23 separate experiments. This summarization clearly suggested that phosphorylation at S300 or S301 was a rare event and that phosphorylation at T48 and T215 was a common event. Thus, "active" Tax protein, which is phosphorylated at S300/301 and dephosphorylated at both T48 and T215, is less abundant than "inactive" Tax protein. The fact that the active/inactive ratio of a biologically potent oncoprotein is skewed toward the inactive state has significant impact upon modeling Tax function. Hypothetically then, function of Tax with respect to promoter activation requires phosphorylation at S300 or S301. Additionally, selective activation of CREB-dependent promoters is achieved by phosphorylation at T48 and dephosphorylation at T215. Thus, discrete regulation of the pleiotropic functionality displayed by the Tax oncoprotein may be reflected in variations of its phosphorylation pattern. This variation is likely dependent upon the host cell type as well as the specific cellular physiological environment. The combined role of Tax post-translational modifications, including phosphorylation, as we have discussed here, and

ubiquitination/sumoylation as has been discussed elsewhere (54,57,58,175), provide a wealth of signals controlling protein structure, stability and localization.

In silico analysis of the sequence surrounding the identified phosphorylation sites in Tax, using ELM (http://elm.eu.org) and MotifScan (http://scansite.mit.edu), revealed several consensus sites for kinase recognition. Serine 336 is located within a proline-dependent serine/threonine kinase consensus motif, and threonine 48 is located within a casein kinase 2 consensus motif. Our data suggests that phosphorylation at T48 results in loss of the ability to transactivate via the NF-κB pathway. Thus, casein kinase 2 activity may provide an important regulatory signal for Tax-mediated activation of the NF-κB pathway. This phosphorylation site lies within the zinc-finger domain of Tax, and may represent a negative regulatory mechanism similar to that described for WT1 (170). Future studies will be aimed at uncovering the kinetic relationship of Tax post-translational modifications and Tax function.

SECTION 5

TAX INTERACTION WITH DNA-PK

Introduction

The human transforming retrovirus, Human T-cell Leukemia Virus Type 1 (HTLV-1) is the causative agent of Adult T-cell Leukemia (ATL), HTLV-1 Associated Myelopathy/Tropical Spastic Paraparesis (HAM/TSP) as well as other subneoplastic conditions (25,36,38,131,132). Cellular transformation can be caused by expression of a single viral transactivating protein, Tax (115). Although the specific mechanism is not fully known, it is evident that Tax affects diverse cellular processes through direct interaction with various cellular proteins involved in cell cycle control and DNA damage repair response (112,114,115,128,130,145). This activity is thought to induce genomic instability, thus contributing to cellular transformation. Identification and functional analysis of Tax-interacting proteins is therefore critical to understanding the mechanism by which Tax induces genomic instability.

Studies showing increased mutation frequency in both Tax-expressing mammalian cells and yeast provide evidence of genomic instability induced by Tax (83,84). These mutations are of a random nature, suggesting impairment of the ability of the cell to repair accumulated DNA damage introduced during its normal life cycle (83). Furthermore, an increase in DNA breaks is observed in Tax-expressing cells as micronuclei (MN), which seem to occur not due to a Tax-induced increase in DNA strand breaks, but due to Tax-induced loss of cellular DNA repair function (128,145). The cell has a variety of mechanisms to repair damaged DNA including base excision repair

(BER), mismatch repair (MMR), and non-homologous end-joining (NHEJ). Tax represses transcription of β–polymerase, an enzyme involved specifically in BER, and BER is suppressed in HTLV-1-transformed cells (125,126). Tax also suppresses NER, which correlates with its ability to *trans*-activate proliferating cell nuclear antigen (PCNA) (114,127). Transcriptional repression of human telomerase (hTert) by Tax may inhibit the addition of telomeric repeats to stabilize the ends of double-strand DNA breaks (128,129). In addition, a reduction or loss of expression of two or more MMR genes was observed in primary leukemic cells from 11 patients with ATL (176). There is further evidence that the ability of Tax to induce micronuclei is dependent on Ku80, a component of the NHEJ pathway of DNA repair (130). Microarray analysis showed that Ku80 gene expression is reduced in Tax-expressing cells (108). Still other effects of Tax were demonstrated by studies in our laboratory and others which show that Tax physically interacts with the DNA damage pathway protein Chk2 (112,143). Tax co-localizes with both Chk2 and 53BP1 at nuclear sites of DNA damage (112). Collectively, these studies demonstrate the wide-ranging effects Tax has on the capacity of the cell to appropriately respond to DNA damage.

In this study, we identified a novel physical interaction between Tax and DNA-dependent Protein Kinase (DNA-PK), an important regulator of the cellular response to double-strand DNA breaks (DSBs). We show that Tax co-localizes within nuclear Tax Speckled Structures (TSS) with forms of the catalytic subunit of DNA-PK (DNA-PKcs) that are phosphorylated at serine residue 2056 (S2056) and threonine residue 2609 (T2609), and that these phosphorylated forms are increased in Tax-expressing cells. The kinase activity of DNA-PK is found to be increased in the presence of Tax. We also

demonstrate that DNA-PK activity mediates Tax activation of Chk2, a known target of DNA-PK phosphorylation (177). Further, while ionizing radiation (IR)-induced phosphor-DNA-PKcs and γ-H2AX DNA damage foci normally resolve within 8 hours post-irradiation, in the presence of Tax these foci remain. Collectively, these data demonstrate that through direct interaction with DNA-PK, Tax interferes with the cellular DNA damage response.

Experimental Procedures

Plasmids

The S-tagged expression vectors *STaxGFP* and *SGFP* were constructed by inserting the *tax-EGFP* fusion or *EGFP* ORF, respectively, into the *Sma*I site of *pTriEx4-Neo* (Novagen, Madison, WI) in frame with the amino-terminal S-tag and His-tag.

Cell Culture and Transfection

293T cells were maintained at 37°C in a humidified atmosphere of 5% CO_2 in air, in Iscove's modified Dulbecco's medium supplemented with 10% fetal bovine serum and 1% penicillin-streptomycin (Invitrogen, Carlsbad, CA).

Transfections were performed by standard calcium phosphate precipitation. Briefly, cells were plated at 1x105 cells/mL. The following day, plasmid DNA in 2M $CaCl_2$ and 2X HBS were added dropwise to cells in fresh medium. Cells were incubated at 37°C for 6 h to overnight and fresh medium was added. The cells were harvested 48 h post-transfection, following a single wash with 1X PBS, in M-Per mammalian protein

extraction reagent (Pierce, Rockford, IL) with protease inhibitor cocktail (Roche, Palo Alto, CA) and immediately frozen at –80°C.

Protein Purification

Prepared cell lysate (1.5 mL) was incubated with 75 μl bed volume of S-protein agarose (Novagen, Madison, WI) for 30 min at room temperature, then washed 3 times with 1 mL Bind/Wash Buffer (20 mM Tris-HCl pH 7.5, 150 mM NaCl, 0.1% TritonX-100). Washed beads were eluted by resuspension in 150 μl Laemmli Sample Buffer (Bio-Rad, Hercules, CA) with β-Mercaptoethanol, followed by boiling for 5 min. Eluates were electrophoresed in a 10% SDS 1-D polyacrylamide gel and visualized by SilverQuest silver staining (Invitrogen, Carlsbad, CA). Bands of interest were manually excised from the gel for further analysis.

Immunoprecipitation

Whole cell lysate (~2 mg) in 500 μl volume was incubated with 5 μl anti-Tax polyclonal antibody at 4°C overnight, with constant rotation. The lysate was then incubated with 100 μl Protein A Sepharose beads (Zymed, San Francisco, CA) while rotating for 1 h at 4°C. The beads were washed 3X with 1 mL each 1X SNNTE buffer (5% sucrose, 500 mM NaCl, 1% Nonidet P-40, 50mM Tris-HCl [pH 7.4], 5 mM EDTA). Proteins were eluted from beads by resuspension in 100 μl Laemmli sample buffer (Bio-Rad, Hercules, CA) with β-mercaptoethanol, and boiled for 5 min.

Immunoblot Analysis

Cell extracts were derived as described above. Total protein concentrations were determined by Protein Assay (Bio-Rad, Hercules, CA). An equal volume of Laemmli sample buffer (Bio-Rad, Hercules, CA) with β-mercaptoethanol was added to the lysate, boiled for 5 min, and a normalized amount of total protein was loaded in each lane and electrophoresed through a 6% or 10% SDS-polyacrylamide gel. In some experiments, protein samples were prepared in 4X LDS Sample Buffer with Sample Reducing Agent, and electrophoresed in a NuPAGE 4-12% Bis-Tris gel using in MES-SDS Running Buffer (Invitrogen, Carlsbad, CA). The proteins were transferred onto Immobilon-P (Millipore, Billerica, MA) membrane using a Trans-blot SD semi-dry transfer cell (Bio-Rad, Hercules, CA) at 400 mA for 50 min or using a Trans-blot electrophoretic transfer cell (Bio-Rad, Hercules, CA) at 800 mA for 4 h in transfer buffer (25 mM Tris, 200 mM glycine, 20% methanol, 0.1% SDS). Following blocking in 5% non-fat milk in PBS/0.1% Tween-20, blots were incubated in primary antibody overnight, followed by 1 h incubation in secondary horseradish-peroxidase conjugated anti-mouse or anti-rabbit antibody (Bio-Rad, Hercules, CA). Immunoreactivity was detected via Immunstar enhanced chemiluminescence protein detection (Bio-Rad, Hercules, CA).

LC-MS/MS Analysis

Protein bands were excised from 1-D polyacrylamide gels. Gel slices were cut into 1-2 mm cubes; washed 3X with 500 μL ultra-pure water and incubated in 100% acetonitrile for 45 minutes. The material was dried in a speed-vac, rehydrated in a 12.5 ng/μL modified sequencing grade trypsin solution (Promega, Madison, WI) and

incubated in an ice bath for 40-45 min. The excess trypsin solution was then removed and replaced with 40-50 µL of 50mM ammonium bicarbonate, 10% acetonitrile, pH 8.0 and the mixture was incubated overnight at 37°C. Peptides were extracted 2X with 25 µl 50% acetonitrile, 5% formic acid and dried in a speed-vac. Digests were resuspended in 20 µL Buffer A (5% acetonitrile, 0.1% formic acid, 0.005% heptafluorobutyric acid) and 3-6 µL were loaded onto a 12-cm x 0.075 mm fused silica capillary column packed with 5 µM diameter C-18 beads (The Nest Group, Southboro, MA) using a N2 pressure vessel at 1100 psi. Peptides were eluted over 55 minutes, by applying a 0-80% linear gradient of Buffer B (95% acetonitrile, 0.1% formic acid, 0.005% heptafluorobutyric acid) at a flow rate of 130 µL/min with a pre-column flow splitter resulting in a final flow rate of ~200 nl/min directly into the source. In some cases the gradient was extended to 150 minutes to acquire more MS/MS spectra. A LCQ™ Deca XP (ThermoFinnigan, San Jose, CA) was run in an automated collection mode with an instrument method composed of a single segment and 4 data-dependent scan events with a full MS scan followed by 3 MS/MS scans of the highest intensity ions. Normalized collision energy was set at 30, activation Q was 0.250 with minimum full scan signal intensity at 5×10^5 and a minimum MS2 intensity at 1×10^4. Dynamic exclusion was turned on utilizing a three minute repeat count of 2 with the mass width set at 1.50 Da. Sequence analysis was performed with TurboSEQUEST™ (ThermoFinnigan, San Jose, CA) or MASCOT (Matrix Sciences, London, GB) using an indexed human subset database of the non-redundant protein database from National Center for Biotechnology Information (NCBI) web site (http://www.ncbi.nlm.nih.gov/). An additional database was created containing only the ORF sequence for the expressed Tax protein.

RT-PCR

Total RNA was extracted from cells transfected with *Hpx* Tax expression vector, or mock transfected, by harvesting in Trizol reagent (Invitrogen, Carlsbad, CA), followed by chloroform extraction. The aqueous layer was transferred to a fresh tube with isopropanol, and the mixture was applied to an RNeasy column (Qiagen, Valencia, CA). RNase-free DNase was added to the wash buffer, and RNA was eluted with RNase-free water. Gene expression was measured using the Access RT-PCR System (Promega, Madison, WI) for coupled reverse transcription and PCR amplification, according to the manufacturer's protocol. Briefly, 10 ng of RNA template was reverse transcribed using AMV Reverse Transcriptase for first strand cDNA synthesis and Tfl DNA Polymerase for second strand cDNA synthesis and DNA amplification. 18S rRNA was amplified as an internal control for equal total RNA using primers: 5'-TGACTCTAGATAACCTCGGG (forward) and 5'-CCCAAGATCCAACTACGAGC (reverse). A 348 bp fragment of DNA-PKcs cDNA (3325-3672 bp) was amplified using primers: 5'-AGGGAAGAAGAGTCTCTGGTGG (forward) and 5'-ATTAGGGGATCTGTTGCCTGGC (reverse).

Deletion Mutagenesis

Deletion mutagenesis was performed using QuikChange XL mutagenesis kit (Stratagene, La Jolla, CA) to delete between 29 to 52 amino acid stretches along the length of the 353-amino acid Tax sequence in the context of the fusion protein, STaxGFP. Forward and reverse primers were designed to anneal to the 5' and 3' regions flanking the desired deletion. Methylated original *STaxGFP* plasmid derived from

bacteria was used as the template, and mutagenic primers were extended with *PfuTurbo* high-fidelity DNA polymerase during an 18-cycle PCR, deleting the desired sequence from the newly synthesized strands. The remaining methylated template was digested by the DpnI provided, and the PCR product was used to transform XL10-Gold competent bacteria. Bacterial colonies growing under ampicillin selection were selected for further processing and correct plasmids were purified using the PureLink HiPure Plasmid Filter Maxiprep Kit (Invitrogen, Carlsbad, CA). Introduction of the correct deletion mutation was confirmed by DNA sequence analysis (Davis Sequencing, Davis, CA), and expression was confirmed by transfection and immunoblot analysis using anti-GFP monoclonal antibody (Santa Cruz Biotechnology, Santa Cruz, CA).

Immunofluorescence

293T cells were seeded onto 22-mm diameter coverslips in 6-well plates at 1×10^5 cells/well. Transfections were performed as described above, and 48 h later cells were washed twice with PBS, fixed in 4% paraformaldehyde and permeabilized with methanol. Coverslips were incubated with primary antibody in 3% BSA/PBS overnight at 4°C, followed by 2 washes in PBS/0.1% Tween20 and 2 washes in PBS. Coverslips were then incubated in secondary antibody with the addition of 1 µM TOPRO-3-iodide (Molecular Probes, Eugene, OR) for 1 h at room temp followed by 2 washes in 3% BSA/PBS and 2 washes in PBS. Coverslips were mounted in Vectashield containing DAPI (Vector Laboratories, Burlingame, CA). Fluorescent images were acquired using a Zeiss LSM 510 confocal microscope at 40X magnification with a 2.8X zoom using

Argon (488 nm), HeNe1 (543 nm), and HeNe2 (633 nm) lasers, and imaged with LSM

Image Browser software (Carl Zeiss, Jena, Germany).

Nuclear Extracts

Five confluent 150-mm plates of transfected 293T cells were washed twice in

cold PBS, and harvested by scraping in 3 mL Buffer A (10 mM HEPES [pH 7.9], 1.5

mM $MgCl_2$, 10 mM KCl, 0.5% Nonidet P-40, 0.5 mM dithiothreitol, protease inhibitor

cocktail [Roche, Indianapolis, IN]). Cell solutions were incubated for 10 min on ice for

lysis. Nuclei were centrifuged at 2000 rpm for 10 min at 4°C. The supernatant was

discarded, and 1 mL Buffer C (20 mM HEPES [pH 7.9], 25% glycerol, 420 mM NaCl,

1.5 mM $MgCl_2$, 0.2 mM EDTA, 0.5 mM dithiothreitol, protease inhibitor cocktail,

[Roche]) was added to the pellet. The resuspended pellet was incubated on ice for 30

min and mixed gently every 5 min by pipetting up and down. The sample was

centrifuged at 14000 rpm for 30 min at 4°C. The supernatant was dialyzed against Buffer

D (20 mM HEPES [pH 7.9], 20% glycerol, 100 mM KCl, 0.2 mM EDTA, 0.5 mM

PMSF, 0.5 mM dithiothreitol) for 5 h to overnight at 4°C. Nuclear extracts were stored

in aliquots at -80°C.

DNA-dependent Protein Kinase Assay

Protein kinase activation was assayed using the SignaTECT® DNA-Dependent

Protein Kinase Assay System (Promega, Madison, WI). Following the manufacturer's

protocol, reactions (25 µl) contained nuclear extract, DNA-PK activation buffer, reaction

buffer, a biotinylated p53-derived peptide containing a serine residue targeted for

phosphorylation by DNA-PK, and 0.5 µCi [γ-^{32}P]ATP (10 mCi/ ml). In some reactions, extracts were pre-incubated with 10 µM DNA-PK inhibitor II (Calbiochem, San Diego,CA) for 1 h on ice before being added to the reaction. Samples were incubated at 30°C for 10 min. Termination buffer containing guanidine hydrochloride was then added and 10 µl of each reaction mixture was spotted onto SAM$^{2®}$ Biotin capture membrane, containing biotin-binding streptavidin matrix. After washing with 2 M NaCl, membranes were dried and incorporated ^{32}P-phosphorylated substrate measured by scintillation counting.

Chk2 Kinase Assay

The plasmid pCDNA4-Chk2 in combination with pCDNA3-Tax (provided by Ralph Grassmann, Germany) or control plasmid expressing non-specific protein was subjected to *in vitro* transcription/translation using the Rabbit Reticulocyte Lysate System (Promega, WI). Standard 50-µl reactions were performed following the manufacturer's protocol. 8 µl of the *in vitro* translation product was mixed with 300 µl NETN buffer (20 mM Tris-HCl [pH 8.0], 0.1 M NaCl, 1 mM EDTA, 0.5% Nonidet P-40, protease inhibitor cocktail [Roche]) for immunoprecipitation using 2 µg of anti-Xpress tag antibody (Invitrogen, Carlsbad, CA) for 3 h. Precipitates were washed twice with NETN buffer lacking protease inhibitors followed by a final wash with 1X kinase assay buffer (20 mM Tris [pH 7.5], 10 mM MgCl$_2$, 10 mM MnCl$_2$, 1 mM dithiothreitol). In some reactions, precipitated Chk2 immune complexes were pre-incubated with 10 µM DNA-PK inhibitor II (Calbiochem, San Diego,CA) for 1 h on ice before being added to the kinase reaction. Reactions were incubated at 30°C for 10 min in 1X kinase assay buffer supplemented

with 2 μM unlabeled ATP and 10 μCi of [γ-^{32}P]ATP (Pierce). The reaction mixture was resolved on a 10% SDS-polyacrylamide gel, dried and subjected to phosphor-imaging using a Typhoon scanner (GE Health Care, NJ). Relative intensity of the bands was calculated by densitometry.

Results

Identification of DNA-PK in Tax Complex

In order to identify cellular proteins that interact with Tax *in vivo*, we created a tandem affinity-tagged Tax construct that could be expressed and purified from mammalian cells in a complex with its cellular binding partners. The previously described *STaxGFP* vector expresses biologically active full-length Tax protein fused to amino-terminal His_6- and S-tags to facilitate affinity purification, and carboxy-terminal green fluorescent protein (GFP) to facilitate monitoring of protein expression and localization (56). We purified S-tagged Tax protein from transiently transfected 293T cells along with interacting cellular proteins and further resolved these proteins by SDS-PAGE and visualized them by silver staining (Fig. 13*A*). Individual bands were manually excised from the gel and proteins were identified by LC-MS/MS analysis. STaxGFP was identified from a band of the expected size on the gel, as indicated (Fig. 13*A*). In addition, a high-molecular weight band was identified as the catalytic subunit of DNA-dependent Protein Kinase (DNA-PKcs). This band was not present in S-tag purifications from control cells transfected with *SGFP*. To confirm the correct identification of the band, replicate samples were resolved by SDS-PAGE and immunoblotted with antibody specific to DNA-PKcs (Fig. 13*B*). This blot clearly indicates that DNA-PKcs is present
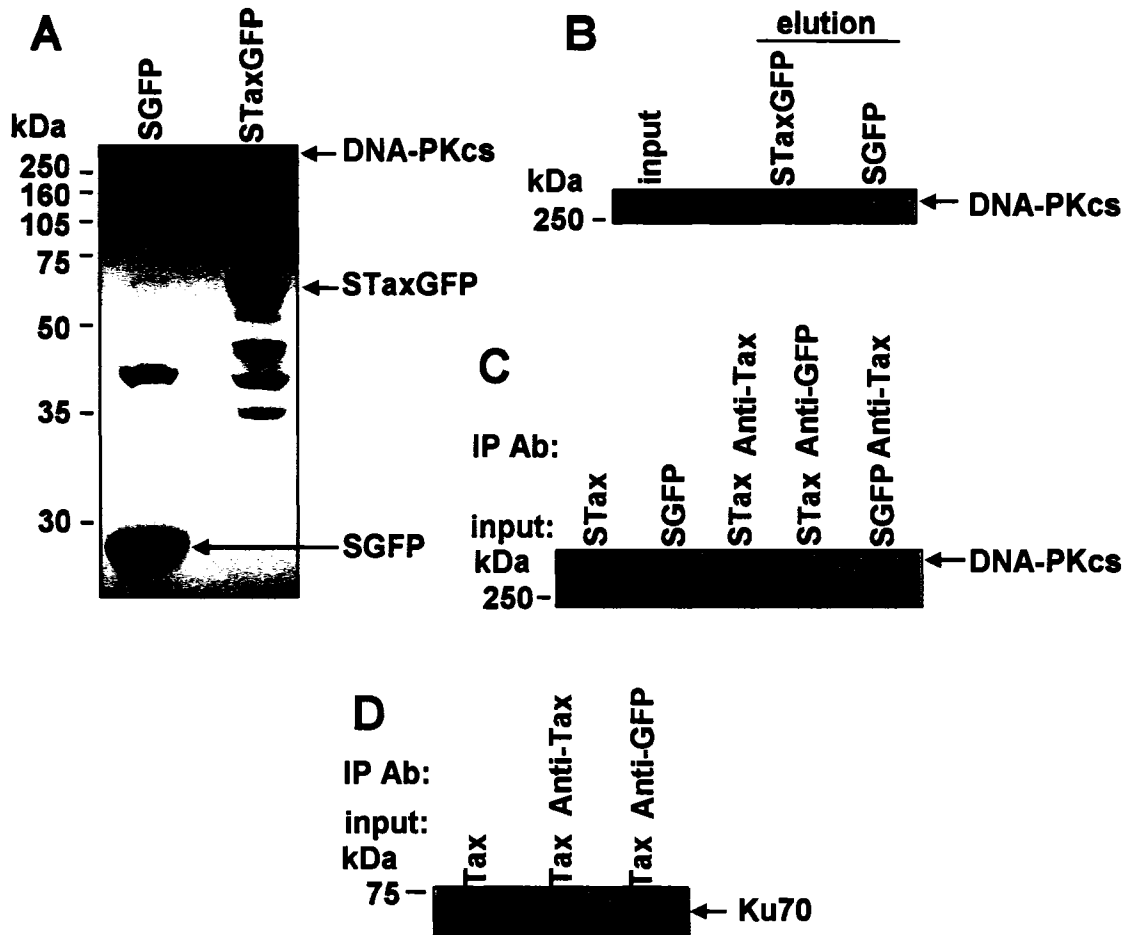
FIG. 13. **Identification of DNA-PK in Tax complex.** Cell lysates from 293T cells transiently transfected with *SGFP* or *STaxGFP* (indicated) were affinity purified on S-protein agarose beads as described under "Experimental Procedures" and subjected to SDS-PAGE and analysis by silver staining (*A*) or immunoblotting with anti-DNA-PKcs antibody (Neomarkers, Fremont, CA) (*B*). The band representing DNA-PKcs is indicated. Crude lysate from STaxGFP-transfected cells was loaded as a control (input) (*B*). *C*, co-immunoprecipitation of Tax and DNA-PKcs from 293T cells. Cell lysates from STax-transfected or SGFP-transfected cells as indicated (*input*), were immunoprecipitated with anti-Tax or anti-GFP polyclonal antibodies as indicated (*IP Ab*). The resulting precipitates were subjected to SDS-PAGE and immunoblot analysis using anti-DNA-PKcs monoclonal antibody (Neomarkers). *D*, co-immunoprecipitation of Tax and Ku70 from 293T cells. Cell lysates from Tax-transfected cells (*input*) were immunoprecipitated with anti-Tax or anti-GFP polyclonal antibodies as indicated (*IP Ab*). The resulting precipitates were subjected to SDS-PAGE and immunoblot analysis using anti-Ku70 monoclonal antibody (Neomarkers).

in the S-tag purification from cells transfected with *STaxGFP*, but not from cells transfected with control *SGFP* (Fig. 13*B*).

We next sought to confirm that Tax interacts with cellular DNA-PK by co-immunoprecipitation experiments. Tax complexes were immunoprecipitated from whole cell lysates with anti-Tax antibody, and an immunoblot with anti-DNA-PKcs antibody revealed that DNA-PKcs is present in the Tax complex (Fig. 13*C*). DNA-PKcs could not be detected when the control anti-GFP antibody was substituted for Tax antibody, or when SGFP was substituted for Tax in the whole cell lysate, indicating the specificity of the Tax-DNA-PKcs interaction (Fig 13*C*).

The DNA-PK holoenzyme consists of a catalytic subunit as well as two regulatory subunits, Ku70 and Ku80 (149,178). Co-immunoprecipitation experiments show that Ku70 is isolated from Tax-expressing cells with anti-Tax antibody but not with control anti-GFP antibody, indicating the Ku70 regulatory subunit of DNA-PK is also in the Tax complex (Fig. 13*D*).

Induction of Phosphorylated DNA-PK by Tax

We next sought to determine whether Tax affects the expression of DNA-PK through its function as a *trans*-activator. Gene expression of DNA-PKcs is not changed in the presence of Tax, as measured by semi-quantitative RT-PCR (Fig. 14*A*). In addition, immunoblot experiments indicate that overall DNA-PKcs protein expression is also unaffected by Tax (Fig. 14*B*). However, this experiment revealed a strong increase in phosphorylated forms of DNA-PKcs in the presence of Tax (Fig. 14*B*). Phosphorylation of DNA-PKcs at S2056 and T2609 has been shown to occur after DNA
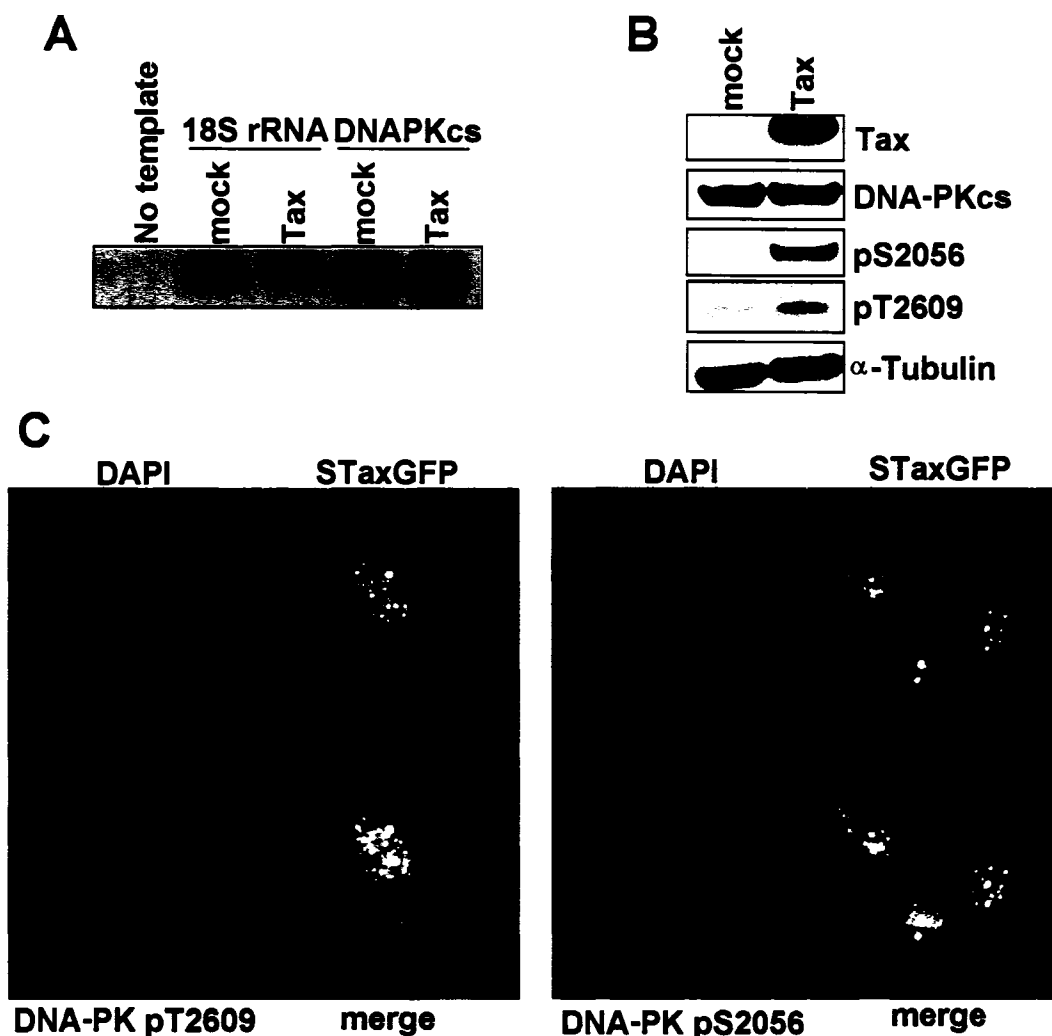
FIG. 14. **Induction of phosphorylated DNA-PKcs by Tax.** *A*, semi-quantitative RT-PCR using primers specific for DNA-PKcs (indicated) or control primers for 18S rRNA (indicated) for normalization to amplify cDNA from untransfected (*mock*) or Tax-transfected (*Tax*) 293T cells. DNA-PKcs-specific primers were included in a negative control reaction with no template DNA (*No template*). *B*, nuclear extracts from untransfected (*mock*) or Tax-transfected (*Tax*) 293T cells were subjected to SDS-PAGE and immunoblot analysis with the indicated antibodies. Alpha-tubulin (*a-Tubulin*) was used as control to demonstrate equal protein loading. *C*, 293T cells were transiently transfected with *STaxGFP* (*green*), fixed and permeabilized, and immunostained with anti-DNA-PKcs (phospho T2609) mouse monoclonal antibody (*DNA-PK pT2609*) or anti-DNA-PKcs (phospho S2056) rabbit polyclonal antibody (*DNA-PK S2056*), followed by the corresponding Alexa-594-conjugated anti-mouse or anti-rabbit secondary antibody (Molecular Probes) (*red*), along with DAPI and TOPRO-3-iodide to stain the nuclei (*blue*). The merged image shows the colocalized area represented in yellow (*merge*).

damage induced by ionizing radiation (IR)(179,180). We found that the expression of Tax alone, without external DNA damage agents, is sufficient to induce phosphorylation of DNA-PKcs. Furthermore, these phosphorylated forms of DNA-PKcs co-localize with Tax in nuclear Tax Speckled Structures (TSS) (Fig. 14C). Immunofluorescence experiments demonstrate that phosphorylated DNA-PKcs is present in characteristic nuclear foci only in the Tax-expressing cells (Fig. 14C). Collectively, the data from the immunoblot and immunofluorescence experiments indicate that Tax induces the phosphorylated form of DNA-PKcs, and specifically co-localizes with it at discrete nuclear sites.

Redistribution of DNA-PK by Tax Deletion Mutants

In order to determine which domains in Tax are required for interaction with DNA-PKcs, we designed a series of deletion mutants along the length of Tax (Fig. 15, *A* and *B*). Using immunofluorescence, we examined the localization of the Tax mutants along with DNA-PKcs (phosphor T2609) (Fig. 16) and DNA-PKcs (phosphor S2056) (data not shown). Both phosphorylated forms of DNA-PKcs showed similar expression patterns. All of the Tax mutants showed cytoplasmic localization, except for the mutants deleted from amino acids 52-99 or 322-353 (Fig. 16). Interestingly, phosphor-DNA-PKcs relocates to the cytoplasm in the presence of the cytoplasmic Tax deletion mutants 1-29, 29-52, and 99-150 (Fig. 16). These data indicate that the Tax regions from amino acids 1-52 and 99-150 are dispensable for interaction with DNA-PKcs. The interaction between the cytoplasmic Tax mutants and DNA-PKcs is strong enough to redistribute DNA-PKcs from the nucleus to the cytoplasm.
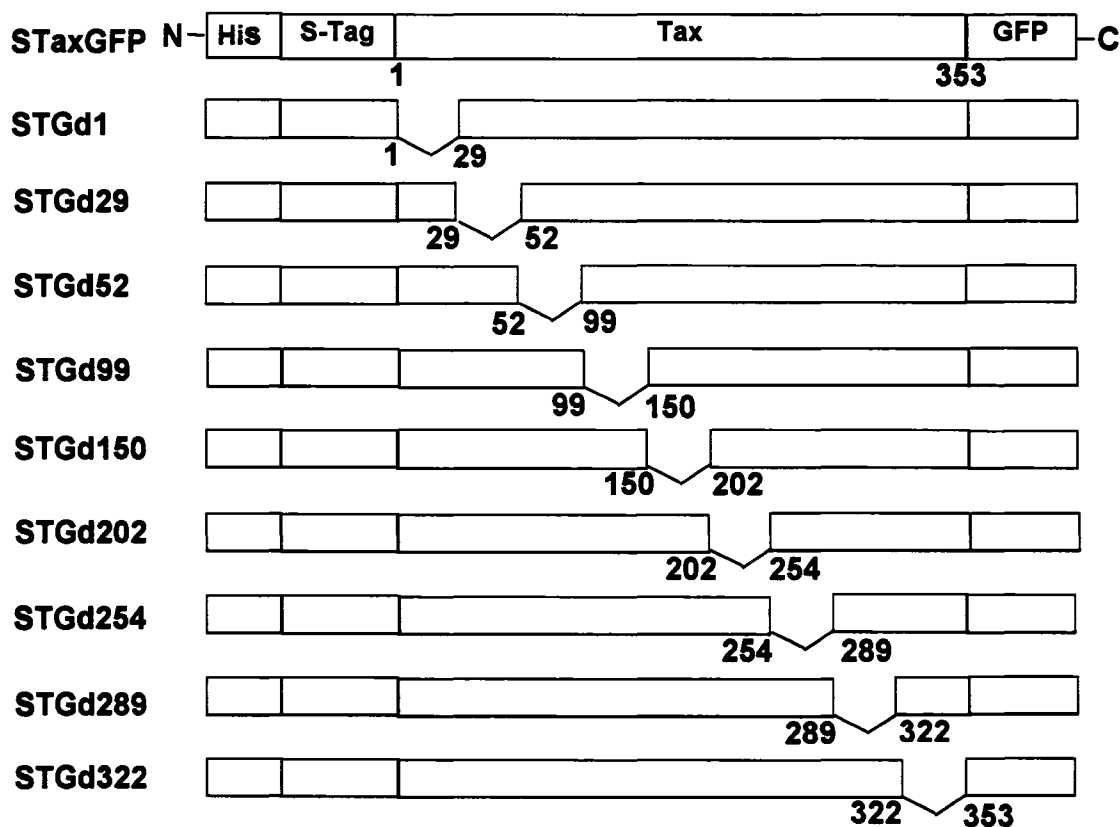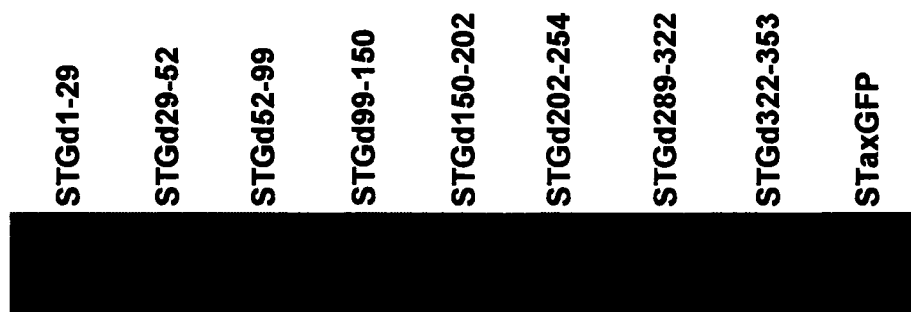
A

B

FIG. 15. **Efficient expression of Tax deletion mutants.** *A*, a depiction of deletion mutants of STaxGFP. The deleted amino acids are indicated. *B*, immunoblot using anti-GFP antibody of whole cell lysates from 293T cells transfected with either wild type Tax (*STaxGFP*) or Tax deletion mutant (indicated).
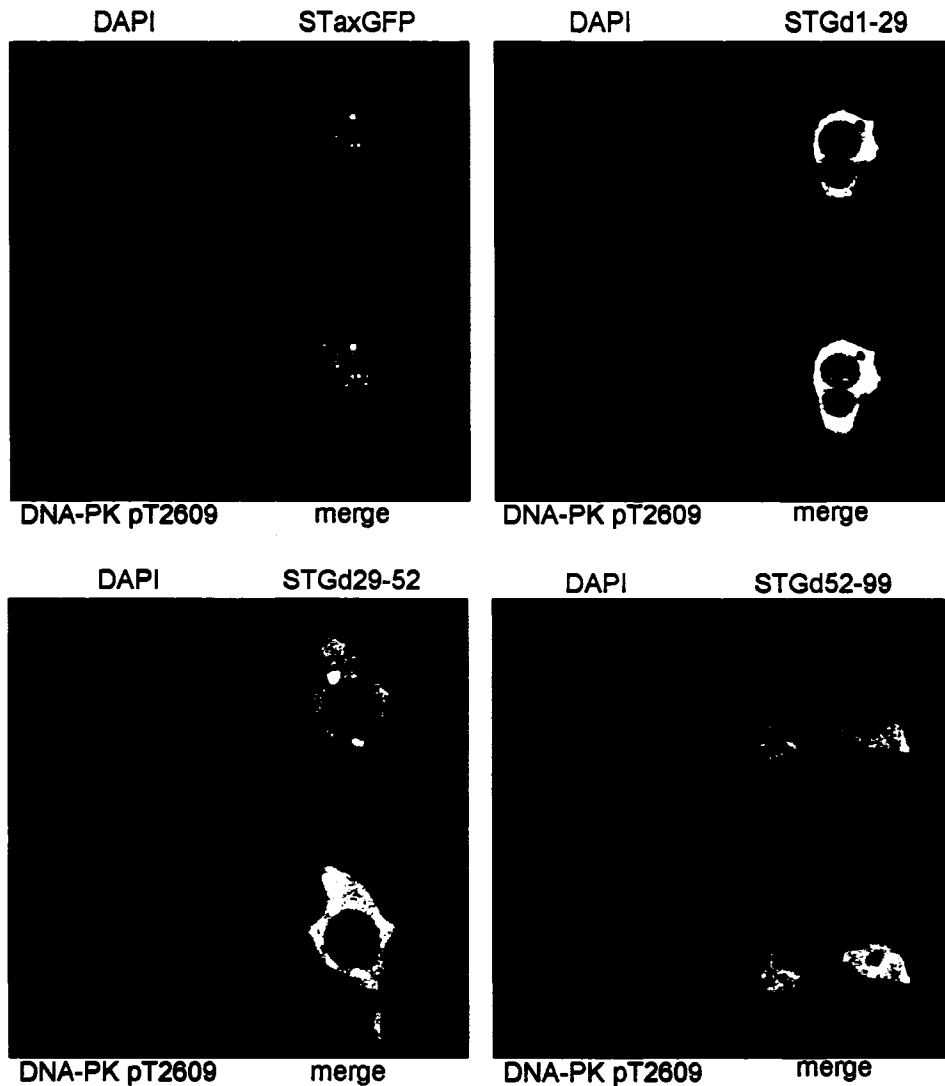
FIG. 16. **Redistribution of DNA-PK by Tax deletion mutants.** 293T cells were transfected with wild type Tax (*STaxGFP*) or Tax deletion mutant (indicated) (*green*), fixed and permeabilized and immunostained with anti-DNA-PKcs (phospho T2609) mouse monoclonal antibody (*DNA-PK pT2609*) followed by Alexa-594-conjugated anti-mouse secondary antibody (*red*), along with DAPI and TOPRO-3-iodide to stain the nuclei (*blue*). The merged image shows the colocalized area represented in yellow (*merge*).
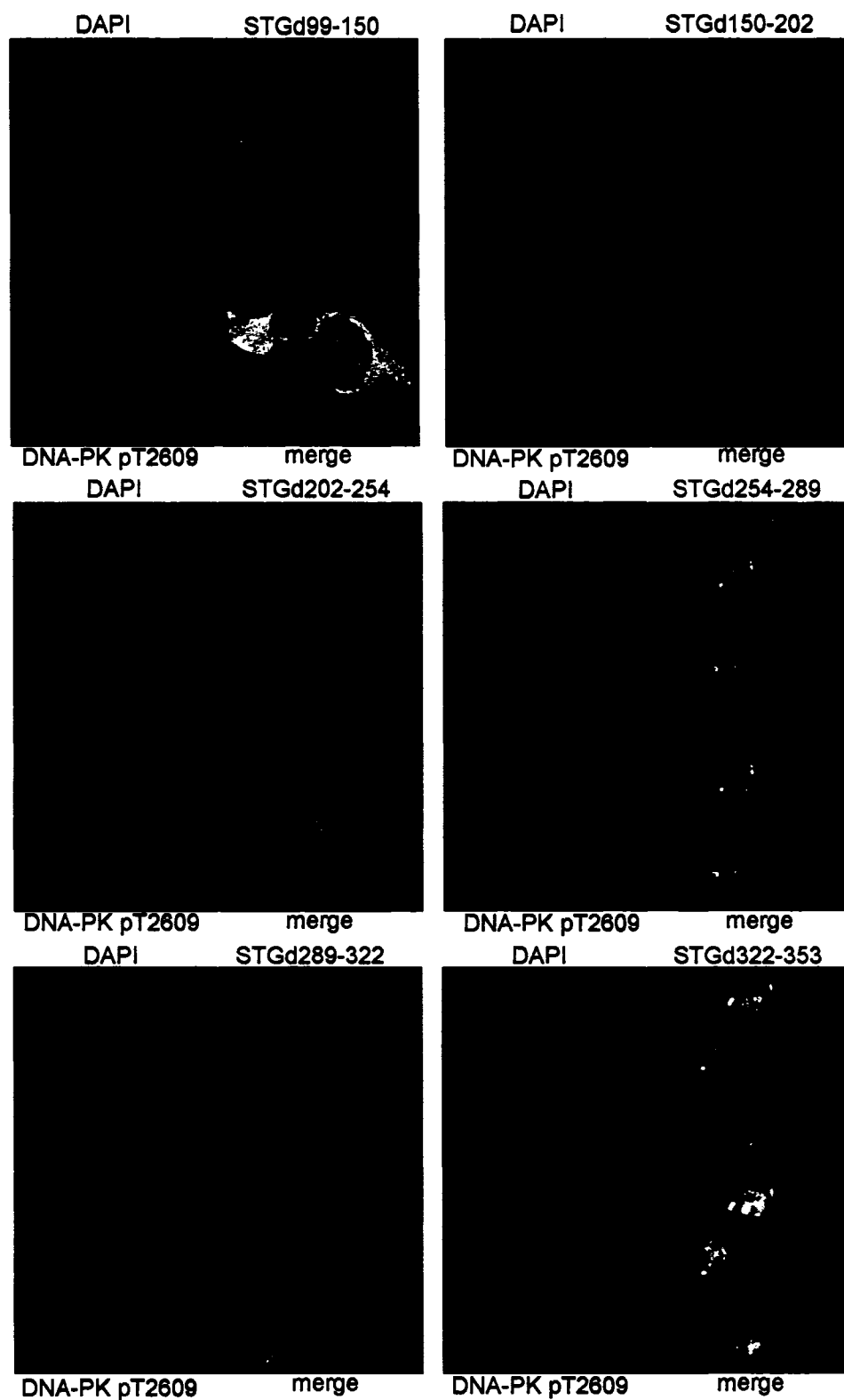
FIG. 16. Continued.

Tax Activation of DNA-PK Kinase Activity

The DNA-PK enzyme functions as a kinase, and therefore, we investigated the effect of Tax expression on DNA-PK kinase activity. Using an *in vitro* kinase assay, we determined that in the presence of Tax, DNA-PK has increased kinase activity (Fig. 17*A*). This assay measures phosphorylation of a p53-peptide substrate that is a known target of DNA-PK, and the specificity of the assay for DNA-PK is demonstrated by the loss of kinase activity in the presence of DNA-PK inhibitor (Fig. 17*A*). One of the known phosphorylation targets of DNA-PK is the DNA damage response protein Chk2, and this phosphorylation at threonine residue 68 activates Chk2, and usually occurs in response to DNA damage (177). Our lab and others have shown that Tax interacts with Chk2 (112,143) and increases its kinase activity (S. Gupta, unpublished data). We demonstrate here that activation of Chk2 by Tax is dependent on DNA-PK, as shown by a decrease in Tax-induced Chk2 activation in the presence of DNA-PK inhibitor (Fig. 17*B*). These data suggest that the increased activity of DNA-PK in Tax-expressing cells contributes to the observed increased Chk2 activity in these cells.

Retention of IR-induced Phosphor-DNA-PK and γ-H2AX Foci by Tax

The formation of γ-H2AX nuclear foci at the site of DNA strand breaks is an early cellular response to a DNA damage event (181). Phosphorylation of DNA-PKcs at S2056 and T2609 also occurs following DNA damage, and phosphor-DNA-PKcs co-localizes with γ-H2AX in nuclear foci (179,180). Since we observed that Tax co-localizes with phosphor-DNA-PKcs in the absence of an external source of DNA
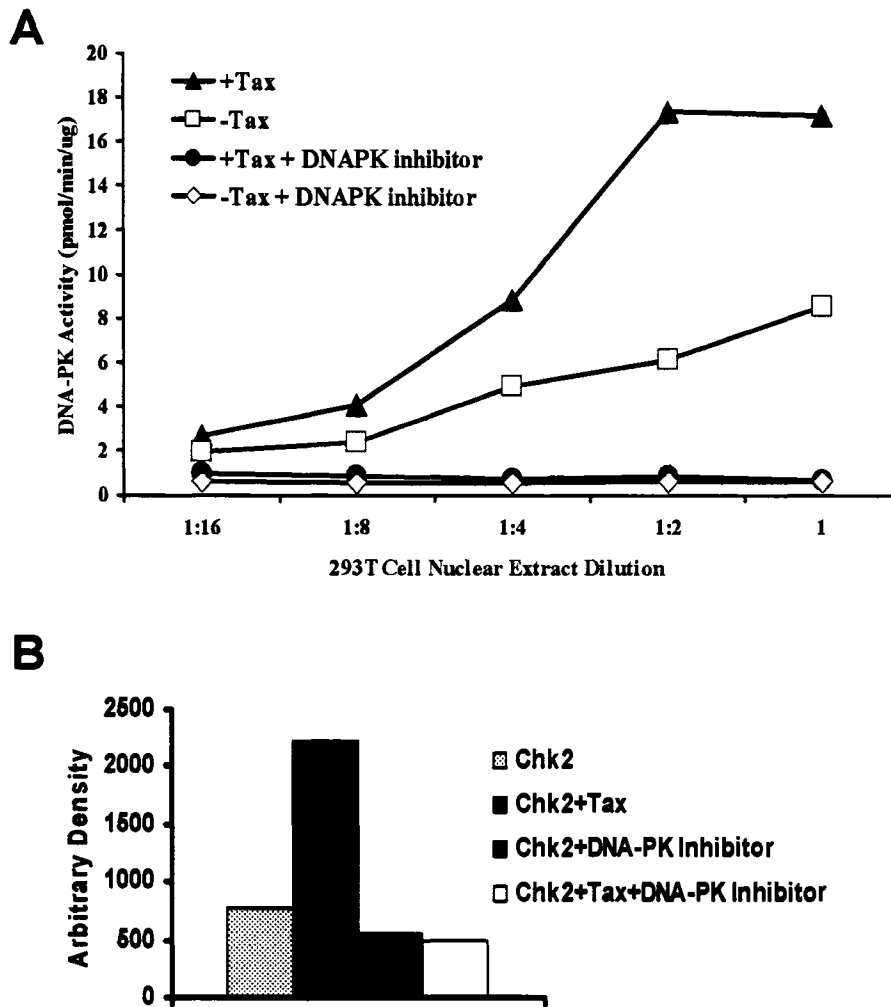
A

B

FIG. 17. **Tax activation of DNA-PK kinase activity.** *A*, dilutions (indicated) of nuclear extracts from 293T cells transfected with Tax (+*Tax*, closed triangle) or untransfected control cells (-*Tax*, open square) were prepared. DNA-PK enzyme activity was quantitated using the SignaTECT® DNA-PK Assay System (Promega), either in the presence (+ *DNAPK inhibitor*, closed circle and open diamond) or absence of DNA-PK inhibitor (Calbiochem) (closed triangle and open square). *B*, DNA-PK activity mediates Tax activation of Chk2 kinase. Kinase assays were performed using *in vitro* transcribed/translated Chk2 and Tax (*Chk2*+*Tax*) or Chk2 alone (*Chk2*), in the presence or absence of DNA-PK inhibitor (indicated). The reaction mixtures were subjected to SDS-PAGE and phosphorimaging analysis. Bands were quantitated by densitometry.

damage, we asked what would happen to IR-induced phosphor-DNA-PKcs and γ-H2AX foci in the presence of Tax. γ-H2AX foci appear within minutes after IR, and phosphor-DNA-PKcs foci are easily observed by 30 min post-IR (179,181). Both foci normally resolve by 6 to 8 h post-IR (179,182). Indeed, we observed a typical time course of DNA damage foci-induction in the absence of Tax, with resolution of phosphor-DNA-PKcs and γ-H2AX foci by 8 h post-IR. However, in Tax-expressing cells at 8 h post-IR, we observe the continued presence of phosphor-DNA-PKcs and γ-H2AX foci (Fig. 18). While a normal cell is able to resolve the DNA damage-induced foci in the appropriate time, Tax-expressing cells do not resolve the foci. These foci are present in conjunction with Tax even in the absence of applied DNA damage (Fig. 18, *No IR*).

Discussion

Oncogenesis can occur through an accumulation of mutations in the cellular genome which can be mechanistically attributed to chromosomal instability or loss of DNA repair function. Chromosomal instability results in polyploidy and aneuploidy, while loss of DNA repair function results in structurally damaged chromosomes bearing point mutations, deletions, substitutions, and translocations. Many of these features are demonstrated in HTLV-1-mediated transformation. Aneuploidy is a striking feature of ATL cells, which have multilobulated nuclei, commonly referred to as "flower" cells (25). Meanwhile, Tax expression alone causes multi-nucleated (polyploid) cells (79,80). HTLV-1-transformed lymphocytes derived from patients contain a variety of chromosomal abnormalities, including translocations, rearrangements, duplications and

FIG. 18. **Retention of IR-induced phosphor-DNA-PK and γ-H2AX foci by Tax.** 293T cells were transfected with Tax (*STaxGFP*), and 48 h later treated with 5 Gy ionizing radiation. Cells were fixed and permeabilized at the indicated times post-irradiation and co-immunostained with anti-DNA-PKcs (phospho T2609) mouse monoclonal antibody (*DNA-PK pT2609*) followed by Alexa-633-conjugated anti-mouse secondary antibody, and anti-γ-H2AX rabbit polyclonal antibody followed by Alexa-594-conjugated anti-rabbit secondary antibody (*γ-H2AX*). The merged image shows the colocalized area (*merge*).

FIG. 18. Continued.

deletions (81). Chromosomal damage is a characteristic of Tax-expressing cells, as observed by the induction of micronuclei (MN), which represent fragmented chromosomes indicative of DNA damage, or defects in DNA repair or in chromosom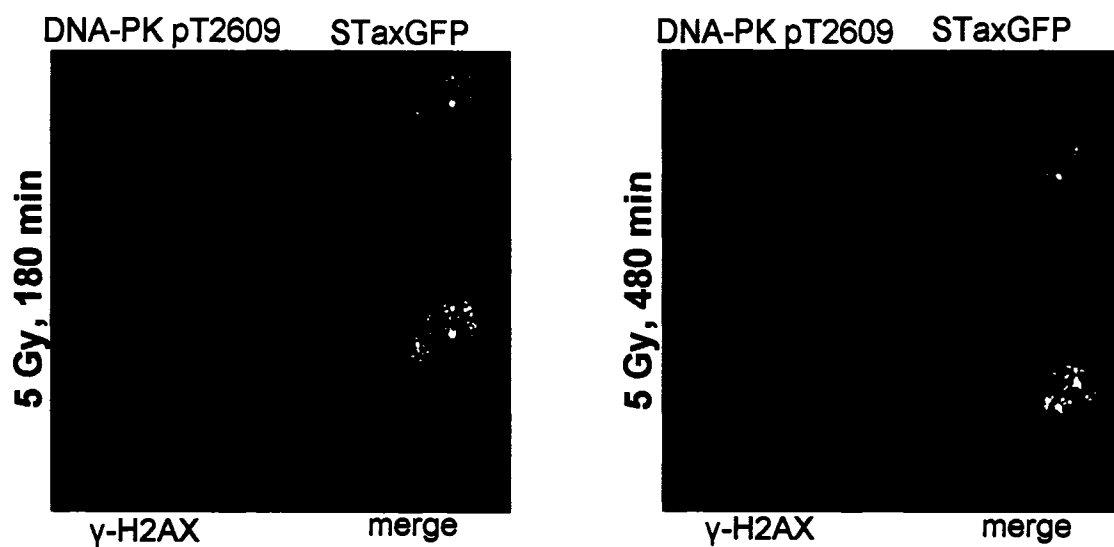al segregation (82). Understanding the interaction of Tax with the cellular DNA damage response pathway is important for elucidating the mechanism of induction of genomic instability.

DNA double strand breaks (DSB) are possibly the most dangerous type of DNA damage. While DSBs can be caused by exposure to ionizing radiation, they can also be caused endogenously by exposure to reactive oxygen species, by-products of cellular metabolism. Impairment of the DSB repair pathway can lead to gross chromosomal abnormalities caused by premature entry of cells into mitosis before DSBs are repaired, by rejoining of DSBs on different chromosomes, by the fusion of chromosome ends with eroded telomeres, or by defective repair (183). DNA repair genes are thus essential for maintaining genomic integrity (184).

The predominant DSB repair pathway in mammalian cells is non-homologous end joining (NHEJ), in which broken DNA ends are rejoined. The DNA-dependent Protein Kinase (DNA-PK) is the key enzyme in the NHEJ pathway of DSB repair (146-149). Along with playing a key role in DNA repair via NHEJ, DNA-PK is also involved in other important responses to DSBs, including cell cycle arrest and apoptosis (148). A further role for DNA-PK has been shown in maintaining telomeres to prevent them from being recognized as DSBs. In fact, in the absence of DNA-PK, cells exhibit telomeric fusions and increased chromosomal instability (150). DNA-PK is thus critically involved

in many important cellular responses to DNA damage and maintenance of genomic integrity.

The DNA-PK enzyme is a nuclear serine/threonine kinase consisting of an approximately 470 kDa catalytic subunit (DNA-PKcs) and a regulatory subunit composed of the Ku70/Ku80 heterodimer. Based on structural homology, DNA-PKcs belongs to a family of protein kinases known as phosphatidylinositol 3-kinase-like protein kinases (PI3KK), which includes DNA damage response proteins, ATM and ATR. The kinase activity of DNA-PKcs is stimulated by physical association with double-strand DNA. The process of NHEJ DSB repair involves recognition and binding of the Ku heterodimer to damaged DNA ends, recruitment and activation of DNA-PKcs and DNA end-processing factors including Artemis, and recruitment of DNA polymerase and XRCC4/ligase IV complex to re-ligate DNA (147). A wide range of proteins have been identified *in vitro* as substrates of DNA-PK kinase activity. These include many proteins in the DNA damage repair complex such as: Ku70 and Ku80, histone H2AX, replication protein A (RPA), XRCC4, and Chk2 (147,177). DNA-PKcs also phosphorylates tumor suppressor protein p53 *in vitro* on serine residues 15 and 37, sites important for regulation of its activity (140). In addition, autophosphorylation of DNA-PKcs at S2056 and T2609 is important for repair activity *in vivo* (179,180,182). Thus, through multiple activities, DNA-PK is an important regulator of the cellular response to DNA damage.

While the mammalian cell relies on the NHEJ pathway for quick repair of DSBs, the processing and rejoining of DNA ends is error-prone, typically involving deletions of 1-10 bases from the ends of broken DNA to regions of microhomology (185).

Significantly, an increase in DNA-PKcs expression and kinase activity is associated with a number of cancers. Gene expression of DNA-PKcs was upregulated in a human hepatoma cell line as compared to normal liver (186). A study comparing tumor tissues and adjacent normal tissues in colorectal cancers found a significant increase in both DNA-PKcs mRNA and protein expression in tumor tissues, as well as increased DNA-PK kinase activity (187). Interestingly, increased DNA-PKcs protein expression and kinase activity were also seen in metastatic and multi-drug resistant cancer cell lines compared to their parental cells (188). The precise regulation of DNA-PK thus seems to be essential for its role as a suppressor of genomic instability.

Autophosphorylation is a major mechanism for regulation of DNA-PKcs function in the repair process. When autophosphorylation is blocked by mutation of specific residues in DNA-PKcs, DSB rejoining is impaired and radiation sensitivity is increased (179,180,182,189). Interestingly, appropriate dephosphorylation appears to be an equally important step in the repair process. In a proposed model of NHEJ, dephosphorylation of DNA-PKcs promotes disassembly of the protein-DNA complex at the end of the repair process and presumably initiates recycling of the component proteins for future repair events (146,190,191). Dephosphorylation of DNA-PKcs is attributed to the activity of protein phosphatase 5 (PP5) (192). Hyperphosphorylation of DNA-PKcs at S2056 and T2609 by a PP5 dominant negative mutant actually resulted in increased radiosensitivity, indicating that prolonged phosphorylation at these sites is detrimental to DNA-PK repair function (192).

In the current study, we found that the HTLV-1 oncoprotein Tax interacts with DNA-PKcs and Ku70 in a complex. Furthermore, Tax induced hyperphosphorylation of

DNA-PKcs at S2056 and T2609, and co-localized with these phosphorylated forms in nuclear foci. Experiments using Tax deletion mutants that are nuclear excluded demonstrated redistribution of phosphor-DNA-PKcs to the sites where the Tax mutants are localized. This provides evidence of a strong interaction of Tax and DNA-PKcs, and the deletion analysis suggests that a large portion of the Tax sequence may be required for the interaction, with the exception of amino acids 1-52 and 99-150 which are dispensable.

In addition to the physical interaction of Tax with DNA-PKcs, we found increased DNA-PK kinase activity in Tax-expressing cells. Elevated DNA-PK kinase activity is correlated with a number of human cancers and with both metastatic and multi-drug resistant phenotypes (185-188). We postulate that the increased DNA-PK activity observed in Tax-expressing cells contributes to the genomic instability observed in these cells. Inappropriate activation of the NHEJ pathway could result in aberrant processing and joining of noncontiguous broken DNA ends, leading to translocations and deletions. Such repair infidelity was observed in myeloid leukemia cells which are characterized by genomic instability, and were shown to have increased DNA-PK activity and DSB misrepair (193). Further studies will be required to determine whether Tax-expressing cells have a higher rate of DSB misrepair.

DNA-PK has multiple phosphorylation targets demonstrated *in vitro* which require appropriate phosphorylation for proper function. Chk2 is a cell cycle checkpoint protein which is activated during the DNA damage response by phosphorylation, and is an *in vitro* substrate for DNA-PK (177). Our laboratory has shown that phosphorylated Chk2 is elevated in Tax-expressing cells and Chk2 activation leads to delayed

progression through the G2/M checkpoint (112). Using DNA-PK inhibitors, we demonstrated that increased Chk2 phosphorylation in Tax-expressing cells is dependent upon DNA-PK kinase activity. Increased DNA-PK activity could thus lead to increased phosphor-Chk2 whose activity results in inappropriate checkpoint activation. Persistant activation of cell cycle checkpoints is an early step in tumorigenesis that leads to genomic instability (183,184).

Another *in vitro* target of DNA-PK is the p53 tumor suppressor, a key protein in the response to DNA damage and cell stress, which has been shown to be phosphorylated by DNA-PK on serine residues 15 and 37 (140). While mutation of p53 is common in human cancers, it is not mutated in most HTLV-1-transformed cells (121). However, there is evidence that Tax can inactivate p53 function through a proposed mechanism involving hyperphosphorylation of p53 at serine 15 and 392, which interferes with the function of p53 as a transcriptional activator (194,195). Although it has been suggested that the phosphorylation mechanism through which Tax inactivates p53 is DNA-PK-dependent (194,195), another study found that Tax-mediated p53 inactivation still occurs in DNA-PKcs-deficient cells (196). However, due to overlapping roles of DNA-PK with other DNA damage response proteins, ATM and ATR (197,198), we cannot rule out the possibility that other proteins in these cells compensated for the lack of DNA-PK.

Another protein that was reported to be a phosphorylated substrate of DNA-PK *in vitro* is the oncoprotein, c-myc (199). Deregulation of c-myc expression is observed in many human tumors, and there is evidence that HTLV-1 Tax can also deregulate c-myc function (200,201). A DNA-PKcs-knockdown study suggested that DNA-PK activity may regulate expression of c-myc protein (202). Considering our current data indicating

an interaction between Tax and DNA-PK and the effect on DNA-PK activity, it is possible that the mechanism of Tax-mediated c-myc deregulation is DNA-PK-dependent. Further studies are required to investigate this hypothesis.

Increased DNA-PK activity may also have detrimental consequences for the maintenance of chromosomal stability in cells expressing Tax, due to its role in telomere capping. Telomeres protect chromosome ends from degradation and prevent chromosomal end fusion (203). DNA-PKcs is critical for telomere capping, and DNA-PKcs-deficiency promotes increased chromosomal instability and telomeric fusions (203,204). A study examining the role of DNA-PKcs in the context of telomerase inactivation proposed a model in which NHEJ-mediated telomere fusions are an outcome of critically short telomeres induced by telomerase deficiency (205). According to this model, an increase in DNA-PK activity would certainly have a detrimental effect in Tax-expressing cells, in which telomerase activity is decreased by Tax-mediated repression of human telomerase reverse transcriptase (hTert) (129). Tax-expressing cells display frequent unstabilized DNA breaks detected as unprotected free 3'-OH DNA ends (128,130). Telomerase inactivation by Tax would promote unstabilized telomeres which could result in end-to-end chromosomal fusions in the context of increased DNA-PK activity, resulting in the cytogenetic abnormalities observed in HTLV-1-infected cells (206).

In this study we provide evidence that Tax alters the function of DNA-PK in response to DNA damage. Tax-expressing cells subjected to ionizing radiation (IR) demonstrated a defect in the DNA damage response by their inability to appropriately resolve damage-induced phosphor-DNA-PKcs and γ-H2AX foci. Treatment of cells with

IR induces DNA-PKcs autophosphorylation and γ-H2AX foci formation, which normally begin to resolve by 8 h post-IR (179-182). Significantly, in Tax-expressing cells we observed prolonged phosphorylation of both DNA-PKcs and H2AX at 8 h post-IR and, indeed, we saw phosphorylation of these damage response proteins even in the absence of IR. The hyperphosphorylation observed in cells expressing Tax indicates a defect in the DNA-PK repair pathway. Further investigation is required to determine whether Tax affects the kinase disassembly step in a proposed model of the repair process (146), interfering with recycling of repair factors for additional rounds of repair.

An interesting question is why a retrovirus would interact with DNA repair proteins. The NHEJ pathway has been implicated in the early steps of retroviral infection. Specifically, DNA-PK may play a role in retroviral DNA integration, as evidenced by inefficient retroviral integration in DNA-PKcs-deficient mouse cells (207). Furthermore, increased apoptotic cell death is observed in these retroviral-infected cells, suggesting DNA-PK protects cells from toxicity caused by infection (207,208). A proposed model suggests that unintegrated retroviral cDNA promotes apoptosis, and activation of the NHEJ pathway protects the cell by recognizing the cDNA double-strand ends and causing circularization (209). It would be beneficial to a retrovirus to activate the NHEJ pathway to evade apoptosis, and is a logical action for the HTLV-1 protein Tax. Unlike HTLV-1, apoptosis is a key feature of the pathogenesis of a different retrovirus, Human Immunodeficiency Virus (HIV), in which apoptosis contributes to T-cell destruction (210). A recent study found decreased DNA-PKcs mRNA and protein expression in cells expressing the HIV protein, Tat, along with reduced DSB repair capacity (211). HIV infection combined with decreased NHEJ could contribute to the

increased apoptosis of infected cells (209). On the other hand, activation of the NHEJ

pathway by HTLV-1 Tax may contribute to the endurance of HTLV-infected cells.

SECTION 6

FUNCTIONAL ROLE OF TAX-DNA-PK INTERACTION

Introduction

Human T-cell Leukemia Virus Type 1 (HTLV-1), a transforming retrovirus, is the etiological agent of Adult T-cell Leukemia (ATL) and HTLV-1 Associated Myelopathy/Tropical Spastic Paraparesis (HAM/TSP), as well as other subneoplastic conditions (31). Expression of the 40-kDa viral transactivating protein, Tax, encoded by HTLV-1, is sufficient to cause cellular transformation (115). Although the specific mechanism is not fully known, it is evident that Tax induces genomic instability through direct interaction with various cellular proteins involved in cell cycle control and DNA damage repair response (112,114,115,128,130,145). Recent evidence in our laboratory indicates that Tax interacts with a key enzyme in the cellular response to DNA damage, the DNA-dependent Protein Kinase (DNA-PK) and affects its activity (S. Durkin, unpublished data). Considering that the fidelity of the DNA repair pathway is critical for maintaining the integrity of the genome, the interaction of Tax with DNA-PK may have negative consequences for the cell.

DNA double strand breaks (DSBs) are the most severe form of DNA damage, and if misrepaired, can lead to chromosomal abnormalities and genomic instability (212). The predominant DSB repair pathway in the mammalian cell is non-homologous end joining (NHEJ), in which broken DNA ends are rejoined. DNA-PK, a nuclear serine/threonine kinase, is the key enzyme in the NHEJ pathway of DSB repair (146-149). The process of NHEJ is rapid and error-prone due to processing and rejoining of

DNA ends using little or no homology to mend the breaks (185). The low fidelity of repair using this pathway can lead to mutations and chromosomal aberrations and, eventually, malignant transformation (213,214). Indeed, increased NHEJ repair activity is itself associated with various human tumors, as measured by increased DNA-PK protein expression and activity (186-188). In this study, we investigated the effect of Tax on NHEJ activity using an *in vivo* plasmid-based end-joining assay to measure overall and precise end-joining efficiency.

Along with playing a key role in DNA repair via NHEJ, DNA-PK is also involved in other important responses to DSBs, including cell cycle arrest and apoptosis (148). Interestingly, cell cycle arrest is a feature of Tax-expressing cells, in which there is delayed progression through the G2/M checkpoint (80,112,122). The mechanism of G2/M accumulation involves direct binding of Tax to the cell cycle checkpoint and DNA damage response protein, Chk2, which is phosphorylated and activated in Tax-expressing cells (112). Suppression of Chk2 using siRNA treatment abrogates the G2/M arrest induced by Tax (112). This effect may also be dependent on DNA-PK. Chk2 is an *in vitro* substrate for phosphorylation by DNA-PK (177), and our laboratory has shown that inhibition of DNA-PK abrogates Tax-induced Chk2 phosphorylation (S. Durkin and S. Gupta, unpublished data). In this study, we investigated the hypothesis that Tax interaction with DNA-PK promotes Chk2 phosphorylation and delays progression through the G2/M checkpoint. Using siRNA to knockdown expression of the catalytic subunit of DNA-PK (DNA-PKcs), we measured the effect on cell cycle in Tax-expressing cells.

This study is designed to determine the functional significance of the interaction of Tax with DNA-PKcs. The results presented here do not suggest a role for Tax in affecting the precision of NHEJ repair, nor do they suggest that DNA-PKcs is required for Tax-induced G2/M accumulation. However, as will be discussed, due to inherent limitations, these assays may not reflect the true situation *in vivo*.

Experimental Procedures

Plasmids

The *STaxGFP* expression vector was constructed by inserting the *tax-EGFP* fusion ORF into the *Sma*I site of *pTriEx4-Neo* (Novagen, Madison, WI) in frame with the amino terminal S- and His-tag.

Cell Culture and Transfection

293T cells were maintained at 37°C in a humidified atmosphere of 5% CO_2 in air, in Iscove's modified Dulbecco's medium supplemented with 10% fetal bovine serum (Cambrex, East Rutherford, NJ) and 1% penicillin-streptomycin (Invitrogen, Carlsbad, CA).

Transfections of 293T cells were performed by standard calcium phosphate precipitation. Cells were plated at 1×10^5 cells/mL. The following day, plasmid DNA in 2M $CaCl_2$ and 2X HBS were added dropwise to cells in fresh medium. Cells were incubated at 37°C for 5 h to overnight and fresh medium was added. The cells were harvested 48 h post-transfection, following a single wash with 1X PBS, in 500 μl M-Per

mammalian protein extraction reagent (Pierce, Rockford, IL) with protease inhibitor cocktail (Roche, Palo Alto, CA) and immediately frozen at –80°C.

Immunoblot Analysis

Cell extracts were derived as described above. Total protein concentrations were determined by Protein Assay (Bio-Rad, Hercules, CA). An equal volume of Laemmli sample buffer (Bio-Rad, Hercules, CA) with β-mercaptoethanol was added to the lysate, boiled for 5 min, and a normalized amount of total protein was loaded in each lane and electrophoresed through a 10% SDS-polyacrylamide gel. The proteins were transferred onto an Immobilon-P (Millipore, Billerica, MA) membrane using a Trans-blot SD semi-dry transfer cell (Bio-Rad, Hercules, CA) at 400 mA for 50 min in transfer buffer (25 mM Tris, 200 mM glycine, 20% methanol, 0.1% SDS). Following blocking in 5% non-fat milk in PBS/0.1% Tween-20, blots were incubated in primary antibody overnight, followed by 1 h incubation in secondary horseradish-peroxidase conjugated anti-mouse or anti-rabbit antibody (Bio-Rad, Hercules, CA). Immunoreactivity was detected via Immunstar enhanced chemiluminescence protein detection (Bio-Rad, Hercules, CA).

In Vivo End-joining Assay

This assay was modified from Zhong, et al. (215). *pGL2-Control* plasmid (Promega, Madison, WI) expressing the *luciferase* gene under control of the SV40 promoter was completely linearized using either *Hind*III or *Eco*RI, as confirmed by agarose gel electrophoresis. The linearized DNA was purified using the Qiaquick PCR Purification kit (Qiagen, Valencia, CA). 2×10^5 293T cells were transfected with 5 μg

STaxGFP or mock transfected using siPORT Amine transfection reagent (Ambion, Austin, TX) and incubated for 24 h. Cells were subsequently transfected with 10 µg either uncut, *Hind*III- or *Eco*RI- linearized *pGL2* DNA using the standard calcium-phosphate method. The transfectants were harvested 48 h post-transfection in Reporter Lysis Buffer (Promega, Madison, WI) and frozen at -80°C for luciferase assays. Luciferase assay substrate was used according to the manufacturer's protocol (Promega), and activity was measured in a TD-20/20 luminometer (Turner Designs, Sunnyvale, CA). Luciferase activity was normalized for total cell protein determined from whole cell extracts by Protein Assay (Bio-Rad, Hercules, CA), according to manufacturer's direction.

Flow Cytometry

To analyze the cell cycle profile, cells were washed once with PBS and centrifuged at 1000 rpm for 10 min at 4°C. The cells were fixed with the addition of 1 mL ice-cold 70 % ethanol and incubated at 4°C overnight. The ethanol was removed by centrifugation and the cell pellet was washed with 2 mL PBS. Cells were resuspended in 1 mL propidium iodide solution (50 µg/mL propidium iodide and 100 units/mL RNase A in PBS) and incubated for 30 min at room temperature with gentle rotation. The cells were washed in PBS and resuspended in 0.5 mL PBS. DNA flow analysis was conducted on a FACScan (BD Biosciences, San Jose, CA) with ModFit LT software (Verity Software House, Topsham, ME).

siRNA Delivery

DNA-PKcs *Silencer* Validated siRNA (PRKDC) or *Silencer* Negative Control #1 siRNA (Ambion, Austin, TX) was delivered to 293T cells in a 6-well plate at 2×10^5 cells/well using 10 μl/well siPORT Amine (Ambion), according to the manufacturer's protocol. In some experiments, 4 μg *STaxGFP* DNA was co-transfected by incubation with the siRNA and siPORT Amine. 48 h later, cells were harvested for further analysis.

Results

Effect of Tax on End-joining Repair

In order to determine the effect of Tax on the NHEJ pathway of repair, we developed an *in vivo* assay to measure end-joining in Tax-expressing cells compared to normal controls. This assay, modified from Zhong et al., measures both overall and precise end-joining repair of a linearized luciferase reporter plasmid, pGL2, transiently transfected into cells in the presence or absence of Tax expression (215). The *luciferase* gene is only expressed after the plasmid is end-joined to re-create the circular form. Relative end-joining efficiency is calculated by comparing luciferase activity of cells transfected with endonuclease-digested reporter plasmid with cells containing uncut plasmid. End-joining of the reporter plasmid linearized with *Hind*III restriction endonuclease, which cleaves at the linker region between the promoter and luciferase coding sequence, is considered overall end-joining activity because any end-joining activity in this region, even that resulting in small deletions or insertions, would not affect luciferase expression. Cleavage of the plasmid at the unique *Eco*RI site located within the luciferase coding region, however, can only produce luciferase activity if end-joined

precisely to restore the original sequence; hence this reflects precise end-joining activity. This assay, therefore, allowed us to measure both the efficiency and precision of end-joining repair capacity in Tax-expressing cells.

Efficient expression of Tax protein in cells prior to assaying for end-joining activity was achieved by transient transfection of *tax* 24 h prior to introduction of the linearized reporter plasmid (Fig. 19*A*). It should be noted that the majority of cells show strong Tax expression, as visualized by fluorescent microscopy of the Tax-green fluorescent protein (GFP) fusion protein (Fig. 19*A*). No significant difference in either overall or precise end-joining efficiency was observed in Tax-expressing cells compared to controls (Fig. 19*B*).

Efficient Knockdown of DNA-PKcs In Vivo

We next sought to determine whether DNA-PKcs plays a functional role in the Tax-induced delay in G2/M progression. Our strategy relied on suppressing DNA-PKcs expression in Tax-expressing cells and analyzing the effect on cell cycle progression. If DNA-PKcs is required for the Tax-induced cell cycle delay, then knocking down DNA-PKcs should remove the delay. Using DNA-PKcs *Silencer* Validated siRNA (*PRKDC*) (Ambion), we achieved efficient knockdown of DNA-PKcs protein expression, as measured by immunoblotting (Fig. 20*A*). The knockdown effect was not seen with delivery of control siRNA directed at a non-specific gene (*Neg. Ctrl*) (Fig. 20*A*). We then delivered both DNA-PKcs siRNA (*PRKDC*) and DNA encoding Tax protein (*STaxGFP*) via transient transfection to achieve knockdown of DNA-PKcs in Tax-expressing cells. DNA-PKcs expression in cells co-transfected with DNA-PKcs siRNA
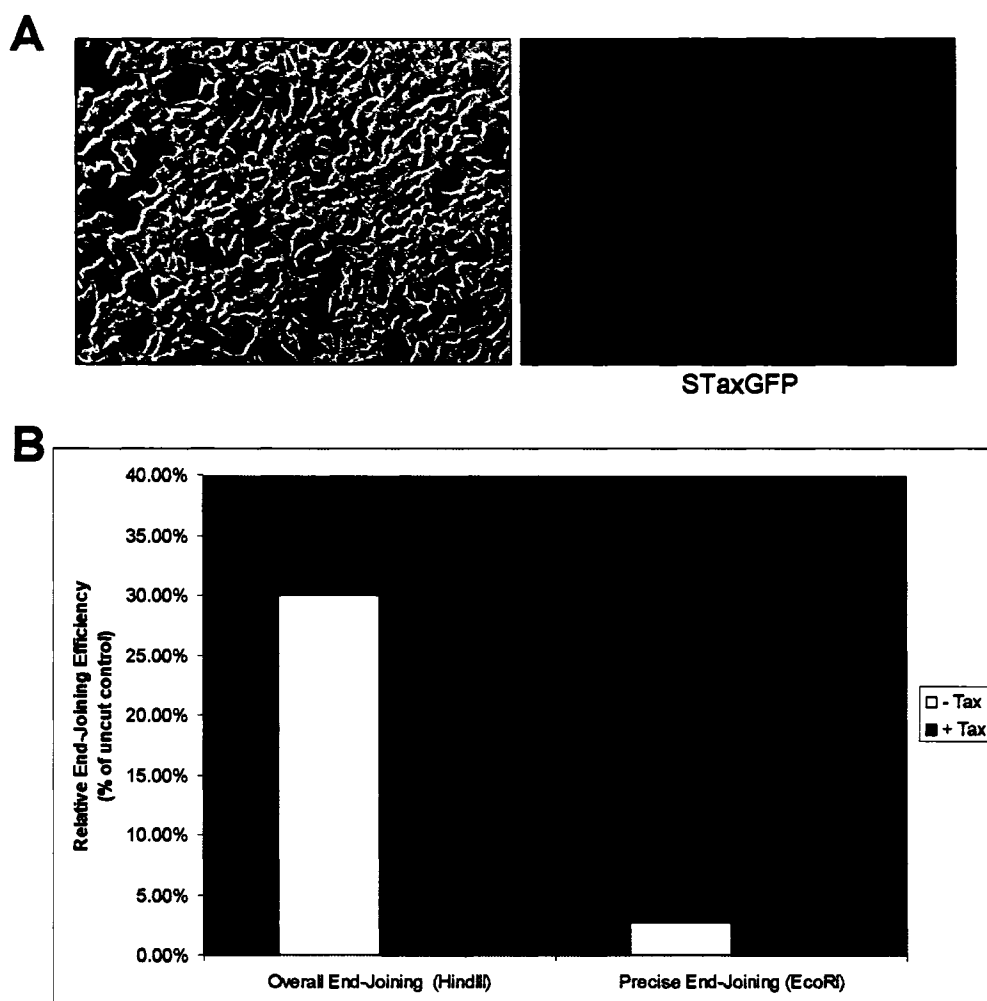
FIG. 19. **Effect of Tax on end-joining repair.** 293T cells were transiently transfected with *STaxGFP* (+*Tax*) or mock-transfected (-*Tax*) and incubated for 24h to allow expression of STaxGFP. The right panel (*A*) represents cells expressing STaxGFP. The left panel (*A*) shows the light field image of the same field of view. Cells were subsequently transfected with uncut, *Hind*III- or *Eco*RI-linearized pGL2 luciferase reporter plasmid. 48 h later, the transfectants were harvested and analyzed for luciferase activity. The relative end-joining efficiency was calculated by comparing luciferase activity in cells transfected with *Hind*III- or *Eco*RI-linearized DNA (indicated) with that of the uncut plasmid (*B*).
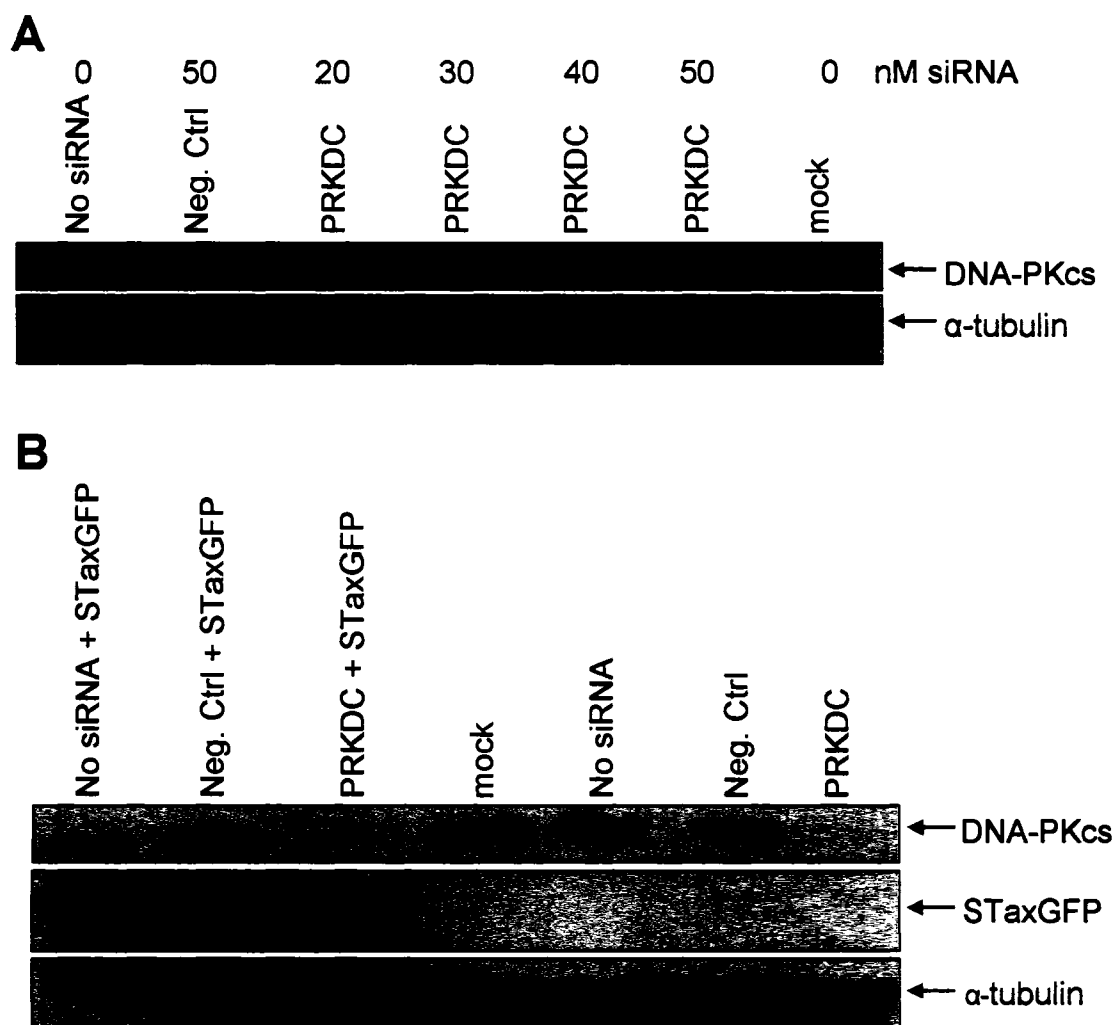
FIG. 20. **Efficient suppression of DNA-PKcs by siRNA.** *A*, 293T cells were transfected with the indicated concentrations of DNA-PKcs *Silencer* Validated siRNA (*PRKDC*) (Ambion) or *Silencer* Negative Control #1 siRNA (*Neg. Ctrl*) using siPORT Amine delivery agent (Ambion). *Mock* samples were treated without siRNA or siPORT Amine, *No siRNA* samples were treated with siPORT Amine alone. 48 h later, cells were harvested and subjected to SDS-PAGE and immunoblot analysis with using anti-DNA-PKcs antibody (Neomarkers). α-tubulin antibody was used as a control to show equal protein loading. *B*, cells were transfected with siRNA in the presence or absence of *STaxGFP* DNA (indicated). Immunoblot analysis using anti-GFP antibody shows expression of STaxGFP.

(*PRKDC*) and S*TaxGFP* was lower than in cells with Negative Control siRNA (*Neg. Ctrl*) and S*TaxGFP* (Fig. 20*B*). However, DNA-PKcs knockdown was not as efficient with co-delivery of S*TaxGFP* when compared to siRNA delivery alone (Fig. 20*B*).

Cell Cycle Analysis of Tax-expressing Cells with Reduced DNA-PKcs Expression

Using flow cytometry to measure fluorescence as well as the cell cycle profile of transfected cells, we were able to analyze the cell cycle of only the population of cells expressing Tax-GFP fusion protein by selecting only green fluorescent cells for analysis. However, we could not select only those cells which had received siRNA, since this population had no fluorescent marker. As expected, Tax-expressing cells show an almost two-fold increase in the percent of cells in G2/M compared to control cells (Fig. 21, *left* panels). The delivery of DNA-PKcs siRNA (*PRKDC*) compared to Negative Control siRNA (*Neg. Ctrl*) had no significant effect on the cell cycle profile (Fig. 21, *upper* panels). Surprisingly, knockdown of DNA-PKcs in Tax-expressing cells had no significant effect on G2/M arrest, as DNA-PKcs siRNA (*PRKDC*) delivery to these cells resulted in the same increase in G2/M as cells with Negative Control siRNA (*Neg. Ctrl*) and Tax (Fig. 21, *lower* panels). Whether this is simply due to inefficient knockdown of DNA-PKcs in many of the analyzed cells is not clear.

Discussion

The aim of this study was to identify a functional role for the interaction of Tax with DNA-PKcs in the DNA damage response pathway, with a specific investigation of the effect on DSB repair and G2/M arrest. We examined the effect of Tax on NHEJ
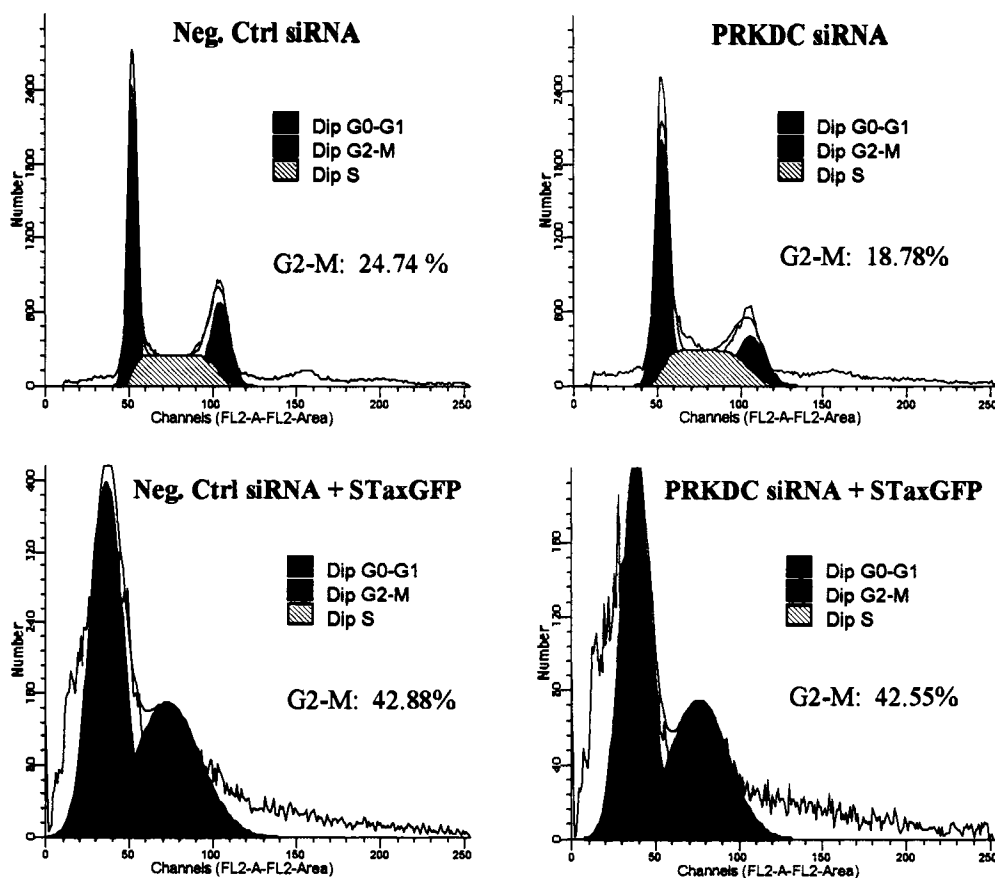
FIG. 21. **Cell cycle analysis of Tax-expressing cells with reduced DNA-PKcs.** The histograms represent the distribution of cells through the cell cycle measured by flow cytometry and analyzed by ModFit. Cells were transfected with *Silencer* Validated DNA-PKcs siRNA (*PRKDC siRNA*) (Ambion) or *Silencer* Negative Control #1 siRNA (*Neg. Ctrl siRNA*) (Ambion) in the presence of absence of *STaxGFP* DNA (indicated). The percentage of cells in G2/M is shown.

repair using an *in vivo* plasmid-based end-joining assay. The findings presented here do not show a significant effect of Tax on end-joining. We also found no significant requirement for DNA-PKcs in Tax-induced G2/M arrest, using siRNA suppression of DNA-PKcs.

Previous work in our laboratory and others has shown evidence of genomic instability in Tax-expressing cells, which may be a result of the impact of Tax on both cell cycle and the DNA damage response (115,145). In fact, Tax-expressing cells show an increased mutation rate, consistent with an effect on cellular DNA repair (83,84). The cell has a variety of mechanisms to repair damaged DNA including base excision repair (BER), mismatch repair (MMR), and non-homologous end-joining (NHEJ). While suppression of both BER and NER activity has been demonstrated in Tax-expressing cells (114,126,127), no studies have addressed the effect of Tax on the NHEJ pathway of repair.

Our laboratory has demonstrated a physical interaction between Tax and DNA-PKcs, a key enzyme involved in NHEJ repair. We also observed increased DNA-PK kinase activity in an *in vitro* assay in the presence of Tax. Furthermore, we found that Tax alters the regulation of this enzyme by increasing the forms of DNA-PKcs phosphorylated at serine 2056 (S2056) and threonine 2609 (T2609). Under normal conditions, following a DNA damage event, DNA-PKcs becomes phosphorylated at S2056 and T2609, and this phosphorylation is resolved after several hours during which time repair occurs (179,180). This event corresponds to the phosphorylation of histone variant H2AX at serine 139 (γ-H2AX), which co-localizes with phosphor-DNA-PKcs at the sites of DNA breaks (179,180). Interestingly, the process appears to be misregulated

in Tax-expressing cells, in which the phosphorylation of both DNA-PKcs and H2AX remains many hours after the DNA damage event. Therefore, we postulate that Tax may affect the NHEJ pathway of repair by influencing the activity of the key regulator, DNA-PK.

In the current study, we were unable to demonstrate a significant effect of Tax on cellular end-joining capacity, as measured by an *in vivo* plasmid-based end-joining assay. We cannot rule out the possibility that limitations in the assay design prevented us from detecting a difference between the repair capacities of cells with and without Tax. For example, the assay measures completed repair at 48 h after introduction of a linearized reporter plasmid. We cannot measure a difference in rates of repair using this approach. Future experiments aimed at measuring rates and fidelity of end-joining in Tax-expressing cells will use a PCR-RFLP-based assay, modified from Wang et al. (216). *Eco*RI-digested pGL2 plasmid will be transfected into cells, and then analyzed at selected time points after transfection for recircularization. A PCR product will be amplified in the linear range by specific primers flanking the *Eco*RI site. If the linearized pGL2 is rejoined precisely, the *Eco*RI site is regenerated and the PCR product can be digested by *Eco*RI to yield two small digestion fragments which can be resolved on an agarose gel containing ethidium bromide and quantified by densitometry. The *Eco*RI-cut fragments represent the fraction of precise end-joining. The PCR product resistant to *Eco*RI-digestion represents the imprecisely end-joined fraction. The effect of Tax on the rate of precise and imprecise end-joining can thus be determined. Furthermore, the exact nature of the misrepaired DNA can be determined by cloning the digestion-resistant fraction of the PCR product in bacteria and sequencing individual colonies. This assay can yield

important information about the impact of Tax on the rate and fidelity of end-joining repair, and may provide more insight than the luciferase-based assay conducted in the current study.

In the current study, we were also unable to demonstrate a role for DNA-PKcs in Tax-induced G2/M arrest. While DNA-PKcs may in fact not be required for this Tax effect, it remains a possibility that efficient siRNA delivery along with Tax was not sufficient to achieve complete knockdown of DNA-PKcs. The residual DNA-PK detected by immunoblot following simultaneous delivery of DNA-PKcs siRNA (*PRKDC*) and Tax (Fig 2*B*) may have been sufficient for activation of the cell cycle checkpoint. Furthermore, efficient siRNA and *STaxGFP* DNA co-delivery to the same cells is required to observe an effect. While cell cycle analysis can be analyzed in the population of cells with Tax-GFP expression due to the fluorescent GFP tag, this population likely only contains a portion of cells which also received siRNA. *Silencer* Validated DNA-PKcs siRNA is now commercially available with a Cy3 fluorescent label (Ambion), which would allow detection of siRNA within cells via flow cytometry. By using this reagent in combination with STaxGFP, we can selectively analyze the cell cycle profile of only the cell population which received both siRNA and *STaxGFP* DNA. Therefore, future studies aimed at optimizing siRNA delivery can readdress the role of DNA-PKcs in Tax-induced G2 arrest.

SECTION 7

CONCLUSIONS

Summary

We have developed two model systems for isolating Tax complexes. Using a stable, inducible cell line Flp-In TREx-293-HisTaxGFP, we demonstrated successful affinity purification of His-tagged Tax and associated proteins using immobilized metal affinity resin. A second model employed affinity purification of S-tagged Tax in complex with cellular binding partners from transiently transfected human cells, using S-protein agarose beads. Using the S-tag model, we successfully isolated Tax complexes and identified the novel Tax-interacting protein DNA-PKcs by LC-MS/MS analysis. We further explored the Tax interactome via bioinformatics analysis. The Human Virus Interactome Resource (HVIR) was developed as an interactive database containing Tax interactions currently documented in the research literature. In addition, we developed a visual map of the direct Tax interactions along with 'second neighbors' of Tax, cellular proteins that interact with Tax-binding partners, as identified by automated searching of publicly available protein interaction databases. Analysis of the resulting Tax interactome suggested that the Tax-DNA-PK interaction could have been predicted with the use of HVIR.

Affinity purification of S-tagged Tax from human cells provided sufficient material to conduct a complete physical mapping of phosphorylation sites in Tax. This analysis, using LC-MS/MS and MALDI-TOF, resulted in identification of four novel sites of phosphorylation at T48, T184, T215 and S336, along with confirmation of the

previously identified phosphorylation at S300/301. Mutational analysis demonstrated phosphorylation at T215 is associated with loss of Tax *trans*-activation of CREB and NF-κB-responsive promoters, while T48 predominantly affects NF-κB-responsive promoters, and T184 and S336 have no effect on these Tax functions.

Following identification of DNA-PKcs in the affinity-purified Tax complex, we confirmed the interaction using co-immunoprecipitation experiments, and also identified the regulatory protein, Ku70, as a binding partner. Semi-quantitative RT-PCR suggests that Tax does not affect the gene expression of DNA-PKcs. While the protein expression of DNA-PKcs is also not affected by Tax, phosphorylated DNA-PKcs is increased in Tax-expressing cells. Furthermore, Tax co-localizes with phosphor-DNA-PKcs in discrete nuclear foci. Select cytoplasmically-localized Tax deletion mutants cause a redistribution of phosphor-DNA-PKcs to the cytoplasm. DNA-PK kinase activity is increased in Tax-expressing cells. We also demonstrated the requirement for DNA-PK for the Tax-induced increase in Chk2 kinase activity. Tax alters the function of DNA-PK in response to DNA damage, as demonstrated by a defect in resolving DNA damage-induced phosphor-DNA-PKcs and γ-H2AX foci in Tax-expressing cells subjected to ionizing radiation.

A plasmid-based *in vivo* end-joining assay demonstrated no significant effect of Tax on cellular end-joining repair capacity. Suppression of DNA-PKcs by siRNA had to significant impact on Tax-induced G2/M arrest.

Significance of Findings

HTLV-1 has a global impact, with an estimated 20-30 million people infected

worldwide (22). HTLV-1 is endemic in distinct geographic areas, and presents a significant public health problem in regions such as the Caribbean, where 3-4% of the population is seropositive, and Japan, where an estimated 1.2 million individuals are infected (24-26). HTLV-1 infection is linked to two life-threatening and incurable diseases, ATL and HAM/TSP. More than 800 cases of ATL are diagnosed in Japan each year (25,26). Chemotherapy is ineffective at treating ATL, and patients with acute ATL have a median survival time of only 13 months, despite aggressive treatment (43).

Study of the molecular pathogenesis of HTLV-1-mediated T-cell transformation is critical to improving ATL treatment regimens. The HTLV-1 viral oncoprotein Tax plays a central role in initiation of cellular transformation (115). While increasing evidence from our group and others has indicated that Tax expression results in loss of genomic integrity, the mechanism by which this occurs in still not known. In the studies presented here, isolation of Tax protein for structural and functional mapping provides important insights into the regulation of Tax protein, and the impact of Tax on the DNA damage response pathway. This represents a significant contribution to understanding the mechanism of genomic instability induced by Tax.

In addition to analyzing Tax complexes *in vivo*, we used a bioinformatics approach to explore the Tax interactome. The HVIR database we developed to map documented Tax interactions provides an important research tool. We demonstrated that this tool can be used to predict Tax-interacting proteins. The interactive design of this database allows the researcher to effectively evaluate what proteins might be logical binding partners of Tax, and this can guide experimentation in the laboratory.

The efficient isolation of Tax from human cells by affinity purification provided

an excellent tool for examining the physical structure of Tax. We successfully generated a complete phosphopeptide map of Tax. Phosphorylation is an important mode of protein regulation. The identification of novel phosphorylation sites, which we further demonstrated are functionally significant for Tax transactivation, provides new information regarding Tax regulation. Since Tax affects so many cellular processes, understanding how it is regulated at the level of post-translational modifications is significant.

In addition to isolating Tax protein from human cells, we were able to pull down Tax-binding proteins in a complex by affinity purification. Further, we identified a novel Tax-interacting protein, DNA-PKcs. DNA-PK is a key enzyme in the cellular response to DNA damage. Since appropriate DNA repair is critical to maintaining the integrity of the genome, the interaction of Tax with DNA-PK is of considerable interest. Significantly, we found that Tax-expressing cells have increased DNA-PK kinase activity. This has serious implications for genomic integrity, as it is evident that a number of tumors present increased DNA-PK activity correlated with chromosomal aberrations and other evidence of genomic instability (186-188). Interestingly, we found that Tax-expressing cells have a defect in resolving DNA damage-induced phosphor-DNA-PK and γ-H2AX foci following ionizing radiation. This observation suggests that Tax alters DNA-PK function, interfering with the appropriate response to DNA damage. Collectively, these data suggest that the interaction of Tax with DNA-PK may contribute to the chromosomal aberrations observed in these cells, due to inappropriate regulation of the DNA repair pathway.

We further addressed the significance of the Tax-DNA-PK interaction by examining end-joining repair and cell cycle control. While we hypothesized that Tax may affect cellular end-joining capacity, we were unable to show such an effect. However, modification of the assay may provide better insight into this function. Further, we were unable to show a requirement for DNA-PK in Tax-induced G2/M arrest. Optimization of the suppression of DNA-PK may better resolve the role of DNA-PK in this function.

The data presented in this work provides a significant contribution to our understanding of the mechanism of Tax-mediated genomic instability. We suggest that Tax interaction with DNA-PK perturbs the cellular response to DNA damage, resulting in inappropriate repair, and the accumulation of chromosomal abnormalities leading to loss of genomic integrity. The models for purification of Tax complexes, along with the HVIR Tax interactome database, provide invaluable tools for the continued analysis of Tax structure and function.

Future Directions

The S-tagged Tax purification system is an incredible tool for identifying Tax-interacting proteins. Continued optimization of the affinity purification protocol can increase the number of proteins that we are able to identify in the Tax complex. One option is to enrich for subsets of proteins that we are interested in. For example, S-tagged Tax can be bound to the beads, and then subsequently incubated with concentrated cellular fractions, such as nuclear extracts, to increase the opportunity for identifying proteins of low-abundance. In addition, the stringency of washes can be regulated to

allow for weaker binding partners to remain bound to the beads, and increase the number of identified proteins. Non-specific proteins can be reduced by utilizing the thrombin cleavage site, such that S-tagged Tax is bound to the beads and the Tax complex is removed by cleavage of the S-tag from the protein using thrombin. This protocol has already successfully been used as an alternative to elution (data not shown). In this way, proteins non-specifically bound to the beads will not be removed by thrombin cleavage as they would be by elution. More sensitive detection of the isolated protein complex can be achieved with 2-D gel electrophoresis. Preliminary experiments indicate that it is critical to decrease non-specific background since this method allows very sensitive protein detection (data not shown). Therefore, thrombin cleavage in combination with 2-D gel analysis may be advantageous.

It is of considerable interest to examine Tax complexes in T-cells, which is the natural cell type for HTLV-1 infection. We are currently working on methods to express S-tagged Tax in T-cells for affinity purification. We have developed a lentiviral-based expression system (Invitrogen) to produce virus expressing STax and STaxGFP which can be used to infect T-cells for efficient expression of S-tagged Tax. Progress has been made in creating the expression vectors, and the production of virus is underway (data not shown). Alternatively, the use of newly-acquired Amaxa Nucleofector technology (Amaxa, Gaithersburg, MD) may provide us with another method for efficiently expressing S-tagged Tax in T-cells.

Besides isolating and identifying Tax-interacting proteins in T-cells, we are also interested in mapping Tax post-translational modifications in this cell type. Efficient expression and purification of S-tagged Tax in T-cells would allow us to perform LC-

MS/MS analysis to determine if the same sites are phosphorylated as in 293T cells. In addition to phosphorylation, other post-translational modifications, such as ubiquitination and sumoylation, can be mapped in either 293T or T-cells by mass spectrometry analysis. We have developed phosphor-specific antibodies to T48, T215 and S300/301 which we can use to further investigate the functional significance of this phosphorylation. Preliminary experiments with these antibodies suggest that they are indeed phosphor-specific (data not shown). The antibodies can be used to assess Tax phosphorylation status in different cell types, the localization of phosphor-forms and other important characteristics. In addition, further studies using the phosphor-specific mutants can be designed to examine the requirement of phosphorylation for other Tax functions, such as interaction with DNA damage response pathway components.

Considering the range of DNA-PK function, there are many questions we can address about the significance of the Tax-DNA-PK interaction. Optimization of the end-joining repair assay, as described in the discussion in Section VI, may show an impact of Tax on this form of repair. In addition, improved suppression of DNA-PKcs would allow better assessment of its role in Tax-induced G2/M arrest. Future studies examining the role of Tax and DNA-PK in myc regulation, p53 function, and telomerase capping would all be valuable.

REFERENCES

1.	Gallo, R. C. (2005) *Retrovirology* **2**(1), 17

2.	Yoshida, M. (2005) *Oncogene* **24**(39), 5931-5937

3.	Coffin, J. M., Hughes, S. H., and Varmus, H. (1997) *Retroviruses*, Cold Spring Harbor Laboratory Press, Plainview, N.Y.

4.	Fields, B. N., Knipe, D. M., and Howley, P. M. (1996) *Fields virology*, 3rd Ed., Lippincott-Raven Publishers, Philadelphia

5.	Le Blanc, I., Grange, M. P., Delamarre, L., Rosenberg, A. R., Blot, V., Pique, C., and Dokhelar, M. C. (2001) *Virus Res* **78**(1-2), 5-16

6.	Shuker, S. B., Mariani, V. L., Herger, B. E., and Dennison, K. J. (2003) *Chem Biol* **10**(5), 373-380

7.	Derse, D., Heidecker, G., Mitchell, M., Hill, S., Lloyd, P., and Princler, G. (2004) *Front Biosci* **9**, 2495-2499

8.	Nicot, C., Harrod, R. L., Ciminale, V., and Franchini, G. (2005) *Oncogene* **24**(39), 6026-6034

9.	Younis, I., and Green, P. L. (2005) *Front Biosci* **10**, 431-445

10.	Kashanchi, F., and Brady, J. N. (2005) *Oncogene* **24**(39), 5938-5951

11.	Grant, C., Barmak, K., Alefantis, T., Yao, J., Jacobson, S., and Wigdahl, B. (2002) *J Cell Physiol* **190**(2), 133-159

12.	Hanon, E., Stinchcombe, J. C., Saito, M., Asquith, B. E., Taylor, G. P., Tanaka, Y., Weber, J. N., Griffiths, G. M., and Bangham, C. R. (2000) *Immunity* **13**(5), 657-664

13.	Semmes, O. J. (2006) *J Clin Invest* **116**(4), 858-860

14.	Manel, N., Kim, F. J., Kinet, S., Taylor, N., Sitbon, M., and Battini, J. L. (2003) *Cell* **115**(4), 449-459

15.	Manel, N., Battini, J. L., Taylor, N., and Sitbon, M. (2005) *Oncogene* **24**(39), 6016-6025

16.	Bangham, C. R. (2003) *J Gen Virol* **84**(Pt 12), 3177-3189

17. Igakura, T., Stinchcombe, J. C., Goon, P. K., Taylor, G. P., Weber, J. N., Griffiths, G. M., Tanaka, Y., Osame, M., and Bangham, C. R. (2003) *Science* **299**(5613), 1713-1716

18. Yamamoto, N., Okada, M., Koyanagi, Y., Kannagi, M., and Hinuma, Y. (1982) *Science* **217**(4561), 737-739

19. Delamarre, L., Rosenberg, A. R., Pique, C., Pham, D., and Dokhelar, M. C. (1997) *J Virol* **71**(1), 259-266

20. Nagy, K., Clapham, P., Cheingsong-Popov, R., and Weiss, R. A. (1983) *Int J Cancer* **32**(3), 321-328

21. Mortreux, F., Kazanji, M., Gabet, A. S., de Thoisy, B., and Wattel, E. (2001) *J Virol* **75**(2), 1083-1089

22. Nicot, C. (2005) *Am J Hematol* **78**(3), 232-239

23. de The, G., and Bomford, R. (1993) *AIDS Res Hum Retroviruses* **9**(5), 381-386

24. Edlich, R. F., Arnette, J. A., and Williams, F. M. (2000) *J Emerg Med* **18**(1), 109-119

25. Matsuoka, M. (2005) *Retrovirology* **2**(1), 27

26. Matsuoka, M., and Jeang, K. T. (2005) *Cancer Res* **65**(11), 4467-4470

27. Okochi, K., Sato, H., and Hinuma, Y. (1984) *Vox Sang* **46**(5), 245-253

28. Hino, S., Yamaguchi, K., Katamine, S., Sugiyama, H., Amagasaki, T., Kinoshita, K., Yoshida, Y., Doi, H., Tsuji, Y., and Miyamoto, T. (1985) *Jpn J Cancer Res* **76**(6), 474-480

29. Murphy, E. L., Figueroa, J. P., Gibbs, W. N., Brathwaite, A., Holding-Cobham, M., Waters, D., Cranston, B., Hanchard, B., and Blattner, W. A. (1989) *Ann Intern Med* **111**(7), 555-560

30. Lee, H., Swanson, P., Shorty, V. S., Zack, J. A., Rosenblatt, J. D., and Chen, I. S. (1989) *Science* **244**(4903), 471-475

31. Proietti, F. A., Carneiro-Proietti, A. B., Catalan-Soares, B. C., and Murphy, E. L. (2005) *Oncogene* **24**(39), 6058-6068

32. Williams, A. E., Fang, C. T., Slamon, D. J., Poiesz, B. J., Sandler, S. G., Darr, W. F., 2nd, Shulman, G., McGowan, E. I., Douglas, D. K., Bowman, R. J., and et al. (1988) *Science* **240**(4852), 643-646

33. Anonymous. (1990) *MMWR* **39**(50), 915,921-924

34. Shuh, M., and Beilke, M. (2005) *Microsc Res Tech* **68**(3-4), 176-196

35. LaGrenade, L., Hanchard, B., Fletcher, V., Cranston, B., and Blattner, W. (1990) *Lancet* **336**(8727), 1345-1347

36. Poiesz, B. J., Ruscetti, F. W., Gazdar, A. F., Bunn, P. A., Minna, J. D., and Gallo, R. C. (1980) *Proc Natl Acad Sci U S A* **77**(12), 7415-7419

37. Hinuma, Y., Nagata, K., Hanaoka, M., Nakai, M., Matsumoto, T., Kinoshita, K. I., Shirakawa, S., and Miyoshi, I. (1981) *Proc Natl Acad Sci U S A* **78**(10), 6476-6480

38. Yoshida, M., Miyoshi, I., and Hinuma, Y. (1982) *Proc Natl Acad Sci U S A* **79**(6), 2031-2035

39. Seiki, M., Hattori, S., Hirayama, Y., and Yoshida, M. (1983) *Proc Natl Acad Sci U S A* **80**(12), 3618-3622

40. Tokudome, S., Tokunaga, O., Shimamoto, Y., Miyamoto, Y., Sumida, I., Kikuchi, M., Takeshita, M., Ikeda, T., Fujiwara, K., Yoshihara, M., and et al. (1989) *Cancer Res* **49**(1), 226-228

41. Daisley, H., Charles, W. P., and Swanston, W. (1999) *Int J STD AIDS* **10**(7), 487-489

42. Shimoyama, M. (1991) *Br J Haematol* **79**(3), 428-437

43. Yamada, Y., Tomonaga, M., Fukuda, H., Hanada, S., Utsunomiya, A., Tara, M., Sano, M., Ikeda, S., Takatsuki, K., Kozuru, M., Araki, K., Kawano, F., Niimi, M., Tobinai, K., Hotta, T., and Shimoyama, M. (2001) *Br J Haematol* **113**(2), 375-382

44. Taylor, G. P., and Matsuoka, M. (2005) *Oncogene* **24**(39), 6047-6057

45. Tan, C., and Waldmann, T. A. (2002) *Cancer Res* **62**(4), 1083-1086

46. Abe, Y., Yashiki, S., Choi, I., Hara, K., Matsushima, T., Nishimura, J., Inaba, S., Nawata, H., and Muta, K. (2002) *Int J Hematol* **76**(1), 91-93

47. Mochizuki, M., Watanabe, T., Yamaguchi, K., Yoshimura, K., Nakashima, S., Shirao, M., Araki, S., Takatsuki, K., Mori, S., and Miyata, N. (1992) *Am J Ophthalmol* **114**(2), 123-129

48. Shida, H., Tochikura, T., Sato, T., Konno, T., Hirayoshi, K., Seki, M., Ito, Y., Hatanaka, M., Hinuma, Y., Sugimoto, M., and et al. (1987) *Embo J* **6**(11), 3379-3384

49. Sundaram, R., Sun, Y., Walker, C. M., Lemonnier, F. A., Jacobson, S., and Kaumaya, P. T. (2003) *Vaccine* **21**(21-22), 2767-2781

50. Sundaram, R., Lynch, M. P., Rawale, S. V., Sun, Y., Kazanji, M., and Kaumaya, P. T. (2004) *J Biol Chem* **279**(23), 24141-24151

51. Kataoka, R., Takehara, N., Iwahara, Y., Sawada, T., Ohtsuki, Y., Dawei, Y., Hoshino, H., and Miyoshi, I. (1990) *Blood* **76**(8), 1657-1661

52. Burton, M., Upadhyaya, C. D., Maier, B., Hope, T. J., and Semmes, O. J. (2000) *J Virol* **74**(5), 2351-2364

53. Semmes, O. J., and Jeang, K. T. (1996) *J Virol* **70**(9), 6347-6357

54. Chiari, E., Lamsoul, I., Lodewick, J., Chopin, C., Bex, F., and Pique, C. (2004) *J Virol* **78**(21), 11823-11832

55. Bex, F., Murphy, K., Wattiez, R., Burny, A., and Gaynor, R. B. (1999) *J Virol* **73**(1), 738-745

56. Durkin, S. S., Ward, M. D., Fryrear, K. A., and Semmes, O. J. (2006) *J Biol Chem*

57. Lamsoul, I., Lodewick, J., Lebrun, S., Brasseur, R., Burny, A., Gaynor, R. B., and Bex, F. (2005) *Mol Cell Biol* **25**(23), 10391-10406

58. Peloponese, J. M., Jr., Iha, H., Yedavalli, V. R., Miyazato, A., Li, Y., Haller, K., Benkirane, M., and Jeang, K. T. (2004) *J Virol* **78**(21), 11686-11695

59. Semmes, O. J., and Jeang, K. T. (1992) *Virology* **188**(2), 754-764

60. Smith, M. R., and Greene, W. C. (1990) *Genes Dev* **4**(11), 1875-1885

61. Alefantis, T., Barmak, K., Harhaj, E. W., Grant, C., and Wigdahl, B. (2003) *J Biol Chem* **278**(24), 21814-21822

62. Semmes, O. J., and Jeang, K. T. (1995) *J Virol* **69**(3), 1827-1833

63. Jin, D. Y., and Jeang, K. T. (1997) *Nucleic Acids Res* **25**(2), 379-387

64. Xiao, G., Harhaj, E. W., and Sun, S. C. (2000) *J Biol Chem* **275**(44), 34060-34067

65. Jin, D. Y., and Jeang, K. T. (1997) *Leukemia* **11 Suppl 3**, 3-6

66. Basbous, J., Bazarbachi, A., Granier, C., Devaux, C., and Mesnard, J. M. (2003) *J Virol* **77**(24), 13028-13035

67. Xie, L., Yamamoto, B., Haoudi, A., Semmes, O. J., and Green, P. L. (2006) *Blood* **107**(5), 1980-1988

68. Rousset, R., Fabre, S., Desbois, C., Bantignies, F., and Jalinot, P. (1998) *Oncogene* **16**(5), 643-654

69. Yan, J. P., Garrus, J. E., Giebler, H. A., Stargell, L. A., and Nyborg, J. K. (1998) *J Mol Biol* **281**(3), 395-400

70. Vendel, A. C., McBryant, S. J., and Lumb, K. J. (2003) *Biochemistry* **42**(43), 12481-12487

71. Harrod, R., Tang, Y., Nicot, C., Lu, H. S., Vassilev, A., Nakatani, Y., and Giam, C. Z. (1998) *Mol Cell Biol* **18**(9), 5052-5061

72. Tanaka, A., Takahashi, C., Yamaoka, S., Nosaka, T., Maki, M., and Hatanaka, M. (1990) *Proc Natl Acad Sci U S A* **87**(3), 1071-1075

73. Pozzatti, R., Vogel, J., and Jay, G. (1990) *Mol Cell Biol* **10**(1), 413-417

74. Grassmann, R., Dengler, C., Muller-Fleckenstein, I., Fleckenstein, B., McGuire, K., Dokhelar, M. C., Sodroski, J. G., and Haseltine, W. A. (1989) *Proc Natl Acad Sci U S A* **86**(9), 3351-3355

75. Grassmann, R., Berchtold, S., Radant, I., Alt, M., Fleckenstein, B., Sodroski, J. G., Haseltine, W. A., and Ramstedt, U. (1992) *J Virol* **66**(7), 4570-4575

76. Nerenberg, M., Hinrichs, S. H., Reynolds, R. K., Khoury, G., and Jay, G. (1987) *Science* **237**(4820), 1324-1329

77. Hinrichs, S. H., Nerenberg, M., Reynolds, R. K., Khoury, G., and Jay, G. (1987) *Science* **237**(4820), 1340-1343

78. Grossman, W. J., Kimata, J. T., Wong, F. H., Zutter, M., Ley, T. J., and Ratner, L. (1995) *Proc Natl Acad Sci U S A* **92**(4), 1057-1061

79. Jin, D. Y., Spencer, F., and Jeang, K. T. (1998) *Cell* **93**(1), 81-91

80. Liang, M. H., Geisbert, T., Yao, Y., Hinrichs, S. H., and Giam, C. Z. (2002) *J Virol* **76**(8), 4022-4033

81. Kamada, N., Sakurai, M., Miyamoto, K., Sanada, I., Sadamori, N., Fukuhara, S., Abe, S., Shiraishi, Y., Abe, T., Kaneko, Y., and et al. (1992) *Cancer Res* **52**(6), 1481-1493

82. Majone, F., Semmes, O. J., and Jeang, K. T. (1993) *Virology* **193**(1), 456-459

83. Miyake, H., Suzuki, T., Hirai, H., and Yoshida, M. (1999) *Virology* **253**(2), 155-161

84. Semmes, O. J., Burton, M., and Epperly, C. D. (1999) *HTLV-I Tax and Loss of Genetic Integrity*, ABI Professional Publications, Arlington, VA

85. Sibon, D., Gabet, A. S., Zandecki, M., Pinatel, C., Thete, J., Delfau-Larue, M. H., Rabaaoui, S., Gessain, A., Gout, O., Jacobson, S., Mortreux, F., and Wattel, E. (2006) *J Clin Invest* **116**(4), 974-983

86. Brady, J., Jeang, K. T., Duvall, J., and Khoury, G. (1987) *J Virol* **61**(7), 2175-2181

87. Jeang, K. T., Boros, I., Brady, J., Radonovich, M., and Khoury, G. (1988) *J Virol* **62**(12), 4499-4509

88. Yin, M. J., and Gaynor, R. B. (1996) *Mol Cell Biol* **16**(6), 3156-3168

89. Goren, I., Semmes, O. J., Jeang, K. T., and Moelling, K. (1995) *J Virol* **69**(9), 5806-5811

90. Kimzey, A. L., and Dynan, W. S. (1999) *J Biol Chem* **274**(48), 34226-34232

91. Jeang, K. T. (2001) *Cytokine Growth Factor Rev* **12**(2-3), 207-217

92. Kwok, R. P., Laurance, M. E., Lundblad, J. R., Goldman, P. S., Shih, H., Connor, L. M., Marriott, S. J., and Goodman, R. H. (1996) *Nature* **380**(6575), 642-646

93. Lenzmeier, B. A., Giebler, H. A., and Nyborg, J. K. (1998) *Mol Cell Biol* **18**(2), 721-731

94. Riou, P., Bex, F., and Gazzolo, L. (2000) *J Biol Chem* **275**(14), 10551-10560

95. Jiang, H., Lu, H., Schiltz, R. L., Pise-Masison, C. A., Ogryzko, V. V., Nakatani, Y., and Brady, J. N. (1999) *Mol Cell Biol* **19**(12), 8136-8145

96. Chu, Z. L., Shin, Y. A., Yang, J. M., DiDonato, J. A., and Ballard, D. W. (1999) *J Biol Chem* **274**(22), 15297-15300

97. Harhaj, E. W., and Sun, S. C. (1999) *J Biol Chem* **274**(33), 22911-22914

98. Jin, D. Y., Giordano, V., Kibler, K. V., Nakano, H., and Jeang, K. T. (1999) *J Biol Chem* **274**(25), 17402-17405

99. Hirai, H., Suzuki, T., Fujisawa, J., Inoue, J., and Yoshida, M. (1994) *Proc Natl Acad Sci U S A* **91**(9), 3584-3588

100. Yoshida, M. (2001) *Annu Rev Immunol* **19**, 475-496

101. Lacoste, J., Petropoulos, L., Pepin, N., and Hiscott, J. (1995) *J Virol* **69**(1), 564-569

102. McKinsey, T. A., Brockman, J. A., Scherer, D. C., Al-Murrani, S. W., Green, P. L., and Ballard, D. W. (1996) *Mol Cell Biol* **16**(5), 2083-2090

103. Mori, N., Fujii, M., Ikeda, S., Yamada, Y., Tomonaga, M., Ballard, D. W., and Yamamoto, N. (1999) *Blood* **93**(7), 2360-2368

104. Shuh, M., and Derse, D. (2000) *J Virol* **74**(23), 11394-11397

105. Fujii, M., Tsuchiya, H., Chuhjo, T., Akizawa, T., and Seiki, M. (1992) *Genes Dev* **6**(11), 2066-2076

106. Azran, I., Schavinsky-Khrapunsky, Y., and Aboud, M. (2004) *Retrovirology* **1**(1), 20

107. Harhaj, E. W., Good, L., Xiao, G., and Sun, S. C. (1999) *Oncogene* **18**(6), 1341-1349

108. Ng, P. W., Iha, H., Iwanaga, Y., Bittner, M., Chen, Y., Jiang, Y., Gooden, G., Trent, J. M., Meltzer, P., Jeang, K. T., and Zeichner, S. L. (2001) *Oncogene* **20**(33), 4484-4496

109. de la Fuente, C., Gupta, M. V., Klase, Z., Strouss, K., Cahan, P., McCaffery, T., Galante, A., Soteropoulos, P., Pumfery, A., Fujii, M., and Kashanchi, F. (2006) *Retrovirology* **3**, 43

110. de La Fuente, C., Deng, L., Santiago, F., Arce, L., Wang, L., and Kashanchi, F. (2000) *AIDS Res Hum Retroviruses* **16**(16), 1695-1700

111. Pise-Masison, C. A., Radonovich, M., Mahieux, R., Chatterjee, P., Whiteford, C., Duvall, J., Guillerm, C., Gessain, A., and Brady, J. N. (2002) *Cancer Res* **62**(12), 3562-3571

112. Haoudi, A., Daniels, R. C., Wong, E., Kupfer, G., and Semmes, O. J. (2003) *J Biol Chem* **278**(39), 37736-37744

113. Lemoine, F. J., and Marriott, S. J. (2001) *J Biol Chem* **276**(34), 31851-31857

114. Haoudi, A., and Semmes, O. J. (2003) *Virology* **305**(2), 229-239

115. Grassmann, R., Aboud, M., and Jeang, K. T. (2005) *Oncogene* **24**(39), 5976-5985

116. Jeang, K. T., Giam, C. Z., Majone, F., and Aboud, M. (2004) *J Biol Chem* **279**(31), 31991-31994

117. Suzuki, T., Kitao, S., Matsushime, H., and Yoshida, M. (1996) *Embo J* **15**(7), 1607-1614

118. Suzuki, T., Narita, T., Uchida-Toita, M., and Yoshida, M. (1999) *Virology* **259**(2), 384-391

119. Haller, K., Wu, Y., Derow, E., Schmitt, I., Jeang, K. T., and Grassmann, R. (2002) *Mol Cell Biol* **22**(10), 3327-3338

120. Kehn, K., Fuente Cde, L., Strouss, K., Berro, R., Jiang, H., Brady, J., Mahieux, R., Pumfery, A., Bottazzi, M. E., and Kashanchi, F. (2005) *Oncogene* **24**(4), 525-540

121. Tabakin-Fix, Y., Azran, I., Schavinky-Khrapunsky, Y., Levy, O., and Aboud, M. (2006) *Carcinogenesis* **27**(4), 673-681

122. Liu, B., Liang, M. H., Kuo, Y. L., Liao, W., Boros, I., Kleinberger, T., Blancato, J., and Giam, C. Z. (2003) *Mol Cell Biol* **23**(15), 5269-5281

123. Liu, B., Hong, S., Tang, Z., Yu, H., and Giam, C. Z. (2005) *Proc Natl Acad Sci U S A* **102**(1), 63-68

124. Peloponese, J. M., Jr., Haller, K., Miyazato, A., and Jeang, K. T. (2005) *Proc Natl Acad Sci U S A* **102**(52), 18974-18979

125. Jeang, K. T., Widen, S. G., Semmes, O. J. t., and Wilson, S. H. (1990) *Science* **247**(4946), 1082-1084

126. Philpott, S. M., and Buehring, G. C. (1999) *J Natl Cancer Inst* **91**(11), 933-942

127. Kao, S. Y., and Marriott, S. J. (1999) *J Virol* **73**(5), 4299-4304

128. Majone, F., and Jeang, K. T. (2000) *J Biol Chem* **275**(42), 32906-32910

129. Gabet, A. S., Mortreux, F., Charneau, P., Riou, P., Duc-Dodon, M., Wu, Y., Jeang, K. T., and Wattel, E. (2003) *Oncogene* **22**(24), 3734-3741

130. Majone, F., Luisetto, R., Zamboni, D., Iwanaga, Y., and Jeang, K. T. (2005) *Retrovirology* **2**(1), 45

131. Gessain, A., Barin, F., Vernant, J. C., Gout, O., Maurs, L., Calender, A., and de The, G. (1985) *Lancet* **2**, 407-410

132. Osame, M., Usuku, K., Izumo, S., Ijichi, N., Amitani, H., Igata, A., Matsumoto, M., and Tara, M. (1986) *Lancet* **1**(8488), 1031-1032

133. Yin, M. J., Christerson, L. B., Yamamoto, Y., Kwak, Y. T., Xu, S., Mercurio, F., Barbosa, M., Cobb, M. H., and Gaynor, R. B. (1998) *Cell* **93**(5), 875-884

134. Geleziunas, R., Ferrell, S., Lin, X., Mu, Y., Cunningham, E. T., Jr., Grant, M., Connelly, M. A., Hambor, J. E., Marcu, K. B., and Greene, W. C. (1998) *Mol Cell Biol* **18**(9), 5157-5165

135. Uhlik, M., Good, L., Xiao, G., Harhaj, E. W., Zandi, E., Karin, M., and Sun, S. C. (1998) *J Biol Chem* **273**(33), 21132-21136

136. Chun, A. C., Zhou, Y., Wong, C. M., Kung, H. F., Jeang, K. T., and Jin, D. Y. (2000) *AIDS Res Hum Retroviruses* **16**(16), 1689-1694

137. Hirata, A., Higuchi, M., Niinuma, A., Ohashi, M., Fukushi, M., Oie, M., Akiyama, T., Tanaka, Y., Gejyo, F., and Fujii, M. (2004) *Virology* **318**(1), 327-336

138. Kim, J. S., and Raines, R. T. (1993) *Protein Sci* **2**(3), 348-356

139. Basu, S., Rosenzweig, K. R., Youmell, M., and Price, B. D. (1998) *Biochem Biophys Res Commun* **247**(1), 79-83

140. Lees-Miller, S. P., Sakaguchi, K., Ullrich, S. J., Appella, E., and Anderson, C. W. (1992) *Mol Cell Biol* **12**(11), 5041-5049

141. Lou, Z., Chen, B. P., Asaithamby, A., Minter-Dykhouse, K., Chen, D. J., and Chen, J. (2004) *J Biol Chem* **279**(45), 46359-46362

142. Lou, Z., Minter-Dykhouse, K., Wu, X., and Chen, J. (2003) *Nature* **421**(6926), 957-961

143. Park, H. U., Jeong, S. J., Jeong, J. H., Chung, J. H., and Brady, J. N. (2006) *Oncogene* **25**(3), 438-447

144. Ressler, S., Morris, G. F., and Marriott, S. J. (1997) *J Virol* **71**(2), 1181-1190

145. Marriott, S. J., and Semmes, O. J. (2005) *Oncogene* **24**(39), 5986-5995

146. Meek, K., Gupta, S., Ramsden, D. A., and Lees-Miller, S. P. (2004) *Immunol Rev* **200**, 132-141

147. Collis, S. J., DeWeese, T. L., Jeggo, P. A., and Parker, A. R. (2005) *Oncogene* **24**(6), 949-961

148. Burma, S., and Chen, D. J. (2004) *DNA Repair (Amst)* **3**(8-9), 909-918

149. Smith, G. C., and Jackson, S. P. (1999) *Genes Dev* **13**(8), 916-934

150. Goytisolo, F. A., Samper, E., Edmonson, S., Taccioli, G. E., and Blasco, M. A. (2001) *Mol Cell Biol* **21**(11), 3642-3651

151. Osame, M., Usuku, K., Izumo, S., Ijichi, N., Amitani, H., Igata, A., Matsumoto, M., and Tara, M. (1986) *Lancet* 1, 1031-1032

152. Poiesz, B. J., Ruscetti, F. W., Gazdar, A. F., Bunn, P. A., Minna, J. A., and Gallo, R. C. (1980) *Proceedings of the National Academy of the Sciences USA* 77, 7415-7419

153. Yoshida, M., Miyoshi, I., and Hinuma, Y. (1982) *Proceedings of the National Academy of the Sciences USA* 79, 2031-2035

154. Sun, S. C., and Yamaoka, S. (2005) *Oncogene* 24(39), 5952-5964

155. Semmes, O. J., and Jeang, K. T. (1992) *J Virol* 66(12), 7183-7192

156. Tootle, T. L., and Rebay, I. (2005) *Bioessays* 27(3), 285-298

157. Jeang, K. T., Brady, J., Radonovich, M., Duvall, J., and Khoury, G. (1988) *p40X trans-activation of HTLV-I LTR Promoter*, Alan R. Liss, Inc., New York

158. Fontes, J. D., Strawhecker, J. M., Bills, N. D., Lewis, R. E., and Hinrichs, S. H. (1993) *J Virol* 67(7), 4436-4441

159. Radonovich, M., and Jeang, K. T. (1989) *J Virol* 63(7), 2987-2994

160. Krause Boehm, A., Stawhecker, J. A., Semmes, O. J., Jankowski, P. E., Lewis, R., and Hinrichs, S. H. (1999) *J Biomed Sci* 6(3), 206-212

161. Loyet, K. M., Stults, J. T., and Arnott, D. (2005) *Mol Cell Proteomics* 4(3), 235-245

162. Gachon, F., Thebault, S., Peleraux, A., Devaux, C., and Mesnard, J. M. (2000) *Mol Cell Biol* 20(10), 3470-3481

163. Gachon, F., Peleraux, A., Thebault, S., Dick, J., Lemasson, I., Devaux, C., and Mesnard, J. M. (1998) *J Virol* 72(10), 8332-8337

164. Tie, F., Adya, N., Greene, W. C., and Giam, C. Z. (1996) *J Virol* 70(12), 8368-8374

165. Kim, J. S., and Raines, R. T. (1993) *Protein Science* 2, 348-356

166. Jaffe, H., Veeranna, and Pant, H. C. (1998) *Biochemistry* 37(46), 16211-16224

167. Yamaoka, S., Inoue, H., Sakurai, M., Sugiyama, T., Hazama, M., Yamada, T., and Hatanaka, M. (1996) *Embo J* 15(4), 873-887

168. Whitmarsh, A. J., and Davis, R. J. (2000) *Cell Mol Life Sci* 57(8-9), 1172-1183

169.   Hunter, T., and Karin, M. (1992) *Cell* **70**(3), 375-387

170.   Sakamoto, Y., Yoshida, M., Semba, K., and Hunter, T. (1997) *Oncogene* **15**(17), 2001-2012

171.   Taylor, W. E., and Young, E. T. (1990) *Proc Natl Acad Sci U S A* **87**(11), 4098-4102

172.   Neubauer, G., and Mann, M. (1999) *Anal Chem* **71**(1), 235-242

173.   Arnott, D., Gawinowicz, M. A., Grant, R. A., Neubert, T. A., Packman, L. C., Speicher, K. D., Stone, K., and Turck, C. W. (2003) *J Biomol Tech* **14**(3), 205-215

174.   McLachlin, D. T., and Chait, B. T. (2001) *Curr Opin Chem Biol* **5**(5), 591-602

175.   Nasr, R., Chiari, E., El-Sabban, M., Mahieux, R., Kfoury, Y., Abdulhay, M., Yazbeck, V., Hermine, O., de The, H., Pique, C., and Bazarbachi, A. (2006) *Blood*

176.   Morimoto, H., Tsukada, J., Kominato, Y., and Tanaka, Y. (2005) *Am J Hematol* **78**(2), 100-107

177.   Li, J., and Stern, D. F. (2005) *J Biol Chem* **280**(12), 12041-12050

178.   Doherty, A. J., and Jackson, S. P. (2001) *Curr Biol* **11**(22), R920-924

179.   Chan, D. W., Chen, B. P., Prithivirajsingh, S., Kurimasa, A., Story, M. D., Qin, J., and Chen, D. J. (2002) *Genes Dev* **16**(18), 2333-2338

180.   Chen, B. P., Chan, D. W., Kobayashi, J., Burma, S., Asaithamby, A., Morotomi-Yano, K., Botvinick, E., Qin, J., and Chen, D. J. (2005) *J Biol Chem* **280**(15), 14709-14715

181.   Takahashi, A., and Ohnishi, T. (2005) *Cancer Lett* **229**(2), 171-179

182.   Cui, X., Yu, Y., Gupta, S., Cho, Y. M., Lees-Miller, S. P., and Meek, K. (2005) *Mol Cell Biol* **25**(24), 10842-10852

183.   Burma, S., Chen, B. P., and Chen, D. J. (2006) *DNA Repair (Amst)* **5**(9-10), 1042-1048

184.   Bartkova, J., Horejsi, Z., Koed, K., Kramer, A., Tort, F., Zieger, K., Guldberg, P., Sehested, M., Nesland, J. M., Lukas, C., Orntoft, T., Lukas, J., and Bartek, J. (2005) *Nature* **434**(7035), 864-870

185.   Chu, G. (1997) *J Biol Chem* **272**(39), 24097-24100

186. Liu, L. X., Jiang, H. C., Liu, Z. H., Zhu, A. L., Zhou, J., Zhang, W. H., Wang, X. Q., and Wu, M. (2003) *Hepatogastroenterology* **50**(53), 1496-1501

187. Hosoi, Y., Watanabe, T., Nakagawa, K., Matsumoto, Y., Enomoto, A., Morita, A., Nagawa, H., and Suzuki, N. (2004) *Int J Oncol* **25**(2), 461-468

188. Um, J. H., Kwon, J. K., Kang, C. D., Kim, M. J., Ju, D. S., Bae, J. H., Kim, D. W., Chung, B. S., and Kim, S. H. (2004) *J Pharmacol Exp Ther* **311**(3), 1062-1070

189. Ding, Q., Reddy, Y. V., Wang, W., Woods, T., Douglas, P., Ramsden, D. A., Lees-Miller, S. P., and Meek, K. (2003) *Mol Cell Biol* **23**(16), 5836-5848

190. Chan, D. W., and Lees-Miller, S. P. (1996) *J Biol Chem* **271**(15), 8936-8941

191. Merkle, D., Douglas, P., Moorhead, G. B., Leonenko, Z., Yu, Y., Cramb, D., Bazett-Jones, D. P., and Lees-Miller, S. P. (2002) *Biochemistry* **41**(42), 12706-12714

192. Wechsler, T., Chen, B. P., Harper, R., Morotomi-Yano, K., Huang, B. C., Meek, K., Cleaver, J. E., Chen, D. J., and Wabl, M. (2004) *Proc Natl Acad Sci U S A* **101**(5), 1247-1252

193. Gaymes, T. J., Mufti, G. J., and Rassool, F. V. (2002) *Cancer Res* **62**(10), 2791-2797

194. Pise-Masison, C. A., Radonovich, M., Sakaguchi, K., Appella, E., and Brady, J. N. (1998) *J Virol* **72**(8), 6348-6355

195. Pise-Masison, C. A., Mahieux, R., Jiang, H., Ashcroft, M., Radonovich, M., Duvall, J., Guillerm, C., and Brady, J. N. (2000) *Mol Cell Biol* **20**(10), 3377-3386

196. Van, P. L., Yim, K. W., Jin, D. Y., Dapolito, G., Kurimasa, A., and Jeang, K. T. (2001) *J Virol* **75**(1), 396-407

197. Durocher, D., and Jackson, S. P. (2001) *Curr Opin Cell Biol* **13**(2), 225-231

198. Yang, J., Yu, Y., Hamrick, H. E., and Duerksen-Hughes, P. J. (2003) *Carcinogenesis* **24**(10), 1571-1580

199. Iijima, S., Teraoka, H., Date, T., and Tsukada, K. (1992) *Eur J Biochem* **206**(2), 595-603

200. Saggioro, D., D'Agostino D, M., and Chieco-Bianchi, L. (1999) *Exp Cell Res* **247**(2), 525-533

201. Semmes, O. J., Barret, J. F., Dang, C. V., and Jeang, K. T. (1996) *J Biol Chem* **271**(16), 9730-9738

202. An, J., Xu, Q. Z., Sui, J. L., Bai, B., and Zhou, P. K. (2005) *Int J Cancer* **117**(4), 531-537

203. Bailey, S. M., and Murnane, J. P. (2006) *Nucleic Acids Res* **34**(8), 2408-2417

204. Gilley, D., Tanaka, H., Hande, M. P., Kurimasa, A., Li, G. C., Oshimura, M., and Chen, D. J. (2001) *Proc Natl Acad Sci U S A* **98**(26), 15084-15088

205. Espejel, S., Franco, S., Sgura, A., Gae, D., Bailey, S. M., Taccioli, G. E., and Blasco, M. A. (2002) *Embo J* **21**(22), 6275-6287

206. Itoyama, T., Chaganti, R. S., Yamada, Y., Tsukasaki, K., Atogami, S., Nakamura, H., Tomonaga, M., Ohshima, K., Kikuchi, M., and Sadamori, N. (2001) *Blood* **97**(11), 3612-3620

207. Daniel, R., Katz, R. A., and Skalka, A. M. (1999) *Science* **284**(5414), 644-647

208. Baekelandt, V., Claeys, A., Cherepanov, P., De Clercq, E., De Strooper, B., Nuttin, B., and Debyser, Z. (2000) *J Virol* **74**(23), 11278-11285

209. Li, L., Olvera, J. M., Yoder, K. E., Mitchell, R. S., Butler, S. L., Lieber, M., Martin, S. L., and Bushman, F. D. (2001) *Embo J* **20**(12), 3272-3281

210. Corbeil, J., and Richman, D. D. (1995) *Adv Exp Med Biol* **374**, 91-99

211. Sun, Y., Huang, Y. C., Xu, Q. Z., Wang, H. P., Bai, B., Sui, J. L., and Zhou, P. K. (2006) *Int J Radiat Oncol Biol Phys* **65**(3), 842-850

212. Jackson, S. P. (2002) *Carcinogenesis* **23**(5), 687-696

213. Shiloh, Y. (2003) *Nat Rev Cancer* **3**(3), 155-168

214. van Gent, D. C., Hoeijmakers, J. H., and Kanaar, R. (2001) *Nat Rev Genet* **2**(3), 196-206

215. Zhong, Q., Chen, C. F., Chen, P. L., and Lee, W. H. (2002) *J Biol Chem* **277**(32), 28641-28647

216. Wang, H. C., Chou, W. C., Shieh, S. Y., and Shen, C. Y. (2006) *Cancer Res* **66**(3), 1391-1400

APPENDIX A

COPYRIGHT PERMISSION

Figures 7-12 and Table II have been reprinted here from Durkin, S.S., Ward, M.D., Fryrear, K.A. and Semmes, O.J. (2006) *J Biol Chem*.

The following copyright permission policy from http://www.jbc.org/misc/Copyright_Permission.shtml has been followed.

Copyright Permission Policy:

ASBMB Journals
Journal of Biological Chemistry
Molecular and Cellular Proteomics
Journal of Lipid Research
Biochemistry and Molecular Biology Education
ASBMB Today

ASBMB does not charge for and grants use without requiring your copyright permission request for:

- Original authors wanting to reproduce portions of their own work; or to republish their material in not-for-profit formats or venues.

- Students wanting to reproduce or republish their work for educational purposes.

- Students using other authors' material for their theses.

- Reproduction or republication of abstracts only.

- Photocopying up to 5 copies for personal use.

- Non-profit educational institutions making multiple photocopies of articles for classroom use; all such reproduction must utilize institutionally owned equipment for this purpose.

APPENDIX B

AUTHORIZATION FOR USE OF RADIOACTIVE MATERIAL

EASTERN VIRGINIA MEDICAL SCHOOL
ENVIRONMENTAL HEALTH AND SAFETY/RADIATION SAFETY PROGRAMS
700 OLNEY ROAD
POST OFFICE BOX 1980
NORFOLK, VIRGINIA 23501

EASTERN VIRGINIA
MEDICAL SCHOOL

TELEPHONE (757) 446-5798
FAX (757) 446-7242

MEMORANDUM

TO: O. John Semmes, Ph.D.   AU#: A158
Department of Microbiology and Molecular Cell Biology

FROM: EVMS Radiation Safety Committee
LaMarr Beuchler, RSO ___ ᒪᐯᗝ ___

DATE: February 24, 2005

SUBJ: Approval of your biennial renewal application dated February 16, 2005

The Radiation Safety Committee approved your renewal application to possess and use the following radioactive material:

1.0 mCi of P-32 as NTP, P04

Your authorization expires on **02/24/2007**. Approval is based on continued work with these materials under conditions specified in your application of 03/21/2003, and this renewal application. If these conditions change, please contact the Radiation Safety Office to amend your authorization. File this approval in your Radiation Safety Notebook.

COMMENTS:

Authorized Users are required to perform and document at least monthly wipe surveys in areas where radioactive material is used and stored.

In addition, individuals working with P-32 shall survey their work areas and self prior to departing the Lab. This survey should be performed with a portable survey instrument capable of detecting P-32.

RSO-40A 04/02

RADIATION SAFETY • LABORATORY SAFETY • HAZARDOUS WASTE DISPOSAL • BIOSAFETY • HAZARD COMMUNICATION

VITA

SARAH SAIONZ DURKIN

Department of study
Eastern Virginia Medical School
Department of Microbiology and Molecular Cell Biology
700 West Olney Road
Norfolk, Virginia 23507

Education
Old Dominion University and Eastern Virginia Medical School
Norfolk, Virginia
Doctor of Philosophy, Biomedical Sciences (August 2002 – December 2006)

University of Pennsylvania
Philadelphia, Pennsyvania
Master of Arts, Biology (August 1998 – August 2000)

University of Pennsylvania
Philadelphia, Pennsyvania
Bachelor of Arts, Biology (August 1996 – May 2000)

Professional Experience
Graduate Research Assistant (August 2002 – December 2006)
Eastern Virginia Medical School
Norfolk, Virginia

Research Scientist I (April 2002 – August 2002)
Pfizer Global Research and Development
La Jolla, California

Adjunct Associate in Molecular Biology (September 2000 – December 2001)
Center for Environmental Diagnostics and Bioremediation, University of West Florida
Pensacola, Florida

Research Assistant (June 1997 – September 2000)
University of Pennsylvania
Philadelphia, Pennsylvania

Summer Intern in Biomedical Research (June 1998 – August 1998)
National Institute of Neurological Disorder and Stroke, NIH
Bethesda, Maryland